Phases and phase transitions of strongly correlated electron systems

by

Pouyan Ghaemi Mohammadi

Submitted to the Department of Physics
in partial fulfillment of the requirements for the degree of

Doctor of Philosophy in Physics

at the

MASSACHUSETTS INSTITUTE OF TECHNOLOGY

August 2008

© Massachusetts Institute of Technology 2008. All rights reserved.

Author .....
Department of Physics
August 5, 2008

Certified by .....
Senthil Todadri
Associate Professor
Thesis Supervisor

Accepted by .....
Thomas J. Greytak
Professor, Associate Department Head on Education

ARCHIVES

MASSACHUSETTS INSTITUTE OF TECHNOLOGY
OCT 0 9 2008
LIBRARIES

Phases and phase transitions of strongly correlated electron systems

by

Pouyan Ghaemi Mohammadi

Submitted to the Department of Physics
on August 5, 2008, in partial fulfillment of the
requirements for the degree of
Doctor of Philosophy in Physics

Abstract

Different experiments on strongly correlated materials have shown phenomena which are not consistent with our conventional understandings. We still do not have a general framework to explain these properties. Developing such a general framework is much beyond the scope of this thesis, but here we try to address some of challenges in simpler models that are more tractable.

In correlated metals it appears as strong correlations have different effect on different parts of fermi surface. Perhaps most striking example of this is normal state of optimally doped cuprates; the quasiparticle peaks on the nominal fermi surface do not appear uniformly. We try to track such phenomena in heavy fermion systems, which are correlated fermi liquids. In these systems, a lattice of localized electrons in f or d orbitals is coupled to the conduction electrons through an antiferromagnetic coupling. Singlets are formed between localized and conduction electrons. This singlet naturally have non-zero internal angular momentum. This nontrivial structure leads to anisotropic effect of strong correlations. Internal structure of Kondo singlet can also lead to quantum Hall effect in Kondo insulator, and formation of isolated points on the fermi surface with fractionalized quasiparticles.

In the second part we study a phase transition in Heisenberg model between two insulating phases, Neel ordered and certain spin liquid state, popular in theories of the cuprates. The existence of such a transition has a number of interesting implications for spin liquid based approaches to the underdoped cuprates and clarifies existing ideas for incorporating antiferromagnetic long range order into such a spin liquid based approach. This transition might also be enlightening, despite fundamental differences, for the heavy fermion critical points where a second order transition between the heavy fermion phase and a metallic phase with magnetic antiferromagnetic order is observed.

Thesis Supervisor: Senthil Todadri
Title: Associate Professor

Acknowledgments

The five years I spent at MIT with all their challenges, were one of the most fruitful periods of my life. I was very lucky that the year I was applying two faculty members from University of Texas at Austin, came to our university for a semester. Professors Cecile Dewitt-Morette and Bryce Dewitt had important effect on my career and indeed opened my path to MIT.

Since the first semester at MIT, I was lucky to learn from the pioneers in the world. Professor Patrick Lee's solid state course was my main motivation to enter hard condensed matter physics. His suggestion to start working with Senthil, even though he had the plan to leave for India, gave me the great chance to have 5 valuable years under his supervision. With professor Kardar's lectures on statistical mechanics I am confident that I will never forgot this core subject and with unique course of quantum field theory by professor Arkani-Hamed I learned the deep physical concepts behind the complicated mathematics of quantum field theory.

I started working with Senthil after the first semester at MIT. From the beginning his wonderful attitude was a great encouragement since I did not have much background in the field when I started. Now that I look back on these years, even the two years when Senthil was away, I see what I learned from him is a valuable baggage that I could not easily gain otherwise. Senthil's deep view of physics of problems was always enlightening and he always gave me confidence in my work. I hope that I have the chance of learning more from him in the future as well. Other great opportunity I had when started research at MIT, was collaboration with professor Ashvin Vishwanath who was a postdoctral fellow at the time. He guided me through my confusions and helped me as an adviser. I am very happy that I will have the chance of collaborating with him in coming years. Later when professor Michael Hermele joined MIT as a post-doc, during the years that Senthil was away, I could enjoy talking with him as well.

In fourth year of my PhD I found the chance to meet two other wonderful faculty members at MIT. I had a course with professor Frank Wilczek, where he presented

new research directions and it lead me to a very fruitful collaboration. His wide and deep vision in physics is well known and I was very lucky to spend hours discussing physics problems with him. I learned so much from him in the last two years and meeting him was such a great honor for me.

Also in the fourth year of my PhD, Senthil introduced me to professor Young Lee's group. This was my first experience with an experimental group. From professor Lee and his students, E. Abel and K. Matan, I learned many things about real challenges that experimentalists face to realize exotic quantum phases of matter. It was so exciting to see how our theoretical expectations are observed in nature. I surely hope to be able to have more collaborations with this and other experimental groups in the future.

MIT opened the way to meet many other scientists out MIT for me. Collaborating with professor Piers Colman and getting to know him was one of them. I never meet him before our paper was submitted, but even then I had learned many things from him. His outstanding view on real materials and experiments is very instructive. I had the pleasure of talking with him later too each time learning new interesting points. Also after professor Subir Sachdev, whose great publications were always great guide for me, joined Harvard I got the chance to learn quantum phase transitions from the pioneer of the field. I meet professor Chamon when he was at MIT and later our long discussions in BU taught me many things.

Many friends and other people in these five years were also very helpful to me. I learned many things from discussions with Dima, Mark, Brian, Maissam, Mohammad and Tarun. An especial person who I am particularly grateful to, because of her endless helps and supports in the times of need was Mahshid. Without her supports I do not know if I could finish my course successfully!

Although the years at MIT where essential in forming my life and interests and I am sure will be a key to my future career, it was not by far the only important period. My parents who where always beside me, my mother Nazy, who wanted nothing in her life but my success and happiness, my father who made me familiar with the joy of reading and learning, and showed me how to look at the world from

science perspective, with spending so much time with me to gather and classify our insects collections, and trying to see the exciting tiny world under the microscope he gave me. Without them I would never had any of my achievements. In high school years I am specially thankful to two of my math teachers. Mr. Honarmandian whose astonishing geometry classes where so joyful, and I really learned organized logical thinking from him, which was always helping me to think on any problem and Mr. Anaraki whose wonderful algebra class was the first place I learned about group theory. Physics Olympiad at the end of high school made me confident about my choice to study physics. I owe all my knowledge in basic physics to that period and particularly professors Shariati and Khorrami.

My undergraduate years in Sharif University were also amongst the best years of my life. Having professor Arfaei as my adviser was essential in my decision to study theoretical physics. I am also thankful to professor Golshani for his amazing quantum mechanics classes, where he spent so much time answering my questions and addressing my confusions to understand a new perspective. Finally I like to thank my aunt Farah because of all her support particularly when I was applying to continue my studies abroad.

To my family

Nazy, Mehdi and Pejman

And my grandmother who always wished to see this but left us before she had the chance.

Although my senses were searching the desert fatigue-lessly; discovering nothing although finding a lot; my soul was illuminated by a thousand suns; but could never ever touch the perfection of a single atom.

Avicenna, 980-1037 C.E.

Contents

List of Figures

List of Tables

Chapter 1

Introduction

Principle of reductionism, that is all the matter around us is governed by the same fundamental laws, is widely accepted among physicists. In high energy physics people try to find the elementary particles forming the matter and discover the fundamental laws governing them. It might seems then, based on reductionism hypothesis, that this is all the fundamental knowledge we need to describe the nature. But the ability to reduce everything to the fundamental laws governing the elementary particles does not imply the ability to start from those laws and reconstruct the universe[5]!

In macroscopic systems consisting of large number of particles, collective behaviors emerge which could not be extracted solely by understanding the physics of their individual elements. To understand the macroscopic properties of materials we need to study these collective behaviors and so we need more than single particle physics.

Thermodynamics and later statistical mechanics were developed to explain macroscopic phenomenas without detail knowledge of the mi-

croscopic properties. With development of quantum mechanics it was also incorporated in describing the properties of matter. Interestingly quantum fluctuations, like thermal fluctuations, can also drive the system through a phase transition[6, 7]. These quantum phase transitions correspond to the change of ground state of the macroscopic system and could have dramatic effects on the properties even at finite (but low) temperatures[3].

Much of our modern understandings of quantum many-body systems are based on two paradigms, both mainly developed by Landau[8]. The first one classifies different phases of matter using the concept of order parameter which is a measure of their broken symmetries. Phase transitions are then described by partial break down of some the symmetries of one phase. In this Landau paradigm, second order phase transitions could happen between two phases where the symmetries of one phase is the subgroup of the symmetries of the other. The other paradigm, fermi liquid theory[9], describes the excitations out of the electronic ground state (i.e. fermi sea) in terms of quasi-particles which retain the electronic integrity, despite their interactions.

Recent experiments have shown that both of these paradigms might break down in systems where there are strong interaction between the particles. A few examples are fractional quantum hall effect, high temperature superconductivity, and heavy fermion phase transitions.

In fractional quantum hall effect, quasi-particles lose their electron integrity and appear as fractional particles which carry only part of

electron quantum numbers[10]. In other systems second order phase transitions are observed which does not seem to fit in Landau theory of phase transitions[3]. Despite wide theoretical investigations, and some developments[11, 12], a general unified theory which explains the behaviors out of Landau paradigms is still lacking.

Developing such a general frame work needs efforts much beyond this thesis; here we try to address some of challenging observations but in simpler models where physics is better understood. We address anisotropic effect of strong correlation which is observed in metallic phase of underdoped high temperature superconductors, in heavy fermions which are strongly correlated fermi liquids and thus more analytically tractable. Also we present a second order phase transition between two insulating phases of a strongly correlated model. This is indeed motivated by observed phases and phase transitions, which are not entirely insulating; but since the actual phase transition is not clearly understood yet, a good strategy might be to address these features in models which are only as close as possible to the real system and can capture some of the essential physics.

Two important classes of unconventional materials are cuprate superconductors and heavy fermion compounds. In this introduction we start by briefly reviewing physics of cuprates particularly in underdoped side. Next we present basic physics of heavy fermions and review the slave particle mean-field theory[13, 14]. This introduction will be finished by an overview of the thesis.

1.1 High temperature superconductivity

High temperature superconductivity was first discovered in 1986[15]. Critical temperature raised fast to well above nitrogen melting point[16]. It was observed in a pretty unexpected material, a transition metal oxide, which made it clear that the mechanism is pretty unconventional[17]. Since then cuprates have been under vast experimental and theoretical investigations. After more than 20 years many of the physical properties of cuprates, particularly in metallic state above superconducting dome, are not understood. There is yet no consensus for mechanism of high T_c superconductivity. But it seems that the basic physics of cuprates is well understood. They all share the layered structure which contains one or more copper oxygen planes. The low energy physics is described by the square lattice Hubbard model[18, 19]:

$$H = -\sum t_{ij} c^{\dagger}_{i\sigma} c_{j\sigma} + H.c. + U \sum_i n_{i\uparrow} n_{i\downarrow} \tag{1.1}$$

In the above Hamiltonian first term corresponds to hopping between sites and the second term is the on-site Columb repulsion which does not like double occupancy. It is well established that in cuprates, strong correlation plays an important role in forming different phases[17]. At zero doping, for large enough U this describes a Mott insulator and have long range antiferromagnetic order. Upon doping with holes antiferromagnetic order disappears quickly (Fig. 1-1). A variety of experiments now support the notion that the underdoped cuprates are usefully re-

garded as doped Mott insulators - in other words proximity to the Mott insulator strongly influences the properties of the underdoped materials[20]. Indeed antiferromagnetic order increases the kinetic energy of the holes. The competition between the kinetic energy of the holes and spin exchange energy forms the phase at small doping, which is known as pseudogap phase.

For spin one half with antiferromagnetic exchange one proposed competing state with Neel ordered phase is known as RVB state, which is a superposition of singlet pairs between different spins[18]. In this configuration the holes can move freely in a background of spin singlet pairs, which does not break any symmetry, and decrease their kinetic energy. This picture is consistent with the important features of the pseudogap phase[21]. Singlet formation explains the decrease of uniform spin susceptibility and reduction of specific heat. In plane conductivity spectral weight scales with number of holes. As will be explained in more details later, photoemission experiments show pull back of leading edge spectral peak which signals the formation of the gap to break a singlet pair. This gap is not uniform over the fermi surface and it is where pseudogap phase got its name.

With more doping at low enough temperature, superconductivity appears which seems to have d-wave structure. Superconducting critical temperature increases with more doping until it reaches its maximum and then decreases to form the superconducting dome. Neutron scattering experiments reveal the existence of a sharp magnetic resonance

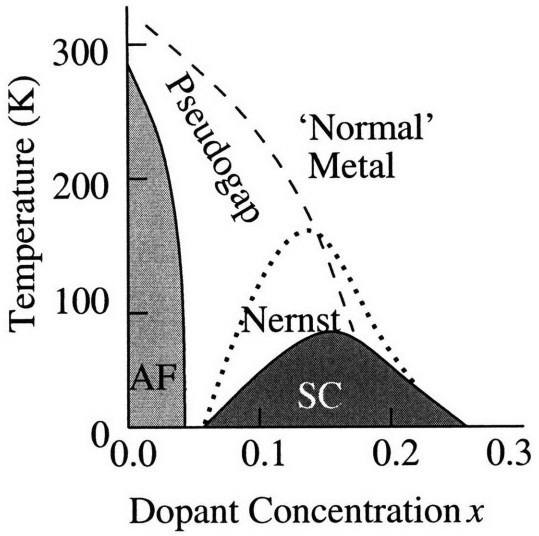

Figure 1-1: Phase diagram of cuprate superconductors

at (π, π) in the doped superconductor [22, 23, 24]. An appealing interpretation of this resonance is as a gapped version of the familiar magnon of a proximate antiferromagnetic state[25, 26, 27]. Interestingly as the doping is reduced, the resonance frequency goes down proportionately to T_c[28, 29]. This suggests that if the doped state is to be viewed as a doped paramagnet, then the latter may at least be connected to the Neel state by a second order transition (see Fig 4-1). Thus we are lead to search for quantum paramagnetic states of spin-1/2 moments on a square lattice that are accessible from the collinear Neel state by a second order transition.

Motivated by these observations in chapter 4 we present a model for the transition from Neel ordered phases to an insulating paramagnetic phase (a spin liquid). Even though the transition in cuprates takes another path (i.e. through doping which takes them out of insulating phase), this model could be enlightening for the nature of the pseudogap

phase.

In the underdoped regime, transport is through holes, but with renormalized hoping parameter. To apply the Luttinger theorem[30] and get the right fermi area, we should consider the fact that antiferromagnetic order folds the Brilloun zone in half. The fermi surface consists of ellipses centered at $(\pm\frac{\pi}{2}, \pm\frac{\pi}{2})$[1]. At larger doping, a fermi liquid metallic phase with a large electron fermi surface develops. We have good understanding of fermi surface in overdoped regime and some theoretical understanding in underdoped regime[17], but what happens in between? Interesting behavior is observed in the normal state of optimally doped cuprates between fermi holes and large fermi surface regimes. This is one of our motivations for the studies in chapter 2.

In cuprates it is known that antiferromagnetic order disappears beyond $x \approx 0.03$ and there is no signature of unit cell doubling. In absence of unit cell doubling, Luttinger theory only gives the right volume for large electron fermi surface. But transport properties seem to be given by the number of the holes. At zero temperature (i.e. ground state) antiferromagnetic phase transform into the superconducting phase where Luttinger theorem does not apply. But at finite temperature in the normal state, on the nominal fermi surface that could be derived from band theory, a true sharp electronic quasiparticle peak does not seem to exist. The electron spectrum - measured through photoemission ex-

[1]Although there are well developed theories for few holes in an antiferromagnetic background [31, 32, 33], there is yet no experimental realization of antiferromagnetic metallic phase with fermi pockets.

periments - shows significant anisotropy on moving around the fermi surface[34, 35, 1](Fig. 1-2).

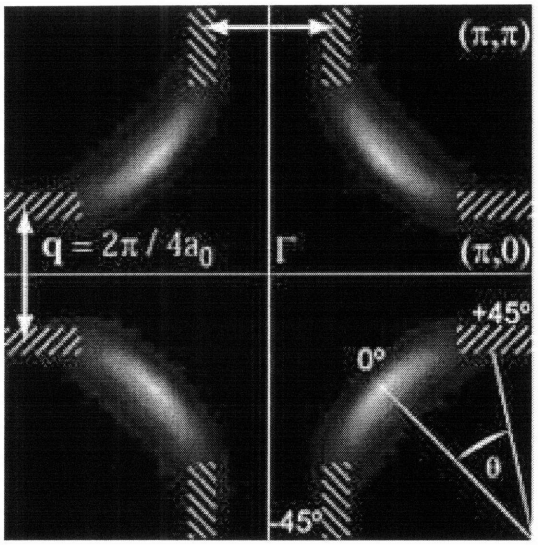

Figure 1-2: Nodal-Antinodal dichotomy from [1]

ARPES measures the spectrum of occupied electron states which could be emptied by the photon. In fermi liquids spectrum consists of sharp quasiparticle peaks at energies $\epsilon_k = E_f$. So as we move the momentum toward the fermi surface a peak appears and disappears as we cross the fermi surface. In the normal state of underdoped side, when we move toward the nominal fermi surface away from diagonal direction quasiparticle peaks which unlike fermi liquids are very broad approach the fermi energy but stop before crossing it. One might think this is what you expect when we have a fermi pocket since you may miss the pocket moving away from diagonal direction; the problem is that when we move along nodal direction, we cross the presumed fermi surface just once, i.e. no back side of the fermi surface is observed. Non existing well defined quasiparticle peaks also signal the fact that this

normal state is not a fermi liquid.

The general message from these results on the cuprates for the study of correlated metals is that correlation effects may not uniformly affect all parts of the fermi surface. Some portions of the fermi surface may be more susceptible to correlation effects than others. This will lead to strong correlation induced anisotropy in physical properties around the fermi surface. Theoretically study of such effects is difficult because electron correlations are typically most easily handled in real space which does not readily distinguish between different parts of the fermi surface. Interesting recent numerical calculations[36] based on cluster extensions of dynamical mean field theory on single band Hubbard models in two dimensions have found such momentum space differentiation in the electronic properties; here we take a different approach. In this thesis, we study the anisotropic effect of correlations in correlated metals which fit in the Landau theory, specifically heavy fermions. This gives us more quantitative handle to study the correlation effects.

1.2 Other correlated metals: heavy fermions

As mentioned before, normal state of optimally doped cuprates does not fit in the Landau fermi paradigm; hence the fermi liquid tools are not fully applicable to study this phase. But cuprates are not the only example of strongly correlated metals. Metals near Mott transition (e.g. $\kappa(BEDT-TTF)_2Cu[N(CN)_2]Cl$ [37]) and heavy fermions [2] are other examples. The later is indeed a strongly correlated fermi liquid.

In the first two chapters of this thesis we focus on the metallic phase of heavy fermions. We show that in this fermi liquid phase, strong correlation could have dramatically anisotropic effect on the fermi surface which is captured through quasiparticles residue (Z)[38].

Heavy fermion compounds present unconventional phases and phase transitions (see table 1.1) as well. Heavy fermion physics was first observed in a Cerium based alloy $CeAl_3$[2]. In these rare earth alloys, a periodic lattice of localized spin-1/2 magnetic moments is coupled through Kondo exchange[39] to a separate band of conduction electrons[40]. An interesting low temperature metallic phase often develops at low temperature where the local moments are absorbed into the fermi sea by a lattice analog of the Kondo effect. The resulting metallic phase is a fermi liquid albeit with strongly renormalized parameters the most dramatic of which is two to three order of magnitude quasiparticle mass enhancement (Fig. 1-3(a) and 1-3(b)), leading to the name 'heavy fermi liquid'.

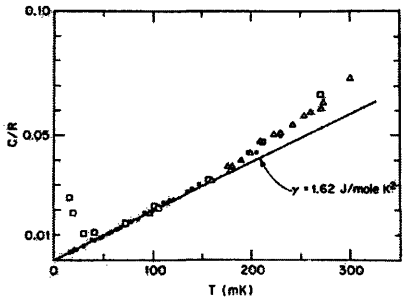

FIG. 1. Specific heat of $CeAl_3$ at very low temperatures in zero field (●, Δ) and in 10 kOe (□).

(a)

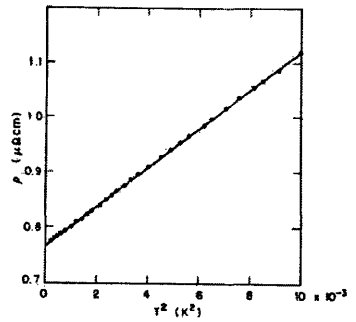

FIG. 3. Electrical resistivity of $CeAl_3$ below 100 mK, plotted against T^2.

(b)

Figure 1-3: Heat Capacity and Resistivit of $CeAl_3$[2]

Concomitantly the quasiparticle residue at the fermi surface is very small (though non-zero). Perhaps most strikingly the fermi surface is large in the sense that its volume satisfies Luttinger's theorem[30] only if the local moments are included in the count of the electron density. This and other universal properties of this fermi liquid are usefully understood in a strong Kondo coupling picture where each conduction electron is trapped into a spin singlet state with a local moment - see Ref. [41].

Theoretically many of the physical properties of heavy fermion compounds, including formation of Kondo singlets, can be captured by the slave particle mean field theory[14, 13]. We will review this method in 1.2.1. Important point to note here is that although the Kondo phase is a fermi liquid, it emerges as a result of large correlations (i.e. large Columb repulsion between two electrons in the same local moment orbital). This could be also noted in original Anderson model for single impurity[42].

Out of this Kondo phase, local moments and conduction sea decouple. Local moments could have antiferromagnetic order (mediated by direct RKKY interactions[43]) and conduction electrons form a small fermi surface. The antiferromagnetic ordering temperature can be driven continuously to zero with pressure, chemical doping or magnetic field[44]. Interestingly behavior above this quantum critical point between magnetic and non-magnetic metallic phases is dramatically different from fermi liquid behaviors [45, 3](see figure 1-4) . Although

scenarios for transition between a heavy fermion phase with large fermi surface and a phase with small fermi surface and local moments in a spin liquid state have been presented[46], the mechanism through which antiferromagnetism transforms into Kondo phase is not understood yet.

Superconductivity also develops in some heavy fermion compounds at low temperatures. UPt_3[47] is one example. By doping UPt_3 with Pd superconductivity disappears quickly and antiferromagnetic order appears through a second order phase transition (within the accuracy of the experiments). This presents a transition contradicting Landau paradigm i.e. direct transition between two phases with different symmetries.

Material	Properties	Resistivity	γ_n $(mJmol^{-1}K^{-2})$
$CeCu_6$	HF Metal	T^2	1600
$CeCu_2Si_2$	HF SC	T^2	800-1250
$CeCoIn_5$	Quasi 2D HF SC	T	750
$CeCu_{6-x}Au_x$	Chemically tuned QCP	T	$\frac{1}{T_0}ln\left(\frac{T_0}{T}\right)$
$YbRh_2Si_2$	Field tuned QCP	T	$\frac{1}{T_0}ln\left(\frac{T_0}{T}\right)$
UPd_2Al_3	AFM+ HF SC	T^2	210

Table 1.1: Heavy fermion compounds and their proporties (HF: Heavy fermion Metal, SC: Superconductivity, AFM: Antiferromagnetic Order, QCP: Quantum Critical Point[4]

In this thesis our main focus is on the heavy fermion metallic phase (chapters 2 and 3). We use tools available in fermi liquid theory to quantify the anisotropic effects of strong correlations which form this phase.

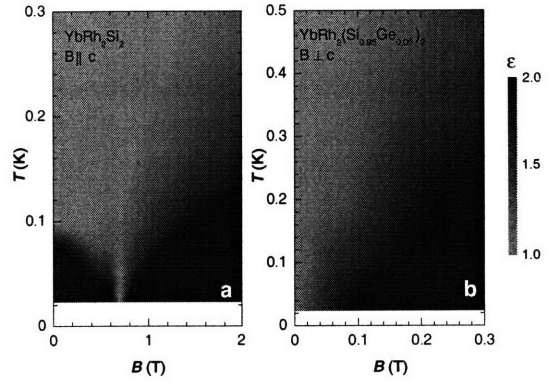

Figure 1-4: Colored plot of resistivity $(dln(\rho)/dln(T))$ close to heavy fermion critical point from[3]

1.2.1 Slave particle mean field theory

As mentioned before, Kondo lattice model describes a lattice of spin-1/2 local moments $\vec{S}_i$ and conduction electrons $c_{i\alpha}$ $(\alpha = \uparrow, \downarrow)$ coupled through Kondo exchange[39].

$$H = -t \sum_{\langle ij \rangle} c_i^\dagger c_j + \frac{J_K}{2} \sum_i \vec{S}_i . c_i^\dagger \vec{\sigma} c_i \tag{1.2}$$

The total number of conduction electrons per site is taken to be some fixed value n_c. A useful mean field treatment is obtained using a fermionic representation of the local moment spin:

$$\vec{S}_i = f_i^\dagger \frac{\vec{\sigma}}{2} f_i \tag{1.3}$$

together with the constraint $f_i^\dagger f_i = 1$ at each site. After some algebra the interaction term (J_K) reduces to:

$$\sum_i f_i^\dagger c_i c_i^\dagger f_i + constant$$

In the corresponding imaginary time path integral for the partition function, this takes the form

$$e^{\int d\tau \sum_i \bar{f}_i c_i \bar{c}_i f_i} \tag{1.4}$$

Using a Hubbard-Stratonovich transformation, this can be decoupled as

$$\int [DV] \ \exp\left(\sum_i \frac{|V(i,\tau)|^2}{4J_k} + (V(i,\tau)\bar{f}_i c_i + V^*(i,\tau)\bar{c}_i f_i)\right) \tag{1.5}$$

Exact integration over $V(i,\tau)$ will produce the original interaction term. But in mean-field approximation, we do the integral using saddle-point method. In addition the constraint $f_i^\dagger f_i = 1$ will be implemented on average. We will choose the mean-field solution with $V(i,\tau) = V$ which leads to the following mean-field Hamiltonian and self consistency equation for V:

$$\begin{aligned} H &= -t\sum_{\langle ij\rangle} c_i^\dagger c_j + h.c \\ &\quad + \sum_i \mu_f f_i^\dagger f_i + V\sum_i (f_i^\dagger c_i + c_i^\dagger f_i) \qquad (1.6) \\ V &= \frac{J_k}{2N}\sum_i \langle f_i^\dagger c_i + h.c.\rangle \qquad (1.7) \\ \langle f_i^\dagger f_i\rangle &= 1 \qquad (1.8) \end{aligned}$$

We have introduced a chemical potential term for the f-fermions which serves to set their average number per site to be one. In addition the fermi energy E_F of the hybridized quasiparticle must be determined by requiring that there are a total of $1 + n_c$ fermions per site. Only states with energy less than E_F are filled in the ground state.

This mean-field Hamiltonian is quadratic and can be diagonalized. To do so, first we write the Hamiltonian in the Fourier space:

$$H = \sum_k \epsilon_{\mathbf{k}} c^\dagger_{\mathbf{k}} c_{\mathbf{k}} + \sum_{\mathbf{k}} \mu_f f^\dagger_{\mathbf{k}} f_{\mathbf{k}} + V \sum_{\mathbf{k}} (f^\dagger_{\mathbf{k}} c_{\mathbf{k}} + c^\dagger_{\mathbf{k}} f_{\mathbf{k}}) \tag{1.9}$$

with $\epsilon_{\mathbf{k}} = -2t\ (\cos(k_x) + \cos(k_y) + \cos(k_z))$. Now it is easy to derive quasi-particle dispersion relation for two bands (fig. 1-5(b)):

$$E^{\pm}_{\mathbf{k}} = \frac{\epsilon_{\mathbf{k}} + \mu_f}{2} \pm \sqrt{(\frac{\epsilon_{\mathbf{k}} - \mu_f}{2})^2 + V^2} \tag{1.10}$$

With this in hand, we can solve the self consistency conditions and calculate physical properties. We first solve the self consistency equation for V:

$$\begin{aligned} V &= \frac{J_k}{2N} \frac{\partial E_g}{\partial V} && (1.11)\\ &= J_k \int_{FS} \frac{d^d k}{(2\pi)^d} \frac{V}{\sqrt{\left(\frac{\epsilon_k - \mu}{2}\right)^2 + V^2}} && (1.12)\\ &= -J_k V \rho(\mu) \log(V/t) && (1.13)\\ &\Rightarrow V \propto e^{-1/J_k \rho(\mu)} && (1.14) \end{aligned}$$

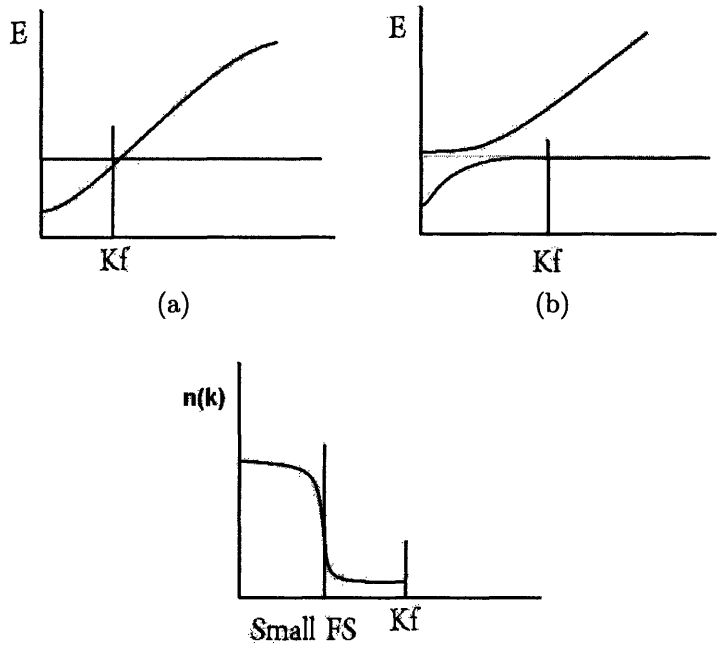

Figure 1-5: a- Mean-field dispersion before Kondo singlets condense b- Mean-field dispersion in Kondo phase c- Electron occupation number

So the hybridization amplitude is exponentially small in $1/J_K\rho(\mu)$. We can also calculate the density of states:

$$\begin{aligned}
\rho(E) &= \int \frac{d^dk}{(2\pi)^d}\delta\left(\frac{\epsilon_k+\mu}{2} - \sqrt{\left(\frac{\epsilon_k-\mu}{2}\right)+V^2}\right) \\
&= \int d\epsilon\rho_c(\epsilon)\delta\left(\frac{\epsilon+\mu}{2} - \sqrt{\left(\frac{\epsilon-\mu}{2}\right)^2+V^2} - E\right) \\
&\approx \int \rho_c(\epsilon)d\epsilon\delta\left(\epsilon - \frac{2V^2}{|\epsilon-\mu|} - E\right) \\
&\approx \rho_c(E)\frac{(E-\mu)^2}{V^2} \\
&\Rightarrow \rho(E) \propto e^{2/J_k\rho(\mu)}
\end{aligned} \tag{1.15}$$

Here we used the fact (as shown in appendix A) that $\epsilon_k < \mu$. $\rho_c(\epsilon)$ is conduction electrons density of states. Here we got a density of states which is exponentially large in $1/J_k$. This gives the large effective mass and hence the name of heavy fermions.

In figure 1.2.1 we present the important features of heavy fermions captured by slave particle mean-field theory in a one dimensional system. In 1-5(a) we present the two bands (free electrons band and localized moments flat band) which are decoupled for $V = 0$. As we turn on V the two bands hybridize and give the dispersions in figure 1-5(b). Only the lower band will be partially filled. The fermi point is at nearly flat part of the band and signals the large effective mass. Another important feature to note here is that the volume of fermi surface is large, compared to fermi surface when $V = 0$ which only contains conduction

electrons, and accommodates both conduction and local electrons. In figure 1-5(c) we present electron occupation number as a function of k. As we pass the momentum corresponding to small fermi surface, there is a large but continues drop corresponding to the drop of electron quasiparticle residue Z. As we pass over large fermi surface, there is a small but discontinues jump which corresponds to the fermi surface and small quasiparticle residue at the fermi surface.

1.3 Overview of the thesis

In this thesis we try to take steps toward clarification of some of strange properties in phases of correlated electronic matter and their phase transitions. In heavy fermion compounds since the Kondo singlet is build of a local moment in say f orbital and a conduction electron, it naturally have non-trivial internal structure[48]. To be more specific, we consider a cerium based heavy fermion compound. Although we simplify the model, we see that correlation induced anisotropies could be seen particularly around the directions that Kondo singlet amplitude vanishes. We present some of observable effects of this model, particularly in ARPES experiments which might be done in near future[35]. Partially motivated by observations in cuprates (see 1.1) we also consider a two dimensional model for heavy fermions (section 1.2) where non-trivial internal structure of Kondo singlet could be studied and leads to dramatically anisotropic effect of interactions in momentum space[49]. We also note that such internal structure could lead to ex-

otic effects. We have quantized Hall effect in Kondo insulators, when internal structure breaks time reversal and in Kondo-Heisenberg model, four isolated points on the fermi surface with vanishing quasiparticle residue, in an otherwise fermi liquid phase!

In first two chapters we consider the fermi liquid metallic phases. As mentioned before although transition between this phase and a spin liquid with small fermi surface have been explored[46] a big challenge is the apparently second order phase transition between this metallic phase with large fermi surface and antiferromagnetic phase with small fermi surface. In chapter 4 we study a phase transition between insulating Neel ordered phase and a paramagnetic phase[50]. Since the scenario for heavy fermion phase transition discuss transition to a paramagnetic phase, along with these developments, our study might be enlightening for the full transition from heavy fermion phase to the antiferromagnetically ordered phase. The transition studied in chapter 4 is more directly relevant to the pseudogap phase in cuprates which should be connected to the Neel phase through a second order phase transition. Here it is important to mention that fundamental models for cuprates and heavy fermions are quite different. Nevertheless studies in each of the two could open paths to study the correlated systems in general. Concluding remarks and directions for future research are presented in the last chapter.

Chapter 2

Higher angular momentum Kondo liquids

As discussed in section 1.2, formation of Kondo singlet leads to many properties of heavy fermions in Kondo phase[41]. The singlet 'molecule' formed out of the local moment and conduction electron is usually taken to be in an s-wave state with zero internal angular momentum. In this chapter we explore metallic states where this singlet has non-zero internal angular momentum. We show that this results in fermi liquid states that have many unusual and interesting properties. For instance such states naturally have large anisotropies in the effective mass, quasiparticle residue and other properties on moving around the fermi surface. Under certain conditions it is even possible for the quasiparticle residue to vanish at isolated points of the fermi surface. The excitations at such points do not have electron quantum numbers but can be understood as a neutral fermionic spin-1/2 'spinon'. Remarkably such a spinon excitation emerges without any associated gauge interaction (unlike the

other many familiar examples[51, 52, 53]). In the special case where the conduction band is half-filled the usual s-wave Kondo singlet formation leads to an insulating state (dubbed the Kondo insulator). If the internal angular momentum is non-zero, interesting varieties of Kondo insulators become possible. For instance we show that in two dimensions with a $d_{x^2-y^2} + id_{xy}$ singlet, the Kondo insulator has a non-trivial quantized electrical Hall conductivity.

Theoretically higher angular momentum Kondo liquids are conveniently accessed through the slave boson mean field review theory[14, 13] in 1.2.1 developed to describe the usual heavy fermi liquid state. In that section we considered the case where the singlet is formed between local moment and conduction electron at the same site. This naturally leads to singlet with s-wave internal structure.

This immediately suggests that Kondo singlets of higher angular momentum can be described by hybridization amplitudes between f_r at site r and $c_{r'}$ at a different site r'. Specifically

$$b_{rr'} = \langle c_r^\dagger f_{r'} \rangle \tag{2.1}$$

may be viewed as the wave function of the Kondo singlet. Thus by choosing the internal angular momentum associated with rotations of the relative coordinate $\vec{r}\,' - \vec{r}$ appropriately Kondo liquids with higher angular momentum may be constructed. In this chapter we will exploit this strategy to construct mean field descriptions of various such Kondo liquid states. Within the mean field description, higher angular

momentum Kondo liquids correspond to a particular form of momentum dependence of the Kondo hybridization amplitude. Momentum dependent hybridization amplitudes have been previously considered in Ref. [54, 55]. Recent optical transport experiments on the 1-1-5 materials have also been interpreted in terms of momentum dependent hybridization amplitudes[56].

2.1 d-wave Kondo liquid

Previously we explained the Physics of Kondo phase by formation of singlets local moments and conduction electrons, which have zero internal angular momentum(i.e. $\langle f_i^\dagger c_i + h.c. \rangle$ is constant). When we assume that the singlet is formed between the local moments and conduction electron at the same site (i.e. singlet is local), the s-wave is the only possibility for internal state of the singlet. In this section we consider modifying the Kondo lattice Hamiltonian so that Kondo singlets with non-zero angular momentum are favored. To that end we consider a generalized Kondo Hamiltonian:

$$H = -\sum_{\langle ij \rangle} t c_i^\dagger c_j + \sum_{ij} J_{ij} \vec{S}_i . \vec{s}_j \tag{2.2}$$

where the Kondo exchange term is not limited to the local moments and conduction electrons at the same site. The simplest case is for J_{ij}

to be non-zero only when i and j denote the nearest neighbor sites:

$$J_{ij} = J_K \quad (i,j) \text{ nearest neighbor} \tag{2.3}$$

$$J_{ij} = 0 \quad \text{otherwise} \tag{2.4}$$

With this choice and after some algebra, similar to what we did in the last section, the Hamiltonian reduces to the following form:

$$H = -\sum_{\langle ij \rangle} t c_i^\dagger c_j + \sum_{\langle ij \rangle} J_{ij}\ f_i^\dagger c_j c_j^\dagger f_i \tag{2.5}$$

Now proceed as before by decoupling the interacting part of the action using an auxiliary field, which this time lives on the bonds of the lattice, instead of the sites:

$$\int [DV] \quad e^{-\left(\int d\tau \sum_{\langle i,j \rangle} \frac{|V(i,j,\tau)|^2}{4J_k} + (V(i,j,\tau)\bar{f}_i c_j + V^*(i,j,\tau)\bar{c}_j f_i)\right)} \tag{2.6}$$

As before, to get the mean-field Hamiltonian, we'll do the integration over V using saddle point approximation (in addition to imposing $\langle f_i^\dagger f_i \rangle = 1$ on average). There are different saddle point solutions (they are basically different local minima in functional space). We will consider two solutions named as s-wave and d-wave (the reason for choosing these names will become clear later). In s-wave solution we consider $V(i,j,\tau) = V$ on all bonds and in d-wave, we consider $V(i,j,\tau) = V$

on x bonds and $V(i,j,\tau) = -V$ on y bonds:

$$H\begin{pmatrix} s \\ d \end{pmatrix} = \sum_{-\langle ij \rangle} t c_i^\dagger c_j + \sum_i \mu_f f_i^\dagger f_i + \sum_{i,x,y} V[(f_i^\dagger c_{i+x} + c_{i+x}^\dagger f_i) \pm (f_i^\dagger c_{i+y} + c_{i+y}^\dagger f_i)] \tag{2.7}$$

It is obvious from this form that these correspond to s-wave and d-wave internal state for the singlet. In momentum space s-wave and d-wave Hamiltonian have the following forms:

$$H_s(\mathbf{k}) = \sum_{\mathbf{k}} \epsilon_{\mathbf{k}} c_{\mathbf{k}}^\dagger c_{\mathbf{k}} + \sum_{\mathbf{k}} \mu_f f_{\mathbf{k}}^\dagger f_{\mathbf{k}} + V \sum_{\mathbf{k}} (\cos(k_x) + \cos(k_y))(f_{\mathbf{k}}^\dagger c_{\mathbf{k}} + c_{\mathbf{k}}^\dagger f_{\mathbf{k}}) \tag{2.8}$$

$$H_d(k) = \sum_{k} \epsilon_{\mathbf{k}} c_{\mathbf{k}}^\dagger c_{\mathbf{k}} + \sum_{\mathbf{k}} \mu_f f_{\mathbf{k}}^\dagger f_{\mathbf{k}} + V \sum_{\mathbf{k}} (\cos(k_x) - \cos(k_y))(f_{\mathbf{k}}^\dagger c_{\mathbf{k}} + c_{\mathbf{k}}^\dagger f_{\mathbf{k}}) \tag{2.9}$$

With this quadratic mean-field Hamiltonian, we can also derive the spectrum and the mean-field parameter V self-consistently:

$$E_\pm^s(\mathbf{k}) = \frac{\epsilon_{\mathbf{k}} + \mu_f}{2} \pm \sqrt{(\frac{\epsilon_{\mathbf{k}} - \mu_f}{2})^2 + V^2(\cos(k_x) + \cos(k_y))^2} \tag{2.10}$$

$$E_\pm^d(\mathbf{k}) = \frac{\epsilon_{\mathbf{k}} + \mu_f}{2} \pm \sqrt{(\frac{\epsilon_{\mathbf{k}} - \mu_f}{2})^2 + V^2(\cos(k_x) - \cos(k_y))^2} \tag{2.11}$$

The ground state is obtained by filling all states upto the fermi level. As before the fermi energy is fixed by requiring that there are $1 + n_c$ fermions in the ground state per site. Note that in both s and d wave cases the + band lies entirely above the − band ($i.e\ min(E_+) \geq max(E_-)$). Therefore in the ground state only the E_- levels are occupied. The ground state energy is

$$E_{gd}^{s,d} = \sum_k \theta(E_F - E_-^{s,d}(\mathbf{k}))E_-^{s,d}(\mathbf{k}) \tag{2.12}$$

The self-consistency equations that determine V and μ_f are now readily obtained. For instance we have

$$1 = \frac{J_k}{2N}\sum_{\mathbf{k}}\theta(E_F - E_-^{s,d}(\mathbf{k}))\times \frac{(\cos(k_x) \pm \cos(k_y))^2}{\sqrt{(\frac{\epsilon_{\mathbf{k}}-\mu_f}{2})^2 + V^2(\cos(k_x) \pm \cos(k_y))^2}} \tag{2.13}$$

In equation 4-4, +(−) corresponds to s-wave(d-wave). In addition we need to impose the condition $\langle f_i^\dagger f_i\rangle = 1$ and $\langle c_i^\dagger c_i\rangle = n_c$.

Let us first specialize to the half-filled case $n_c = 1$. In this case the microscopic model has a particle-hole symmetry under which

$$c_{i\alpha} \rightarrow -i\epsilon_r \sigma^y_{\alpha\beta} c^\dagger_{i\beta} \tag{2.14}$$

where $\epsilon_r = (-1)^{(x+y)} = \pm 1$ on the A and B sublattices of the two dimensional square lattice. As the total number of fermions per site $1 + n_c = 2$ in this case, all the E_- levels are filled. At the level of the

approximate mean field Hamiltonians Eqn. 2.7, under the particle-hole transformation

$$f_{i\alpha} \rightarrow -i\epsilon_r \sigma^y_{\alpha\beta} f^\dagger_{i\beta} \tag{2.15}$$

$$\mu_f \rightarrow -\mu_f \tag{2.16}$$

$$V \rightarrow V \tag{2.17}$$

Thus a particle-hole symmetric mean field state (which we assume) requires $\mu_f = 0$.

With this in hand we proceed to compare the ground state energy of the s-wave and d-wave mean field Hamiltonians in half-filled case. First consider self-consistency equation for s-wave case:

$$\frac{1}{J_k} = \frac{1}{2N} \sum_{\mathbf{k}} \frac{(\cos(k_x) + \cos(k_y))^2}{\sqrt{(\frac{\epsilon_\mathbf{k}}{2})^2 + V^2(\cos(k_x) + \cos(k_y))^2}} \tag{2.18}$$

It is obvious that the right hand side of equation 2.18 is monotonically decreasing function of $|V|$. So it has its maximum value for $V = 0$:

$$\frac{1}{J_k} = \frac{1}{2N\sqrt{2t}} \sum_{\mathbf{k}} |\cos(k_x) + \cos(k_y)| \tag{2.19}$$

The right hand-site of the above equation is finite. So there is a maximum value of $1/J_k$ for which we can find a solution for V in equation 2.18. On the other hand the self consistency equation for d-wave at $\mu_f = 0$ takes the form:

$$\frac{1}{J_k} = \frac{1}{2N} \sum_{\mathbf{k}} \frac{(\cos(k_x) - \cos(k_y))^2}{\sqrt{(\frac{\epsilon_\mathbf{k}}{2})^2 + V^2(\cos(k_x) - \cos(k_y))^2}} \tag{2.20}$$

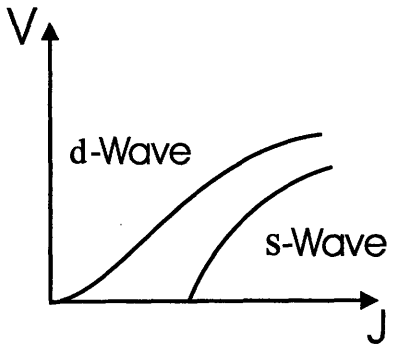

Figure 2-1: V versus J for s-wave and d-wave self consistency equation

Like s-wave, the right hand site of equation is maximum for $V = 0$. But in this case the right hand side of equation 2.20 is divergent as $V \to 0$. So for d-wave, the self-consistency solution exist for any value of J_k. A schematic graph of V versus J_k for s-wave and d-wave is plotted in figure 2-1.

As it is also clear from the figure, there is at least a region of small J_k for which V for d-wave is larger than V for s-wave (in fact we can have a region with finite V for d-wave but s-wave V as small as we want). Now if we look at the lower band spectrum (eqn. 2.10 and 2.11) this proves that there is at least a region for small J_k where d-wave ground state energy is lower than s-wave.

Upon moving away from half-filling, we expect that the value of ground state energy starts changing continuously; so we still have at least a region of small J_k and small doping, for which d-wave mean-field Hamiltonian is a better approximation than s-wave. We have confirmed this by a direct numerical solution of the self-consistency equations.

2.2 Properties of d-wave Kondo liquid

We now study the properties of the d-wave mean-field state away from half-filling. We will see that d-wave singlet formation provides a natural route toward very anisotropic properties over the fermi surface. Before getting into the details of these properties, we will examine some aspects of d-wave dispersion in equation 2.11. A schematic graph of fermi surface for finite doping in the first Brillouin zone, as well as dispersion along a specific path, are given in figures 2-2 and 2-3 respectively. One important feature of the spectrum in figure 2-3 (which is also easily proved analytically in appendix A) is that the maximum value of energy in the Brillouin zone is μ_f, that is the energy of the points along diagonal direction, where $\mu_f < \epsilon_{\mathbf{k}}$. This shows that fermi surface crosses the diagonal direction at a point where $E^d_{\mathbf{k}} < \mu_f$ (since E_f has to be less than μ_f). In diagonal direction the spectrum is $E^d_{\mathbf{k}} = \frac{\epsilon_{\mathbf{k}}+\mu_f}{2} - |\frac{\epsilon_{\mathbf{k}}-\mu_f}{2}|$ which can be written as:

$$\begin{cases} E^d_{\mathbf{k}} = \epsilon_{\mathbf{k}} & for \quad \epsilon_{\mathbf{k}} < \mu_f \\ E^d_{\mathbf{k}} = \mu_f & for \quad \epsilon_{\mathbf{k}} > \mu_f \end{cases}$$

combining this with the condition $E^d_{\mathbf{k}} < \mu_f$ shows that fermi surface should cross the diagonal direction at a point where the quasiparticles energy is equal to $\epsilon_{\mathbf{k}}$. This result is in fact the basic foundation for the interesting properties that will be studied in the next sections i.e. over the fermi surface, in diagonal direction, quasi-particles are c-electron type; the f-electron properties appear, as we go away from the diagonal

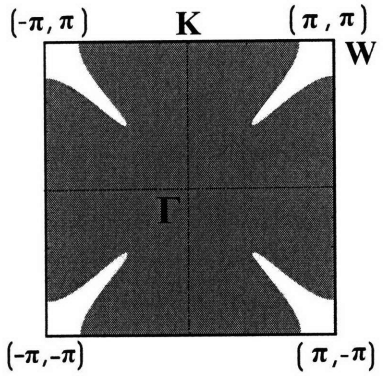

Figure 2-2: fermi surface in the first Brillouin zone. Occupied region is plotted in gray.

direction. In the following section we will present the result of numerical calculation of properties over fermi surface.

The self consistency equation for parameter V could also be studied analytically (appendix B). We see that for d-wave Kondo model, similar to the on site s-wave Kondo, we have $V \propto e^{-\frac{C}{J_k}}$. Density of states at fermi energy is also studied analytically (appendix C), it again shows exponential dependence on coupling constant:

$$\rho(E_f) \propto V^{-2} \propto e^{\frac{2C}{J_k}} \tag{2.21}$$

These results were also checked and confirmed numerically.

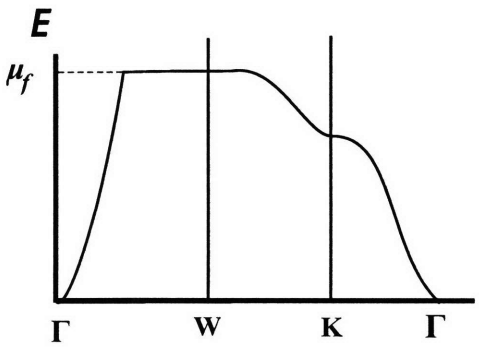

Figure 2-3: Spectrum along the lines $(0,0) \rightarrow (\pi,\pi) \rightarrow (0,\pi) \rightarrow (0,0)$

In the following sections we present the effective mass and quasi-particle residue on fermi surface, as a function of angle (from the center of Brillouin zone). We will see that these properties are very anisotropic as we move along the fermi surface.

2.2.1 Effective mass

The effective mass of quasi-particles is defined through second derivative of energy with respect to $k_\perp$ which is the momentum in direction perpendicular to fermi surface:

$$\frac{1}{m} = \frac{\partial^2 E^d_{\mathbf{k}}}{\partial^2 k_\perp} \tag{2.22}$$

A closed form for the effective mass could be derived. In figure 2-4 we have plotted the inverse effective mass over fermi surface near diagonal direction. As we expected, along diagonal direction the effective mass matches the electron effective mass. As we go far away from the diagonal direction, effective mass becomes very large. This is because away from the diagonal direction, the quasiparticle is essentially an f-fermion with some weak admixture with the c-electron. Between these two limits we see the strange anisotropic behavior where second derivative of energy goes from electron type, positive value to large negative value. A comparison with quasi-particle residue plot (figure 2-6) shows that this behavior occurs where the quasi-particles are a complete mixture of c-electron and f-fermion.

This weird behavior could be traced by looking closer at the spec-

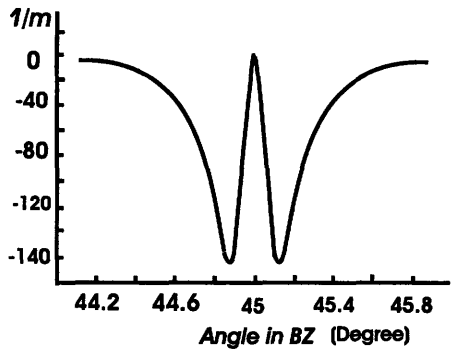

Figure 2-4: Second derivative of energy respect to $k_\perp$ in direction perpendicular to fermi surface.

trum in the Brillouin zone. First consider diagonal direction (figure 2-5). We see that moving along this line we go from region where $E_{\mathbf{k}}^- = \epsilon_{\mathbf{k}}$ to region where $E_{\mathbf{k}}^- = \mu_f$ (see figure 2-3). So if we plot first derivative of energy with respect to $k_\perp$ (which is diagonal direction for points along diagonal direction), as seen in figure 2-5, there is a jump from a finite value to zero at the point where $\epsilon_{\mathbf{k}} = \mu_f$. In this direction, as shown before, at the fermi surface $E_{\mathbf{k}}^- = \epsilon_{\mathbf{k}}$ so there is a finite value for second derivative. As we move away from diagonal direction, the jump softens slightly (because $V_{\mathbf{k}}$ moves slightly from zero). But still first derivative have a large decrease in a small interval and so the second derivative is large negative number; interestingly, fermi surface does cross this region at some points. This behavior is very strange. In fact we see points at which the effective mass is much smaller than free electron mass.

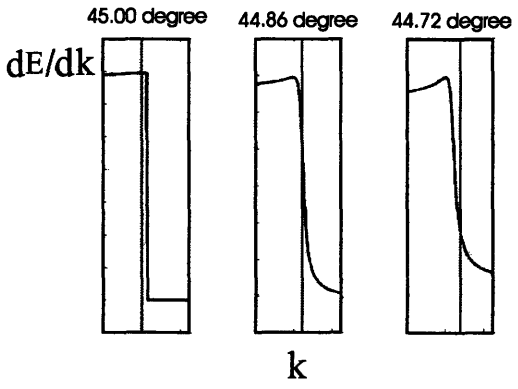

Figure 2-5: First derivative of the energy with respect to $k_\perp$. Vertical axis, in each plot, is $\frac{\partial E_k^-}{\partial k_\perp}$ and $k_\perp$ is the momentum in direction perpendicular to the fermi surface at the point defined by the angle on the top. Vertical line shows the position of the fermi surface

2.2.2 Quasi-particle residue

The electron-electron green function is given by[38]:

$$G(k, i\omega_\nu) = \int_0^\beta d\tau e^{i\omega_\nu \tau} \langle T_\tau c(k,\tau) c^\dagger(k,0) \rangle \tag{2.23}$$

Suppose $\gamma_{\mathbf{k}}^+$ and $\gamma_{\mathbf{k}}^-$ are annihilation operators for quasi-particles in upper and lower bands respectively, in terms of which the Hamiltonian is diagonal. The c-electron annihilation operators could be written as:

$$\begin{aligned} c_{\mathbf{k}} &= u_{\mathbf{k}}\, \gamma_{\mathbf{k}}^+ + v_{\mathbf{k}}\, \gamma_{\mathbf{k}}^- \\ v_{\mathbf{k}}^2 &= \frac{(E_{\mathbf{k}}^+ - \epsilon_{\mathbf{k}})^2}{(E_{\mathbf{k}}^+ - \epsilon_{\mathbf{k}})^2 + V_{\mathbf{k}}^2} \\ u_{\mathbf{k}}^2 &= \frac{V_{\mathbf{k}}^2}{(E_{\mathbf{k}}^+ - \epsilon_{\mathbf{k}})^2 + V_{\mathbf{k}}^2} \\ u_{\mathbf{k}} &= -\frac{V_{\mathbf{k}} v_{\mathbf{k}}}{E_{\mathbf{k}}^+ - \epsilon_{\mathbf{k}}} \end{aligned} \tag{2.24}$$

Using this form (and the fact that Hamiltonian is diagonal in terms

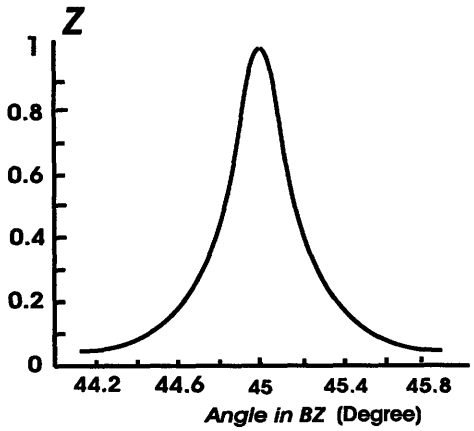

Figure 2-6: Quasi-particle residue on the fermi surface

of $\gamma_{\mathbf{k}}^{\pm}$ operators):

$$\langle c(\mathbf{k},\tau)c^{\dagger}(\mathbf{k},0)\rangle = u_{\mathbf{k}}^2\langle\gamma_{\mathbf{k}}^{+}(\tau)\gamma_{\mathbf{k}}^{+\dagger}(0)\rangle + v_{\mathbf{k}}^2\langle\gamma_{\mathbf{k}}^{-}(\tau)\gamma_{\mathbf{k}}^{-\dagger}(0)\rangle$$

Rewriting the Hamiltonian in term of γ operators ($H = \sum_{\mathbf{k}}(E_{\mathbf{k}}^{+}\gamma_{\mathbf{k}}^{+\dagger}\gamma_{\mathbf{k}}^{+} + E_{\mathbf{k}}^{-}\gamma_{\mathbf{k}}^{-\dagger}\gamma_{\mathbf{k}}^{-})$) we get:

$$\langle\gamma_{\mathbf{k}}^{\pm}(\tau)\gamma_{\mathbf{k}}^{\pm\dagger}(0)\rangle = e^{-E_{\mathbf{k}}^{\pm}\tau}$$

Putting these into equation 2.23 gives:

$$G(k,i\omega_\nu) = \frac{u_{\mathbf{k}}^2}{E_{\mathbf{k}}^{+} - i\omega_\nu} + \frac{v_{\mathbf{k}}^2}{E_{\mathbf{k}}^{-} - i\omega_\nu} \tag{2.25}$$

By analytically continuing this to real frequencies and taking the imaginary part we get the spectral function[38]:

$$A(k,\omega) = u_{\mathbf{k}}^2\delta(\omega - E_{\mathbf{k}}^{+}) + v_{\mathbf{k}}^2\delta(\omega - E_{\mathbf{k}}^{-}) \tag{2.26}$$

This consists of two peaks and the weight under the low energy peak will give us the quasiparticle residue (Z). We have plotted Z for

the points near diagonal direction in figure 2-6. Again as we expect, the quasiparticle residue near diagonal direction is of order one (electron type excitations) and gets very small away from diagonal direction.

2.3 d-wave Kondo liquid in a Kondo-Heisenberg model: fermi liquid with spinons

We now study the properties of the d-wave Kondo liquid state in a model which allows for explicit Heisenberg exchange interactions between the local moments. Remarkably we will show that the quasiparticle residue vanishes at isolated points of the fermi surface in such a state. The excitation at such points is a free neutral fermionic spinon. In a subsequent Section, we show that this spinon survives even when fluctuations beyond the mean field are included. Thus this d-wave Kondo liquid is a fermi liquid state that supports spinons at isolated fermi points. Specifically we consider the model

$$H = \sum_{\langle ij \rangle} t_{ij} c_i^\dagger c_j + J_K \sum_{\langle ij \rangle} \vec{S}_i . \vec{s}_j + J_H \sum_{\langle ij \rangle} \vec{S}_i . \vec{S}_j \qquad (2.27)$$

We proceed as before using the d-wave mean-field approximation to treat $\vec{S}_i . \vec{s}_j$ term; but here, we have another interacting term, which is the direct Heisenberg exchange between the local moments. Expressing this in terms of the f-fermions gives rise to a four fermion term. We treat this in mean field theory as well. While a number of different mean field decouplings are possible, we focus here on one in the particle-hole

channel which endows the f-fermions with a uniform non-zero hopping χ. This is in turn determined self-consistently through the equation

$$\chi = J_H \langle f_i^\dagger f_j \rangle \tag{2.28}$$

Using this, we get the following mean-field Hamiltonian:

$$\begin{aligned} H_H(k) = &\sum_k \epsilon_{\mathbf{k}} c_{\mathbf{k}}^\dagger c_{\mathbf{k}} + \sum_{\mathbf{k}} \epsilon_{f\mathbf{k}} f_{\mathbf{k}}^\dagger f_{\mathbf{k}} \\ &+ V \sum_{\mathbf{k}} (\cos(k_x) - \cos(k_y))(f_{\mathbf{k}}^\dagger c_{\mathbf{k}} + c_{\mathbf{k}}^\dagger f_{\mathbf{k}}) \end{aligned} \tag{2.29}$$

where $\epsilon_{f\mathbf{k}} = \mu_f - \chi\ (\cos(k_x) + \cos(k_y))$. With this quadratic Hamiltonian, we can again get the spectrum:

$$\begin{aligned} E_\pm^H(\mathbf{k}) = &\frac{\epsilon_{\mathbf{k}} + \epsilon_{f\mathbf{k}}}{2} \pm \\ &\sqrt{(\frac{\epsilon_{\mathbf{k}} - \epsilon_{f\mathbf{k}}}{2})^2 + V^2(\cos(k_x) - \cos(k_y))^2} \end{aligned} \tag{2.30}$$

Now let us have a closer look at this Hamiltonian and spectrum. When $V = 0$, local moments and conduction electrons are not hybridized and we have two separated fermi surfaces. The electron fermi surface is identified by spectrum $\epsilon_{\mathbf{k}}$ and is small. Spinon fermi surface, contains one moment per site and covers half the Brillouin zone[46].

Now assume turning on non-zero V. If V is small enough, both bands intersect the fermi energy. The resulting fermi surface then consists of two sheets (each identified with one of the bands). Consider the quasiparticle residue on each band. From Eqn. 2.26, it is clear that on the

fermi surface of the E_-^H band, quasi-particle residue is given by $v_{\mathbf{k}}^2$ while on the other sheet (associated with E_+^H) it is given by $u_{\mathbf{k}}^2$. $v_{\mathbf{k}}$ and $u_{\mathbf{k}}$ are defined in Eqn. 2.24 and satisfy

$$\begin{aligned} u_{\mathbf{k}} &= -\frac{V(\cos(k_x)-\cos(k_y))}{E_+^H(\mathbf{k})-\epsilon_{\mathbf{k}}}\, v_{\mathbf{k}} \\ u_{\mathbf{k}}^2 &+ v_{\mathbf{k}}^2 = 1 \end{aligned} \tag{2.31}$$

Using this we see that the fermi surface of the $-$ band has large quasiparticle residue and thus has essentially c-electron character (with weak admixture to f-fermions). On the other hand the $+$ fermi surface has small quasiparticle residue and has essentially f-fermion character with weak admixture to c-electrons. Following reference [[46]] we name the $-$ and $+$ fermi surfaces as cold and hot surface respectively. Remarkably the quasiparticle residue on the hot fermi surface vanishes at four isolated points (which are along the diagonal directions). At these four points the excitation is a pure f-fermion with *no* admixture to the c-electron. Thus at these isolated points the excitation is a neutral fermionic spinon even though spinons do not exist elsewhere on the fermi surface.

2.4 Quantum Hall Kondo insulators

In this Section we describe an interesting Kondo insulating state that is possible if the Kondo singlet has nontrivial internal angular momentum. Consider the generalized Kondo Hamiltonian again (2.2) and assume

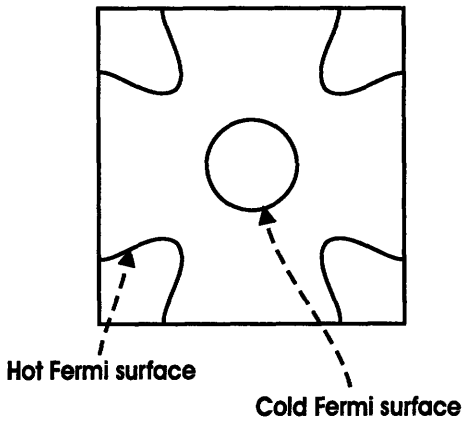

Figure 2-7: fermi surface of the d-wave Kondo liquid in the Kondo-Heisenberg model

J_{ij} is non-zero for nearest (J_1) and next nearest neighbors (J_2). Now, as before, we decouple the interacting term using an auxiliary field and consider the saddle point solution with nearest neighbor $V(\tau, i, j)$ the same as d-wave, and next nearest neighbor equal to iV_2 along one diagonal direction and $-iV_2$ along the other. Clearly this coresponds to a Kondo singlet with internal angular momentum $d_{x^2-y^2} + id_{xy}$, and describes a mean field state that spontaneously breaks time reversal symmetry. This leads to the following mean-field Hamiltonian:

$$\begin{aligned} H_{d+id}(\mathbf{k}) = &\sum_{\mathbf{k}} \epsilon_{\mathbf{k}} c^\dagger_{\mathbf{k}} c_{\mathbf{k}} + \sum_{\mathbf{k}} \mu_f f^\dagger_{\mathbf{k}} f_{\mathbf{k}} \\ &+ V_1 \sum_{\mathbf{k}} (\cos(k_x) - \cos(k_y))(f^\dagger_{\mathbf{k}} c_{\mathbf{k}} + c^\dagger_{\mathbf{k}} f_{\mathbf{k}}) \\ &+ V_2 \sum_{\mathbf{k}} i \sin(k_x) \sin(k_y)(c^\dagger_{\mathbf{k}} f_{\mathbf{k}} - f^\dagger_{\mathbf{k}} c_{\mathbf{k}}) \end{aligned} \tag{2.32}$$

We now specialize to a half-filled conduction band $n_c = 1$. Diagonalizing this Hamiltonian, we readily see that the ground state in this case is a Kondo insulator with a gap. However we now show that the broken time reversal symmetry leads to a non-vanishing quantized electrical

Hall conductivity. Thus this state provides an interesting example of a quantum Hall effect in a local moment system driven by the Kondo effect. To expose this physics it is convenient to rewrite the Hamiltonian in terms of a two-component fermion operator $\psi_{\mathbf{k}}$:

$$\psi_{\mathbf{k}} = \begin{pmatrix} c_{\mathbf{k}} \\ f_{\mathbf{k}} \end{pmatrix}$$

We have

$$H = \sum_{\mathbf{k}} \psi^{\dagger}_{\mathbf{k}} \left(\frac{\epsilon_{\mathbf{k}} + \mu_f}{2} + \vec{m}(\mathbf{k}).\vec{\tau} \right) \psi_{\mathbf{k}} \tag{2.33}$$

Here $\vec{\tau}$ are Pauli matrices operating on the two components of $\psi_{\mathbf{k}}$ and $\vec{m}_{\mathbf{k}}$ is a 3-dimensional vector defined in the two dimensional Brillouin zone:

$$\begin{aligned} \vec{m}_{\mathbf{k}} = \; & V_1(\cos(k_x) - \cos(k_y))\hat{x} \\ & + V_2 \sin(k_x) \sin(k_y)\hat{y} \\ & + \frac{\epsilon_{\mathbf{k}} - \mu_f}{2} \hat{z} \end{aligned} \tag{2.34}$$

Note that if $|\vec{m}| \neq 0$ over the Brillouin zone, $\vec{m}/|\vec{m}|$ is topologically a mapping from a torus (Brillouin zone) to the unite sphere. To calculate the Hall conductivity, we need the current operator. Note that in this mean field Hamiltonian, charge conservation symmetry is realized as invariance under $\psi_{\mathbf{k}} \rightarrow e^{i\alpha}\psi_{\mathbf{k}}$. Thus though the f-fermions start off as neutral, the mean field condensation of V has endowed them with

physical charge. This observation then leads to the current operator:

$$J_\mu(\mathbf{k}) = \frac{\partial}{k_\mu} H \tag{2.35}$$

We can now calculate σ_{xy} using the Kubo formula[57]. The details of the calculation are in Appendix D. We get

$$\sigma_{xy} = \frac{e^2}{4\pi h} \int d^2k \frac{\vec{m}.(\partial_x \vec{m} \times \partial_y \vec{m})}{|\vec{m}|^3} \tag{2.36}$$

The value of σ_{xy} is then invariant under smooth change of $\vec{m}$. It is thus a topological invariant of the kind considered previously by Volovik[58]. We can now change $\vec{m}$ smoothly to a mapping for which integration 2.36 could be calculated easily and gives twice the surface area of a unit sphere so that

$$\sigma_{xy} = \frac{2e^2}{h} \tag{2.37}$$

This is also confirmed with direct numerical integration. The essential physics is also simply illustrated by the following argument. As the relevant integral is a topological invariant we first imagine a smooth deformation to make V_2 infinitesimally small. In the limit when $V_2 = 0$ the gap closes and $|\vec{m}(\mathbf{k})|$ has four zeroes in the Brillouin zone on the diagonal directions where $\epsilon_\mathbf{k} = \mu_f$. At low energies, the physics will be dominated by modes near these nodes. On turning on a small value of V_2, we expect that the universal physics is still correctly captured, in an approximation that is legitimate for modes near the nodes. So we expand $\vec{m}(\mathbf{k})$ near these nodes and take the integral over k_x and k_y

from $-\infty$ to ∞. After the expansion, we get (for the node at (k_p, k_p) in the first quadrant of the Brilloun zone):

$$\begin{aligned} \vec{m}_q = \; & V_1 \sin(k_p) \frac{q_x - q_y}{2} \hat{x} \\ & + V_2 \sin^2(k_p) \hat{y} \\ & + t \sin(k_p) \frac{q_x + q_y}{2} \; \hat{z} \end{aligned} \tag{2.38}$$

Here $q_i = k_i - k_p$ and $\cos(k_p) = \frac{\mu_f}{4t}$. After renaming $q_x - q_y$ as k_x, $q_x + q_y$ as k_y, $V_1 \sin(k_p)$ as v_x, $t \sin k_p/2$ as v_y and $V_2 \sin(k_p)^2$ as Δ, along with 90° rotation of $\vec{m}$ around x axis, we get the following simple form:

$$\vec{m}(\mathbf{k}) = v_x k_x \hat{x} + v_y k_y \hat{y} + \Delta \hat{z} \tag{2.39}$$

From this we trivially see that $\hat{m}(\mathbf{k}) = \frac{\vec{m}(\mathbf{k})}{|\vec{m}(\mathbf{k})|}$ points along $\hat{z}$ at $k_x = k_y = 0$ and points along radial direction in k_x, k_y plane as $\sqrt{k_x^2 + k_y^2} \to \infty$. So this vector covers half the sphere and contributes 2π to the integral in Eqn. 2.36. Exactly the same contribution arises from the other nodes and so we get $4 \times 2\pi = 8\pi$. Putting this in 2.36 gives the result quoted above for the electrical Hall conductivity.

Thus the $d_{x^2-y^2} + id_{xy}$ Kondo insulator has a quantized electrical Hall conductivity. A similar result - a spin and thermal quantum Hall effect - was established for two dimensional $d_{x^2-y^2} + id_{xy}$ *superconductors* in Ref. [59].

Chapter 3

Anisotropic quasiparticle weight in Cerium based Heavy fermions

The main purpose of this chapter is to discuss the variation in the quasiparticle weight Z on moving around the fermi surface, in a more realistic model relevant to heavy fermion alloys. Indeed Z is a convenient measure of the extent to which fermi liquid theory works in a fermi liquid. The theoretical approach we use is the standard hybridization mean field theory for Kondo lattice models of the rare earth alloy. The variation of Z may be linked to the internal orbital structure of the Kondo singlet that forms between the local moments and the conduction electrons. This internal orbital structure derives from the symmetries of the atomic orbital occupied by the local moment and the conduction electron band it is coupled to. In the hybridization mean field theory this leads to angle dependence of the hybridization on going around the fermi surface. The most dramatic variation occurs when the hybridization vanishes along some directions. Along such hybridization nodes

$Z \sim o(1)$ but can become very close to zero along other directions. We demonstrate the possibility of such hybridization nodes in a simplified model appropriate for a Ce-based cubic system. Recent angle resolved photoemission experiments[35, 34] have begun to probe the structure of the electronic excitations of the heavy fermi liquid. We expect that the physics described here may be probed in the near future.

Very recently experiments on $CeCoIn_5$ have reported a striking anisotropic violation of the Wiedemann-Franz law at the critical point[60]. Ref. [60] suggested that this might be caused by Z vanishing on some extended portions of the fermi surface but not on others. The state we study in this chapter is a fermi liquid state and hence does not violate the Wiedemann-Franz law. Nevertheless the strongly angle dependent Z that we find might provide some hints on the fundamental question of whether Z can at all vanish on some but not all portions of the fermi surface.

Inspired by these calculations appropriate to heavy electron systems, we consider the possibility that the pseudogap regime of the underdoped cuprates may actually have a large band-structure fermi surface but with strongly angle dependent Z. Several experimental results on the underdoped cuprates are examined in this light. Such a pseudogap state has some attractive phenomenological features - in particular it provides one possible reconciliation between recent high field quantum oscillation experiments[61, 62, 63] and older ARPES reports of gapless 'fermi arcs'. However such a large fermi surface fermi liquid state also has a number

of problems with other experiments making it unappealing as a serious theory of the underdoped cuprates. A *non-fermi liquid* version of such a large fermi surface state might perhaps resolve these difficulties but theoretical description of such a state remains out of reach.

3.1 Kondo singlets with internal orbital structure

As we saw before, the heavy fermion materials are conveniently modeled as Kondo lattices, *i.e.* a periodic lattice of local moments coupled by magnetic exchange to a separate band of conduction electrons[40]. At low temperatures the local moments are absorbed into the fermi sea of the metal through Kondo singlet formation. In a typical heavy electron metal the local moments occupy atomic f-orbitals. The conduction electrons derive from bands with different symmetry (s, p or d). The Kondo singlet that forms between a local moment and a conduction electron will therefore have nontrivial internal orbital structure. In the low temperature heavy fermi liquid phase this orbital structure leads to pronounced anisotropies between various parts of the fermi surface. A close analogy is with the physics of unconventional superconductors where Cooper pairs with non-trivial internal orbital structure condense leading to anisotropic superconductivity. In the heavy fermi liquid case such anisotropic effective masses are known to occur and have been discussed theoretically using a renormalized band theory approach[64].

In the present chapter we will mainly focus on the quasiparticle spectral weight Z which is a measure of the extent to which fermi liquid

theory works. To illustrate our point we focus specifically on Ce based heavy electron materials with the Ce ion in a f^1 state[65]. We also assume cubic symmetry. Such a Ce ion has, after considering the effect of spin-orbit coupling and crystal field splitting, a low energy Kramers doublet that couples to a separate conduction band. Again we treat the corresponding Kondo lattice model within the slave boson mean field approach (review in 1.2.1) [14, 13]. We show that Kondo singlet amplitude has strong momentum dependence coming from the symmetry of the f-orbital. Thus the true quasiparticles at the fermi surface are angle dependent admixtures of the f-fermions and the conduction electrons. Most remarkably we show that our simplified model naturally has directions where the hybridization vanishes. These hybridization nodes have a number of consequences. Most importantly it leads to a fermi surface structure where along the hybridization nodes the true (large) fermi surface is contained within the original small fermi surface of the conduction electrons. Thus along these directions the true quasiparticle mostly has c-character with weak admixture to f. Along other directions the situation is reversed. Now the physical electron spectral weight depends on the extent to which the conduction electron contributes to the quasiparticle state of the true large fermi surface. This then leads to the dramatic variation of the quasiparticle weight discussed before.

3.2 Anderson Model for a Cerium ion

We begin by briefly reviewing the Anderson model describing a Cerium f^1 impurity in a metallic host. The f states have orbital angular momentum $l = 3$ so that on including the spin there are $2\ (2 \times 3 + 1) = 14$ quantum states in this orbital. Spin-orbit coupling breaks the degeneracy of this orbital into two sets of states with $J = 7/2$ and $J = 5/2$ where J is the total angular momentum ($J = s + l$). The $J = 5/2$ states have lower energy and so we will concentrate on them. In a cubic environment crystal fields will further split the $J = 5/2$ states into a doublet (lower energy) and a quadruplet (higher energy) states. We will concentrate on the lower energy Kramer's doublet, described by $|M\rangle = |\pm\rangle$, where [65]:

$$\begin{aligned} |+> = & \left(\frac{1}{6}\right)^{1/2} |J_z = -\frac{5}{2}\rangle - \left(\frac{5}{6}\right)^{1/2} |J_z = \frac{3}{2}\rangle, \\ |-> = & \left(\frac{1}{6}\right)^{1/2} |J_z = \frac{5}{2}\rangle - \left(\frac{5}{6}\right)^{1/2} |J_z = -\frac{3}{2}\rangle. \end{aligned} \tag{3.1}$$

Now consider coupling this doublet to a band of conduction electrons $c_{\mathbf{k}\sigma}$. We assume that the f-electron in a state M can hybridize with the appropriate partial wave of the c-electron also in the partial-wave state M. The coupling may therefore be modeled by the Anderson impurity

Hamiltonian[42]:

$$H = \sum_{k,M} \varepsilon_{\mathbf{k}} c^{\dagger}_{\mathbf{k}} c_{\mathbf{k}} + \mu_f \sum_{M} f^{\dagger}_{M} f_{M} + U \sum_{M,M'} n_{M} n_{M'} + \sum_{k,M} V_k c^{\dagger}_{kM} f_{M} + V^{*}_{k} f^{\dagger}_{M} c_{kM}, \tag{3.2}$$

with the electron partial wave operator $c_{k,M}$, corresponding to representation in total angular momentum and magnitude k bases. The transformation between this bases and usual spin σ and vector momentum $\mathbf{k}$ bases is given through:

$$c^{\dagger}_{k,M} = \sum_{\sigma} \int \frac{d\Omega_{\hat{\mathbf{k}}}}{4\pi} c^{\dagger}_{\mathbf{k},\sigma} \langle \mathbf{k}, \sigma | k, M \rangle, \tag{3.3}$$

where the integral is taken over all directions of the vector $\hat{k}$. For simplicity we assume further that $V_k = V$ independent of $\mathbf{k}$.

Focussing now on the strong correlation limit of large U we restrict the f-occupation to be one, imposing the constraint

$$\sum_{M} f^{\dagger}_{M} f_{M} = 1. \tag{3.4}$$

The standard Schrieffer-Wolf transformation[66, 67] then gives the "Kondo" effective Hamiltonian with an interaction

$$H_I = -J \sum_{k,k',M,M'} f^{\dagger}_{M} c_{k,M} c^{\dagger}_{k',M'} f_{M'} \tag{3.5}$$

with $J = V^2 U / [\mu_f (\mu_f + U)]$. This is a Kondo type[39] interaction and describes the coupling of the fluctuating M state at the Ce site to the

conduction band. Alternately we may write

$$H_I = -J \sum_{\mathbf{k},\mathbf{k}',\sigma,\sigma',M,M'} < \mathbf{k}'\sigma'|k'M' >< kM|\mathbf{k}\sigma > \times f^\dagger_M c_{\mathbf{k}\sigma} c^\dagger_{\mathbf{k}',\sigma'} f_{M'}, \tag{3.6}$$

3.3 Kondo lattice model

We now generalize the description of a single Ce impurity ion of the previous section to a lattice of Ce ions. We first introduce operators $f_{M,\mathbf{R}}$ for the local moments at site $\mathbf{R}$ of the lattice. The generalization of the Kondo interaction H_I is clearly

$$H_K = -J \sum_{\mathbf{R}} \sum_{\mathbf{k},\sigma,\mathbf{k}',\sigma',M,M'} \langle \mathbf{k}', \sigma'|k', M', \mathbf{R}\rangle\langle k, M, \mathbf{R}|\mathbf{k}, \sigma\rangle \times f^\dagger_{\mathbf{R},M} c_{\mathbf{k},\sigma} c^\dagger_{\mathbf{k}',\sigma'} f_{\mathbf{R},M'}, \tag{3.7}$$

where $|k, M, \mathbf{R}\rangle$ is a c-electron partial wave centered at site $\mathbf{R}$. We have

$$|k, M, \mathbf{R}\rangle = e^{i\hat{\mathbf{P}}\cdot\mathbf{R}}|k, M\rangle, \tag{3.8}$$

where $\hat{\mathbf{P}}$ is the momentum operator (generator of translation) and $|k, M\rangle$ is a partial wave centered at the origin. Thus we get:

$$\langle \mathbf{k}, \sigma|k, M, \mathbf{R}\rangle = \langle \mathbf{k}, \sigma|e^{i\hat{\mathbf{P}}\cdot\mathbf{R}}|k, M\rangle = e^{i\mathbf{k}\cdot\mathbf{R}}\langle \mathbf{k}, \sigma|k, M\rangle, \tag{3.9}$$

since $\langle \mathbf{k}, \sigma|$ is momentum eigen state. With Fourier transforming the $c_{\mathbf{k}}$ electrons back to real space ($c_{\mathbf{k},\sigma} = \sum_{\mathbf{r}} e^{i\mathbf{k}\cdot\mathbf{r}} c_{\mathbf{r},\sigma}$) we get:

$$H_K = -J \sum_{\mathbf{R}} \sum_{\mathbf{r},\mathbf{r}',M,M'} f^{\dagger}_{M,\mathbf{R}} \left[\sum_{\mathbf{k},\sigma} \langle k, M|\mathbf{k},\sigma\rangle e^{i\mathbf{k}\cdot(\mathbf{r}-\mathbf{R})} c_{\mathbf{r},\sigma} \right] \left[\sum_{\mathbf{k}',\sigma'} \langle \mathbf{k}',\sigma'|k',M'\rangle e^{-i\mathbf{k}'\cdot(\mathbf{r}'-\mathbf{R})} c^{\dagger}_{\mathbf{r}',\sigma'} \right] f_{M',\mathbf{R}}. \tag{3.10}$$

It is convenient now to define real space operators

$$\Gamma_{\mathbf{r},\mathbf{R},M} = \sum_{\mathbf{k},\sigma} \langle k, M|\mathbf{k},\sigma\rangle e^{i\mathbf{k}\cdot(\mathbf{r}-\mathbf{R})} c_{\mathbf{r},\sigma}, \tag{3.11}$$

which are a mixture of spin up and down electrons. In terms of these real-space operators, the Kondo interaction assumes simple form:

$$H_K = -J \sum_{\mathbf{R}} \sum_{\mathbf{r},\mathbf{r}'} \sum_{M,M'} f^{\dagger}_{M,\mathbf{R}} \Gamma_{\mathbf{r},\mathbf{R},M} \Gamma^{\dagger}_{\mathbf{r}',\mathbf{R},M'} f_{M',\mathbf{R}'}. \tag{3.12}$$

The full Kondo lattice model then takes the form

$$H = H_c + H_K \tag{3.13}$$

$$H_c = \sum_{\mathbf{k},\sigma} \varepsilon_{\mathbf{k}} c^{\dagger}_{\mathbf{k},\sigma} c_{\mathbf{k},\sigma}, \tag{3.14}$$

together with the constraints

$$\sum_{M} f^{\dagger}_{M,\mathbf{R}} f_{M,\mathbf{R}} = 1, \tag{3.15}$$

at each site $\mathbf{R}$. Note that due to this constraint it is no longer ap-

propriate to think of the f-operators as describing physical electrons. Rather at this stage they should be viewed as neutral fermions that carry spin alone. As is well known this representation is redundant and introduces an extra $U(1)$ gauge structure associated with the freedom to change the phase of f independently at each site.

3.4 Slave boson mean field theory

We now discuss the fermi liquid phases described by this Kondo lattice model within the slave boson mean field approximation. In simpler Kondo lattice models this technique correctly captures the essential physics of the fermi liquid state[13, 14]. In the mean field we impose the constraint of Eqn. 3.15 on average with a chemical potential μ_f for the f-fermions and replace the Kondo interaction by a self-consistently determined hybridization between the c and f operators. The mean field Hamiltonian reads

$$\begin{aligned} H_{MF} = & \sum_{\mathbf{k}\sigma} \varepsilon_{\mathbf{k}} c^{\dagger}_{\mathbf{k}\sigma} c_{\mathbf{k}\sigma} + \mu_f \sum_{M\mathbf{R}} f^{\dagger}_{M,\mathbf{R}} f_{M,\mathbf{R}} \\ & + b \sum_{M\mathbf{R}} \left(f^{\dagger}_{M\mathbf{R}} \sum_{\mathbf{r}} \Gamma_{\mathbf{r}\mathbf{R}M} + h.c \right). \end{aligned} \tag{3.16}$$

The mean field parameters μ_f, b must be determined self-consistently through the equations

$$1 = \sum_M \langle f^\dagger_{M,\mathbf{R}} f_{M,\mathbf{R}} \rangle, \tag{3.17}$$

$$b = J \langle \sum_M f^\dagger_{M\mathbf{R}} \sum_{\mathbf{r}} \Gamma_{\mathbf{r}\mathbf{R}M} \rangle. \tag{3.18}$$

Note that we have chosen b to be real in this mean field. Parenthetically we note that a non-zero mean field hybridization parameter b should really be viewed as a Higgs condensate for the $U(1)$ gauge structure introduced when we represent the spins in terms of the f-fields. In this Higgs phase the internal gauge charge of the f-fermions is screened by the condensate and the resulting screened gauge neutral object has the same quantum numbers as the electron. This structure of the low energy electrons manifests itself as a small electron quasiparticle weight at the heavy electron fermi surface.

To diagonalize this mean field Hamiltonian we go to momentum space. We write $f_{M,\mathbf{R}} = \sum_{\mathbf{q}} e^{-i\mathbf{q}\cdot\mathbf{R}} f_{M,\mathbf{q}}$ and put in original form of Γ

operators in terms of c. The hybridization term then becomes

$$\begin{aligned} H_{MF} &= b \sum_{\mathbf{R},\mathbf{r}} \sum_{\mathbf{q}} e^{i\mathbf{q}\cdot\mathbf{R}} f^{\dagger}_{M,\mathbf{q}} \sum_{\mathbf{k},\sigma} \langle k, M|\mathbf{k},\sigma\rangle e^{i\mathbf{k}\cdot(\mathbf{r}-\mathbf{R})} c_{\mathbf{r},\sigma} \\ &\quad + h.c. \\ &= b \sum_{\mathbf{q},\mathbf{k},\sigma} \left(\sum_{\mathbf{R}} e^{i(\mathbf{q}-\mathbf{k})\cdot\mathbf{R}} \right) f^{\dagger}_{M,\mathbf{q}} \, \langle k, M|\mathbf{k},\sigma\rangle \\ &\quad \times \left(\sum_{\mathbf{r}} e^{i\mathbf{k}\cdot\mathbf{r}} c_{\mathbf{r},\sigma} \right) + h.c. \\ &= b \sum_{\mathbf{k}} \langle k, M|\mathbf{k},\sigma\rangle \; f^{\dagger}_{M,\mathbf{k}} \; c_{\mathbf{k},\sigma} + h.c. \; . \end{aligned} \tag{3.19}$$

Thus the momentum dependence of the hybridization is captured through the $\langle \mathbf{k},\sigma|k,M\rangle$ matrix element, which we calculate in the Appendix.

We define the four component field $\Psi_{\mathbf{k}}$

$$\Psi_{\mathbf{k}} = \begin{bmatrix} c_{\mathbf{k}\uparrow} \\ c_{\mathbf{k}\downarrow} \\ f_{k,1} \\ f_{k,2} \end{bmatrix},$$

in terms of which, the Hamiltonian becomes

$$H_{MF} = \sum_{\mathbf{k}} \Psi^{\dagger}_{\mathbf{k}} \begin{bmatrix} \varepsilon_{\mathbf{k}}\mathbf{I} & b\; M(\mathbf{k}) \\ b\; M^{\dagger}(\mathbf{k}) & \mu_f \mathbf{I} \end{bmatrix} \Psi_{\mathbf{k}}. \tag{3.20}$$

Here $M(\mathbf{k})$ is a 2×2 matrix given by

$$M(\mathbf{k}) = \begin{bmatrix} B(\mathbf{k}) & A^*(\mathbf{k}) \\ A(\mathbf{k}) & -B^*(\mathbf{k}) \end{bmatrix}. \tag{3.21}$$

The functions $A(\mathbf{k}), B(\mathbf{k})$ are defined in the Appendix.

Now we look for operators $\gamma_i(\mathbf{k})$ that satisfy $[H_{MF}, \gamma_i^\dagger(\mathbf{k})] = \lambda_i(\mathbf{k})\gamma_i^\dagger(\mathbf{k})$, in term of which H^{MF} is diagonal:

$$H_{MF} = \sum_{\mathbf{k},i} \lambda_i(\mathbf{k})\gamma_i^\dagger(\mathbf{k})\gamma_i(\mathbf{k}). \tag{3.22}$$

If we express $\gamma_i(\mathbf{k})$ as:

$$\gamma_i(\mathbf{k}) = u_i^1(\mathbf{k})c_{\mathbf{k}\uparrow} + u_i^2(\mathbf{k})c_{\mathbf{k}\downarrow} + u_i^3(\mathbf{k})f_{\mathbf{k}1} + u_i^4(\mathbf{k})f_{\mathbf{k}2}, \tag{3.23}$$

where the coefficients $u_i^\alpha(\mathbf{k})$ are determined through the eigenvalue equation:

$$\begin{bmatrix} \varepsilon_{\mathbf{k}}\mathbf{I} & b\ M(\mathbf{k}) \\ b\ M^\dagger(\mathbf{k}) & \mu_f\mathbf{I} \end{bmatrix} \begin{bmatrix} u_i^1(\mathbf{k}) \\ u_i^2(\mathbf{k}) \\ u_i^3(\mathbf{k}) \\ u_i^4(\mathbf{k}) \end{bmatrix} = \lambda_i(\mathbf{k}) \begin{bmatrix} u_i^1(\mathbf{k}) \\ u_i^2(\mathbf{k}) \\ u_i^3(\mathbf{k}) \\ u_i^4(\mathbf{k}) \end{bmatrix} \tag{3.24}$$

From this we get the four eigenstates and the corresponding dispersion

of four bands:

$$\begin{aligned}
\lambda_1(\mathbf{k}) &= \lambda_2(\mathbf{k}) = \frac{\varepsilon_\mathbf{k} + \mu_f}{2} \\
&- \sqrt{\left(\frac{\varepsilon_\mathbf{k} - \mu_f}{2}\right)^2 + b^2(|A(\Omega_\mathbf{k})|^2 + |B(\Omega_\mathbf{k})|^2)}, \\
\lambda_3(\mathbf{k}) &= \lambda_4(\mathbf{k}) = \frac{\varepsilon_\mathbf{k} + \mu_f}{2} \\
&+ \sqrt{\left(\frac{\varepsilon_\mathbf{k} - \mu_f}{2}\right)^2 + b^2(|A(\Omega_\mathbf{k})|^2 + |B(\Omega_\mathbf{k})|^2)}
\end{aligned}$$

At each $\mathbf{k}$ obviously we have $\lambda_1(\mathbf{k}) = \lambda_2(\mathbf{k}) \leq \lambda_3(\mathbf{k}) = \lambda_4(\mathbf{k})$, so we have two sets of doubly-degenerate bands. The degeneracy is a consequence of time reversal and inversion symmetries which have been assumed in the original model.

Let us assume that there are n_c conduction electrons per unit cell with $n_c < 1$. Once combined with single f-fermion per unit cell, we then need to fill these bands up to the fermi energy to give a total particle number of $1 + n_c$ per unit cell. Only only states in the lower bands λ_1 and λ_2 are e filled, and the fermi surface always lives in these two bands. Clearly the fermi surface is large in that its volume counts both the conduction electrons and the f-fermions. The shape of the fermi surface corresponding to our simple model is shown shown in Fig. 3-1.

We note that the hybridization matrix $bM(\vec{k})$ vanishes along the (100) and symmetry related directions (see Appendix). These hybridization nodes lead to striking fermi surface anisotropies as discussed

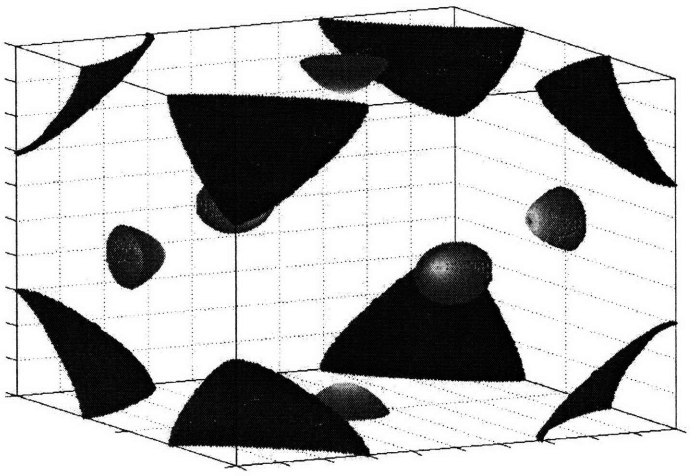

Figure 3-1: Z on fermi surface. Red denotes larger Z close to one and blue denotes Z close to zero. Red points are along (0,0,1),(0,1,0) and (0,0,1) directions.

in detail below. For now we note that along these 'nodal' directions the fermi surface coincides within the original *small* conduction electron fermi surface. To see this consider the spectrum of the partially occupied band. It is obvious that $\lambda(\mathbf{k}) = \lambda_1(\mathbf{k}) < \frac{\varepsilon_\mathbf{k}+\mu_f}{2} - |\frac{\varepsilon_\mathbf{k}-\mu_f}{2}|$. On the other hand $\frac{\varepsilon_\mathbf{k}+\mu_f}{2} - |\frac{\varepsilon_\mathbf{k}-\mu_f}{2}| = min\{\varepsilon_\mathbf{k}, \mu_f\}$ so that for all $\mathbf{k}$, $\lambda(\mathbf{k}) \leq \mu_f$ (equality only holds for the points where $b(\mathbf{k}) = b^2(|A(\Omega_\mathbf{k})|^2 + |B(\Omega_\mathbf{k})|^2) = 0$). So for $n_c < 1$, $E_f < \mu_f$. Now if we consider points on the fermi surface where $b(\mathbf{k})$ vanishes, again for such points $\lambda(\mathbf{k})$ is equal to either μ_f for points where $\varepsilon_\mathbf{k} > \mu_f$ and $\varepsilon_\mathbf{k}$ for points where $\varepsilon_\mathbf{k} < \mu_f$. Since $E_f < \mu_f$ for such points we have $\lambda(\mathbf{k}) = \varepsilon_\mathbf{k}$; so the fermi surface coincides with the small fermi sea of conduction electrons at the points where $b(\mathbf{k}) = 0$. Thus along the nodal directions of the hybridization the quasiparticles at the fermi surface are almost entirely composed of conduction-electrons. However, on moving away from these nodal directions the quasiparticles quickly acquire an almost complete f-character with a weak conduction electron admixture.

3.5 Implications for photoemission experiments

The anisotropic hybridization leads, as discussed below, to anisotropic quasiparticle spectral weight. This can be probed by angle resolved photoemission spectroscopy (ARPES). We begin with a general discussion of the physical electron Green function in Kondo lattice systems.

Let us start with Anderson model given in equation 3.2. In ARPES by interaction with a light beam electrons are extracted from the sample. These electrons in principle could be extracted form any of the two bands (see Equation 3.2). However processes where the f-occupation is changed cost large energy in the strong correlation limit. On the other hand, processes where the removed f-electron is replaced by tunneling of a c-electron into the unoccupied f-site can occur at order(V/U) and will have matrix elements in the low energy "Kondo" subspace. To discuss this physics let us start from a single Anderson impurity and consider the operator $\psi_{\mathbf{k},\sigma}$ that corresponds to extracting a electron with momentum $\mathbf{k}$ and spin σ out of the sample:

$$\psi_{\mathbf{k},\sigma} = c_{\mathbf{k},\sigma} + \sum_{M} \langle \mathbf{k}, \sigma | M \rangle f_M. \tag{3.25}$$

In the strong correlation limit we need to perform the Schrieffer-Wolff transformation for this operator. Below we use an equivalent alternate procedure. We first consider the ground state. In the limit of infinite U it consists of half filled f orbital coexisting with a conductino band filled up to the fermi energy: we name this state $|g_0\rangle$. In the limit of

large but finite U to first order in V/U the ground state becomes:

$$|g_1\rangle = |g_0\rangle + \sum_{n,M,\mathbf{k},\sigma} |n\rangle \frac{\langle n|V\left(f_M^\dagger c_{\mathbf{k},\sigma} + c_{\mathbf{k},\sigma}^\dagger f_M\right)|g_0\rangle}{U}, \tag{3.26}$$

where, for simplicity we have assumed that the energy to add, or remove an f-electron is U. Here $|n\rangle$ denote the first excited states. To a good approximation, the state-vector in the second term is given by $\left(f_M^\dagger c_{\mathbf{k},\sigma} + c_{\mathbf{k},\sigma}^\dagger f_M\right)|g_0\rangle$. Now when we annihilate an electron by acting with ψ on $|g_1\rangle$ state, only final states which lie within the manifold of states with single f-occupancy at the impurity, site will contribute to the photoemission intensity at low energy. There are two such states, one corresponding to the action of c on the $|g_0\rangle$ component of the ground state, and the other corresponding to the action of f on the second term in $|g_1\rangle$ (*i.e* on the $f^\dagger c|g_0\rangle$ term). The net action of $\psi_{\mathbf{k},\sigma}$ on $|g_0\rangle$ is then:

$$\begin{aligned}\psi_{\mathbf{k},\sigma} \sim c_{\mathbf{k},\sigma} + (V/U) \sum_{\mathbf{k}',\sigma',M',M} & \langle k', M'|\mathbf{k}', \sigma'\rangle \\ & \times \langle \mathbf{k}, \sigma|k, M\rangle \; f_{M'}^\dagger c_{\mathbf{k}',\sigma'} f_M.\end{aligned} \tag{3.27}$$

The first term corresponds to the knocking off an electron from the c band and second term corresponds to the first order process where an electron from an f orbital is knocked off and an electron from c band replaces it. Now for a lattice of impurities, we should consider processes where f electrons from different sites are knocked out:

$$\psi_{\mathbf{k},\sigma} \sim c_{\mathbf{k},\sigma} + (V/U) \sum_{\mathbf{R}} \sum_{\mathbf{k}',\sigma',M',M} \langle k', M', \mathbf{R}|\mathbf{k}', \sigma'\rangle \times \langle \mathbf{k}, \sigma|k, M, \mathbf{R}\rangle f^{\dagger}_{M',\mathbf{R}}\, c_{\mathbf{k}',\sigma'} f_{M,\mathbf{R}}. \tag{3.28}$$

It is convenient to reexpress this in real space. The procedure is the same we did in section 3.4:

$$\begin{aligned}
&\sum_{\mathbf{R}} \sum_{\mathbf{k}',\sigma',M'} \langle k', M', \mathbf{R}|\mathbf{k}', \sigma'\rangle \langle \mathbf{k}, \sigma|k, M, \mathbf{R}\rangle f^{\dagger}_{M',\mathbf{R}} c_{\mathbf{k}',\sigma'} f_{M,\mathbf{R}} \\
&= \sum_{\mathbf{R}} \sum_{\mathbf{k}',\sigma',M'} \langle k', M'|\mathbf{k}', \sigma'\rangle e^{i\mathbf{k}'.(\mathbf{r}-\mathbf{R})} f^{\dagger}_{M',\mathbf{R}} c_{\mathbf{r},\sigma'} \\
&\qquad \langle \mathbf{k}, \sigma|k, M\rangle e^{i\mathbf{k}.\mathbf{R}} f_{M,\mathbf{R}} \\
&= \sum_{\mathbf{R}} \sum_{M'} f^{\dagger}_{M',\mathbf{R}} \left[\sum_{\mathbf{k}',\sigma} \langle k', M'|\mathbf{k}', \sigma'\rangle e^{i\mathbf{k}'.(\mathbf{r}-\mathbf{R})} c_{\mathbf{k}',\sigma'} \right] \\
&\qquad \sum_{M} e^{i\mathbf{k}.\mathbf{R}} f_{M,\mathbf{R}} \\
&= \sum_{\mathbf{R}} \sum_{M'} f^{\dagger}_{M',\mathbf{R}} \Gamma_{\mathbf{r},\mathbf{R},M'} \sum_{M} \langle \mathbf{k}, \sigma|k, M\rangle f_{M,\mathbf{R}}.
\end{aligned} \tag{3.29}$$

Within the slave boson mean field approximation we replace the product $f^{\dagger}c$ (or equivalently $f^{\dagger}\Gamma$) term in the second term by its average to get:

$$\psi_{\mathbf{k},\sigma} \sim c_{\mathbf{k},\sigma} + (b/V) \sum_{M} \langle \mathbf{k}, \sigma|k, M\rangle f_{M}. \tag{3.30}$$

The ARPES intensity may now be calculated from the Greens func-

tion of this ψ operator. Its trace is given by

$$\begin{aligned} Tr\left[G_{\sigma,\,\sigma'}(k,i\omega_\nu)\right] &= \int_0^\beta d\tau e^{i\omega_\nu \tau} \\ &\langle T_\tau \left[\psi_\uparrow(k,\tau)\psi_\uparrow^\dagger(k,0) + \psi_\downarrow(k,\tau)\psi_\downarrow^\dagger(k,0)\right]\rangle, \end{aligned} \tag{3.31}$$

where the expectation value is taken in the ground state. From equation 3.30 it is obvious that this Green function consists four different terms. For this calculation, we need to have c_σ and f_M operators, in term of γ operators. To make this calculation more transparent, it is useful to introduce the unitary matrix U as:

$$U = \begin{bmatrix} u_1^1 & u_1^2 & u_1^3 & u_1^4 \\ u_2^1 & u_2^2 & u_2^3 & u_2^4 \\ u_3^1 & u_3^2 & u_3^3 & u_3^4 \\ u_4^1 & u_4^2 & u_4^3 & u_4^4 \end{bmatrix}, \tag{3.32}$$

where:

$$\begin{bmatrix} \gamma^1 \\ \gamma^2 \\ \gamma^3 \\ \gamma^4 \end{bmatrix} = U \begin{bmatrix} c_\uparrow \\ c_\downarrow \\ f_1 \\ f_2 \end{bmatrix}. \tag{3.33}$$

Here $\mathbf{k}$ index is suppressed for notational convenience. Inverting we get

$$c_\uparrow^\dagger = u_1^1\gamma_1^\dagger + u_2^1\gamma_2^\dagger + u_3^1\gamma_3^\dagger + u_4^1\gamma_4^\dagger, \tag{3.34}$$

$$c_\downarrow^\dagger = u_1^2\gamma_1^\dagger + u_2^2\gamma_2^\dagger + u_3^2\gamma_3^\dagger + u_4^2\gamma_4^\dagger, \tag{3.35}$$

$$f_1^\dagger = u_1^3\gamma_1^\dagger + u_2^3\gamma_2^\dagger + u_3^3\gamma_3^\dagger + u_4^3\gamma_4^\dagger, \tag{3.36}$$

$$f_2^\dagger = u_1^4\gamma_1^\dagger + u_2^4\gamma_2^\dagger + u_3^4\gamma_3^\dagger + u_4^4\gamma_4^\dagger. \tag{3.37}$$

Using this result, we can expand imaginary part of the trace of the Green function to obtain the zero temperature spectral function. This has four terms corresponding to the operator combinations $cc^\dagger$,$ff^\dagger$, $fc^\dagger$ and $cf^\dagger$. Let us calculate them one by one. The $cc^\dagger$ term is:

$$\begin{aligned} A_{cc}(\mathbf{k},\omega) =& (|u_1^1(\mathbf{k})|^2 + |u_1^2(\mathbf{k})|^2)\ \delta(\lambda_1(\mathbf{k}) - \omega) \\ &+ (|u_2^1(\mathbf{k})|^2 + |u_2^2(\mathbf{k})|^2)\ \delta(\lambda_2(\mathbf{k}) - \omega). \end{aligned} \tag{3.38}$$

We then get the following form for the quasi-particle residue on the fermi surface:

$$Z_{cc}(\mathbf{k}|\lambda_2(\mathbf{k}) = E_f) = |u_2^1(\mathbf{k})|^2 + |u_2^2(\mathbf{k})|^2 = \frac{b(\mathbf{k})^2}{b(\mathbf{k})^2 + \left(\frac{\varepsilon(\mathbf{k})-\mu_f}{2} + \sqrt{(\frac{\varepsilon(\mathbf{k})-\mu_f}{2})^2 + b(\mathbf{k})^2}\right)^2} \tag{3.39}$$

Now for ff term (noting $u_1^3 = u_2^4 = 0$) we have:

$$A_{ff}(\mathbf{k},\omega) = \left(\frac{b(\mathbf{k})}{V}\right)^2 |u_4^1(\mathbf{k})|^2\ \delta(\lambda_1(\mathbf{k}) - \omega) + \left(\frac{b(\mathbf{k})}{V}\right)^2 |u_2^3(\mathbf{k})|^2\ \delta(\lambda_2(\mathbf{k}) - \omega). \tag{3.40}$$

This gives the residue:

$$Z_{ff}(\mathbf{k}|\lambda_2(\mathbf{k}) = E_f) = \frac{\left(\frac{\varepsilon(\mathbf{k})-\mu_f}{2} + \sqrt{(\frac{\varepsilon(\mathbf{k})-\mu_f}{2})^2 + b(\mathbf{k})^2}\right)^2}{b(\mathbf{k})^2 + \left(\frac{\varepsilon(\mathbf{k})-\mu_f}{2} + \sqrt{(\frac{\varepsilon(\mathbf{k})-\mu_f}{2})^2 + b(\mathbf{k})^2}\right)^2} \left(\frac{b(\mathbf{k})}{V}\right)^2. \tag{3.41}$$

The last contribution will be:

$$Z_{cf}(\mathbf{k}|\lambda_2(\mathbf{k}) = E_f) = -\frac{2(b^2/V)\left(\frac{\varepsilon(\mathbf{k})-\mu_f}{2} + \sqrt{(\frac{\varepsilon(\mathbf{k})-\mu_f}{2})^2 + b(\mathbf{k})^2}\right)}{b(\mathbf{k})^2 + \left(\frac{\varepsilon(\mathbf{k})-\mu_f}{2} + \sqrt{(\frac{\varepsilon(\mathbf{k})-\mu_f}{2})^2 + b(\mathbf{k})^2}\right)^2} \times \Re\left(A^2(\Omega_\mathbf{k}) + B^2(\Omega_\mathbf{k})\right), \tag{3.42}$$

where $b(\mathbf{k}) = b\sqrt{|A(\Omega_\mathbf{k})|^2 + |B(\Omega_\mathbf{k})|^2}$. In Fig. 3-1 we have also indicated the total residue Z_{total} which is the sum of these three contributions.

Using the fact that $|b(\mathbf{k})|$ is small, we can investigate the behavior of Z_{total} at least for the points where $|b(\mathbf{k})| \ll |\varepsilon(\mathbf{k}) - \mu_f|$. For such points we see that whenever $\epsilon_\mathbf{k} > \mu_f$ the dominant term (of order b^2/V^2) is

Z_{ff} and it varies since $b(\mathbf{k})$ is angle dependent. On the other hand, when $\epsilon_{\mathbf{k}} < \mu_f$, the dominant contribution is Z_{cc} which is of order one. This information could be summarized in the following form:

$$Z(\mathbf{k}|\lambda_2(\mathbf{k}) = E_f) = \\ b^2 \frac{h(\mathbf{k})}{(\varepsilon(\mathbf{k}) - \mu_f)^2} \Theta(\varepsilon(\mathbf{k}) - \mu_f) + \Theta(\mu_f - \varepsilon(\mathbf{k})). \tag{3.43}$$

where $h(\mathbf{k})$ is given by:

$$h(\mathbf{k}) = \left(|A^2(\Omega_{\mathbf{k}})| + |B^2(\Omega_{\mathbf{k}})|\right)(1 + (\varepsilon(\mathbf{k}) - \mu)^2/V^2) \\ - 2\Re\left(A^2(\Omega_{\mathbf{k}}) + B^2(\Omega_{\mathbf{k}})\right)(\varepsilon(\mathbf{k}) - \mu)/V \tag{3.44}$$

A key result of this calculation is that for the points where $\varepsilon(\mathbf{k}) > \mu_f$, Z is small and of order $\frac{b(\mathbf{k})^2}{(\varepsilon(\mathbf{k})-\mu_f)^2}$; this quantity varies by about 20% due to the angle dependent $b(\mathbf{k})$. But for the points where $\mu_f > \varepsilon(\mathbf{k})$, the quasi-particle residue will be of order one and will exhibit no strong variations. The small region in the middle of fermi surface in Fig. 3-1 with $Z \sim 1$ corresponds to these points. These regions are centered along (100) and symmetry related directions. As discussed in the previous section the hybridization matrix has nodes in these special directions and the corresponding quasiparticles are essentially conduction electrons with $Z \sim 1$. On the other hand further away from these nodal directions the quasiparticles develop f-character and $Z \sim o(b^2)$ along these other directions.

There is thus a dramatic anisotropy in Z on moving around the fermi surface. We note that ARPES experiments will naturally be able

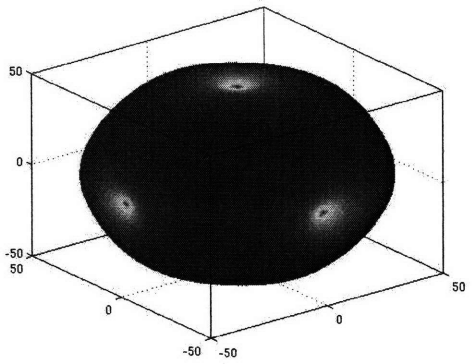

Figure 3-2: Large closed fermi surface. Red large ARPES intensity Blue small ARPES intensity

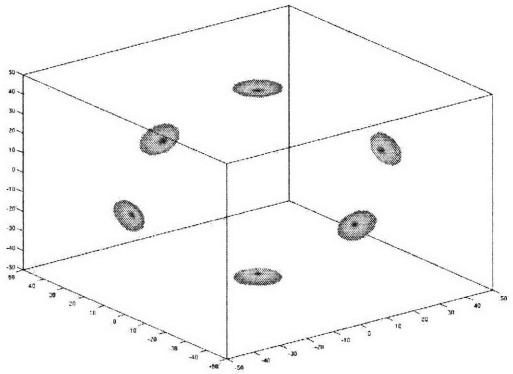

Figure 3-3: fermi patches as might appear in ARPES without large enough intensity. Red large ARPES intensity Blue small ARPES intensity

to resolve the quasiparticle peak along high-Z directions. However a low resolution ARPES study may well not be able to resolve the small-Z quasiparticles at all and may incorrectly conclude that the fermi surface consists only of finite open ended pieces??

3.6 Momentum dependent effective mass

It is well known that the effective mass m^* in a heavy fermion system can be very anisotropic on the fermi surface. How do these anisotropies

correlate with the anisotropic Z? It is precisely the combination $Z \times m^*$ that determines the *tunneling* density of states. It is therefore also interesting to look at $m^*(\mathbf{k})$ variations over the fermi surface. The effective mass can be calculated by taking the second derivative of energy with respect to momentum in direction perpendicular to the fermi surface i.e. $\frac{\partial^2 \lambda_2(\mathbf{k})}{\partial k_\perp^2}$:

$$\begin{aligned} 1/(m^*(\mathbf{k})) = 1/2m_e^* \Bigg[1 - \frac{\frac{\varepsilon_\mathbf{k} - \mu_f}{2}}{\sqrt{\left(\frac{\varepsilon_\mathbf{k} - \mu_f}{2}\right)^2 + |b(\mathbf{k})|^2}} \\ + \frac{b^2(\varepsilon_\mathbf{k} - \mu_f) f(\mathbf{k})}{\left(\left(\frac{\varepsilon_\mathbf{k} - \mu_f}{2}\right)^2 + |b(\mathbf{k})|^2\right)^{3/2}} \Bigg] \\ \approx 1/m_e^* \left[\Theta\left(\mu_f - \varepsilon(\mathbf{k})\right) + \frac{b^2}{(\varepsilon_\mathbf{k} - \mu_f)^2} g(\mathbf{k}) \right] \end{aligned} \tag{3.45}$$

where m_e^* is the free electron effective mass ($1/m_e^* = \frac{\partial^2 \varepsilon_\mathbf{k}}{\partial k_\perp^2}$), and in the last step we used the approximation $|\varepsilon_\mathbf{k} - \mu_f| \gg |b(\mathbf{k})|$. $f(\mathbf{k})$ and $g(\mathbf{k})$ are dimensionless functions of $\mathbf{k}$ where $g(\mathbf{k}) = 2\ sign(\varepsilon_\mathbf{k} - \mu_f)\left(4f(\mathbf{k}) + |A(\Omega_\mathbf{k})|^2 + |B(\Omega_\mathbf{k})|^2\right)$ (numerical calculations show no $\mathbf{k}$ point where $g(\mathbf{k})$ vanishes). Inverting this we get:

$$m^*(\mathbf{k}) \approx m_e^* \left[\Theta\left(\mu_f - \varepsilon(\mathbf{k})\right) + \Theta\left(\varepsilon(\mathbf{k}) - \mu_f\right) \frac{(\varepsilon_\mathbf{k} - \mu_f)^2}{g(\mathbf{k}) b^2} \right] \tag{3.46}$$

We see a similar behavior with $Z(\mathbf{k})$. Again for points with $\varepsilon_\mathbf{k} > \mu_f$ we have quasiparticles with large effective mass, but for $\varepsilon_\mathbf{k} < \mu_f$ quasiparticles are free electron types and have effective mass corresponding to

small, conduction electrons effective mass. We see that we have large effective mass in the points where Z is small. So indeed variations of effective mass are correlated with variations of $1/Z$. The approximate invariance of the product $Z(\mathbf{k})m^*(\mathbf{k})$ is a momentum-space variant of Langreth theorem, which states that the single particle density of states in the Anderson impurity model is an adiabatic invariant, independent of the strength of the interaction[68, 69].

This is interesting since it shows us that the strong angle dependent anisotropy does not apparently have large observable consequence on ordinary tunneling measurements. However it may possibly show up in the amplitude of the Friedel oscillations of the tunneling conductance around an impurity, and may therefore be accessible through Fourier transform scanning tunneling spectroscopy.

3.7 Underdoped cuprates: Pseudogaps and fermi arcs in a large fermi surface metal?

We now compare the phenomena described with observations on the normal state of the cuprate materials. As discussed above in the heavy fermion context there are portions of the fermi surface where $Z \sim o(1)$, and ARPES experiments may conclude that the fermi surface consists of open ended pieces. This is strongly reminiscent of the fermi arc phenomena reported by ARPES in the pseudogap regime of the underdoped cuprates. It is tempting therefore to imagine that a similar

mechanism is operational in the cuprates. More specifically is it possible that the underdoped cuprates actually have a large band-structure-like fermi surface but the Z is $o(1)$ only along the observed fermi arcs and becomes very small away from it so that those portions are not easily observed? The antinodal pseudogap itself must then be associated with a gap in the incoherent part of the electron spectrum with the gapless coherent part not resolved due to the smallness of Z.

In considering this question we first observe that in the heavy fermion system the smallness of Z goes hand-in-hand with the largeness of effective mass. More generally the effective mass is not directly related to Z (it is only in cases where the electron self energy is momentum independent that Z determines the mass renormalization). So phenomenologically we need to first suppose that the small Z antinodal regions do not have mass enhancement. Such a fermi liquid state for the pseudogap regime has some attractive features. Consider first the gapless fermi arcs. Several popular theories attempt to view the arcs as part of a true fermi surface which consists of small closed hole pockets whose *back* portions are not observed in ARPES due to a small Z. However, the observed fermi arc coincides with band structure fermi surface and shows no tendency to bend away into a closed hole pocket. In contrast in the state discussed above the true fermi surface is simply the band structure one but the antinodal sections would be unobservable due to a small Z.

Consider next recent observations of quantum oscillations at high

fields and low temperatures in some underdoped cuprates[61, 62]. The oscillation frequency seems consistent with a small fermi pocket. A key issue is to reconcile this with the fermi arcs reported in photoemission, and a few different ideas have been proposed[70, 17]. An interesting feature of the high field experiments is a negative Hall constant which has been interpreted as evidence for an *electron* pocket[71]. Recently Millis and Norman[72] have proposed that the oscillations and negative Hall constant should be with a 1/8th filling antiphase stripe order, which folds the band structure fermi surface to create a pocket. One issue with the proposal is that the electron pocket is near the edges of the full Brillouin zone - precisely the region where a big pseudogap is seen by ARPES in zero field in the normal state above T_c. For the theory of Ref. [72] to apply it is apparently necessary that the $60T$ fields used in the quantum oscillation experiment wipe out the pseudogap[1]. This may seem unnatural but is not prohibited. This difficulty is overcome in the large fermi surface pseudogap envisaged in this section. A low temperature 1/8 antiphase stripe instability arising from that state will retain all the same transport properties as that in the theory of Ref. [72]. This is because the smallness of Z does not affect transport phenomena. On the other hand the ARPES pseudogap (which in this state is the gap of the incoherent part of the spectrum) will survive intact. Thus this kind of large fermi surface state provides a possible route to a reconciliation between the quantum oscillation and

[1]This issue was raised by Patrick Lee.

ARPES experiments.

However a number of difficulties exist with the idea that the pseudogap state has a large fermi surface state with strong angle dependent Z. First, the density of states as measured by thermodynamic measurements actually decreases on entering the pseudogap state by cooling. This requires that the effective mass at the antinodal regions is *suppressed* (rather than enhanced) in the pseudogap state which is rather unnatural. Besides such behavior should signal an increase in the Drude weight in optical transport in the pseudogap state which is not seen. Finally this is also inconsistent with the scaling of the superfluid density with the density of doped holes.

In light of these difficulties it seems unlikely that a fermi liquid state with a large fermi surface of the kind discussed here is a serious candidate for the pseudogap state. These difficulties may perhaps be overcome by a non-fermi liquid version which retains the large fermi surface and the strong variation of the low energy spectral density. However a description of such a state does not currently exist.

3.8 Discussion

The most interesting aspect of our work is the possibility of large variations in the quasiparticle weight (and concomitantly the effective mass) on moving around the fermi surface. This anisotropy is linked to the internal orbital structure of the Kondo resonance, derived from the f-symmetry of the orbitals occupied by the local moments. In the hy-

bridization mean field theory the most dramatic variation occurs when there are 'hybridization nodes', *i.e* directions along which the hybridization vanishes. We have demonstrated the possibility of these nodes in a simple model of a Ce-based cubic heavy fermion system with cubic symmetry. Hybridization nodes lead to the possibility that some portions of the large fermi surface are actually contained within the original small fermi surface of the conduction electrons. In those regions the quasiparticles essentially have c-electron character with very little admixture to the f-fermions. The quasiparticle weight is correspondingly large (of order 1). The opposite is true in other portions where the quasiparticles mostly have f-character and have small Z. This then leads to a strong angle dependence of the quasiparticle weight.

Real heavy electron materials have much more complicated band structures than in the simplified model considered here. Nevertheless there exists in general the possibility of hybridization nodes which will greatly affect their low temperature physics. Consider for instance heavy electron superconductivity. At least in some cases the superconductivity may be driven by formation of singlet bonds between neighbouring local moments due to RKKY interactions. In combination with Kondo hybridization this leads to superconductivity. Formally the singlet formation may be described as $< ff >$ pairing while the Kondo hybridization has non-zero $< c^\dagger f >$. This then leads to non-zero $< cc >$, *i.e* superconducting order[73, 74]. If the hybridization has nodes then this will lead to extra nodes in the physical superconducting

order parameter over and above any nodes inherited from the singlet bond $< ff >$ amplitude[75].

The large variation of the Z also has potential implications for current thinking on the nature of the quantum critical point between the heavy fermi liquid and the antiferromagnetic metal. It has been suggested that this transition is accompanied by the loss of Kondo screening resulting in a reconstruction of the fermi surface[44, 46, 76]. Such a reconstruction presumably requires Z to vanish through out the large fermi surface on approaching the transition from the paramagnetic side. For a discussion on Z vanishing at the heavy fermion quantum critical points see [77]. The variation of Z described in this chapter raises the question of whether the manner in which Z vanishes also varies around the fermi surface.

Chapter 4

Neel order, spin liquids and quantum criticality in two dimensions

In this chapter, we change gear and study a strongly correlated model in insulating phase. As mentioned before although there are scenarios for direct transition between heavy fermion phase and a spin liquid with small fermi surface([46]), full direct transition to Neel ordered phase is not explained yet. The model in this section, although is in insulating phase of one band Hubbard model, describe the other halfway from spin liquid to Neel state. We emphasis here that although this model is not directly relevant to heavy fermions, it might open some roats for future investigations in this system.

This chapter is more directly relevant to cuprates in underdoped side. Despite many theoretical and experimental developments[17], questions remain on connection between the paramagnetic phase and occurrence

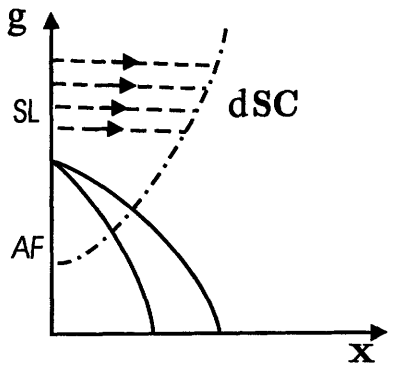

Figure 4-1: Zero temperature phase diagram showing the route from Mott insulating antiferromagnet to d-wave superconductor (dashed-dot line). Horizontal axis refers to doping and vertical axis refers to frustrating spin interactions that destabilize the Neel state. The thesis of the spin liquid approach is that the intermediate and long scale physics of the doped system may be fruitfully viewed as those of a doped spin liquid Mott insulator. Doping the spin-liquid phase naturally leads to d-wave superconducting state. (dashed lines).

of antiferromagnetic long range order.

Early work[18, 78] suggested that the undoped magnetically ordered Mott insulator is close to being disordered by quantum fluctuations into a paramagnetic featureless "spin liquid" phase. Such a spin liquid state was postulated to have neutral spin-1/2 spinon excitations and preserve all the symmetries of the underlying microscopic spin Hamiltonian (including spin rotation). Further it was argued that doping a spin liquid could possibly lead to high temperature superconductivity[18, 78].

Despite its original appeal, this scenario was subsequently questioned by a number of significant theoretical developments. Calculations in a controlled large-N expansion of quantum Heisenberg spin models concluded that the natural result of destruction of collinear Neel order was not a featureless spin liquid but (for spin-1/2) a valence bond solid (VBS), which breaks various lattice symmetries[79]. (Here natu-

ral refers to the possibility that the quantum paramagnet in question is potentially separated from the Neel state by a second order transition.) The VBS state also does not support fractionalized spinon excitations. This was supported by a number of other indirect arguments - for instance by studies of quantum dimer models on the square lattice[80]. It was shown however that destruction of non-collinear Neel order could indeed lead to a fractionalized spin liquid state that preserves all lattice symmetries[51].

These calculations lead to the following folk wisdom (for a review see Ref. [81]): "*In two spatial dimensions collinear ordered magnets naturally give way to confined VBS paramagnets when disordered by quantum fluctuations while non-collinear magnets naturally lead to spin liquids*". As the magnetic ordering is undoubtedly collinear in the cuprates this folk wisdom apparently spells doom for the view of the cuprates as doped spin liquid paramagnetic Mott states.

In this chapter we revisit these issues. We will first argue that, if at all a spin liquid based approach is to be pursued, experiments suggest a certain kind of paramagnetic spin liquid state as natural candidate 'parent' states of the doped cuprates. Next we argue that the existing theoretical work does not rule out a direct second order transition between the Neel state and this particular kind of spin liquid state. Finally we outline in some detail a theory for just such a direct second order transition. Thus our work calls into question the folklore described above and potentially frees the spin liquid based approach to

the cuprates from one of its theoretical criticisms.

Based on these results we will develop a qualitative picture of the neutron resonance mode seen in experiments in the doped system and its relationship with other aspects of the observed spin physics. Our description will naturally unify two popular views of the resonance mode - one as a soft mode associated with antiferromagnetic long range order[25, 26, 27], and the other as a spin exciton formed as a triplet particle-hole collective mode of fermionic quasiparticles[82, 83, 84, 85, 86].

We begin with experiments. It is by now quite clearly established that the cuprate superconductors are d-wave paired and furthermore have nodal BCS-like quasiparticles. The existence of the nodal quasiparticles is theoretically significant. Indeed the possibility of d-wave paired superconductors without nodal quasiparticles has been much emphasized by Kivelson and coworkers (for a review see Ref. [87]). It is therefore of some interest to ask whether there exist paramagnetic Mott states that already have gapless nodal excitations. Such a state then builds-in enough of the spin physics seen in the experiments at finite doping that it would be an attractive 'parent' Mott insulator as a basis for a theory of the underdoped cuprates.

Remarkably such states are known to exist as stable quantum phases[53, 88] of quantum antiferromagnets magnets on a two dimensional square lattice, at least within an appropriate large-N expansion. Here we will focus on one such state that has played a central role in some previous

theoretical work[89, 90, 91, 92, 93, 94] on the cuprate problem. This state - dubbed the d-wave RVB or staggered flux (sF) spin liquid - is a quantum paramagnet that nevertheless has gapless spin carrying excitations. Recent theoretical work[88] has established the stability of such a state (in a suitable large-N expansion). A low energy description of the physics is usefully provided in terms of a theory of gapless nodal fermionic spinons coupled minimally to a fluctuating $U(1)$ gauge field. Despite this however there really is no true quasiparticle description of the low energy spectrum[93, 95].

4.1 Mean field theory

Consider a generic $SU(2)$ symmetric spin-$1/2$ model on a square lattice with predominantly antiferromagnetic short ranged interactions:

$$\mathcal{H} = J \sum_{<rr'>} \vec{S}_r \cdot \vec{S}_{r'} + \cdots \tag{4.1}$$

Here $J > 0$ (antiferromagnetic exchange), and the ellipsis represent frustrating interactions that can be used to tune quantum phase transitions. We will require that the full Hamiltonian be invariant under $SU(2)$ spin rotations, time-reversal, and the full space group of the square lattice. It is well known that the nearest neighbour model has a Neel ordered ground state. Various paramagnetic ground states can be accessed (in principle) by appropriate frustrating interactions. As explained in the introduction, here we will focus on a particular para-

magnetic state that is known as the dRVB algebraic spin liquid (also often referred to as the staggered flux spin liquid). A mean field theory for this state has been described several times in the literature and is well-known[89]. First the spin is formally rewritten as a bilinear of fermionic "spinon" operators

$$\vec{S}_r = \frac{1}{2} f^\dagger_{r\alpha} \vec{\sigma}_{\alpha\beta} f_{r\beta}. \tag{4.2}$$

Here $\alpha = 1, 2$, corresponding to spin up/spin down fermions. This is an exact rewriting when combined with the local constraint $f^\dagger_\alpha f_\alpha = 1$. In the mean field approximation the exact Hamiltonian is replaced by one quadratic in the spinon operators but with self-consistently determined parameters. For the dRVB state, the mean field Hamiltonian takes the form

$$H_{sF} = -\sum_{<rr'>} \left((\chi_{rr'} + i\Delta_{rr'}) f^\dagger_r f_{r'} + h.c \right) \tag{4.3}$$

Here we take r to belong to one sublattice of the square lattice. So that r' belongs to the opposite sublattice. The constants $\Delta_{rr'} = +\Delta$ on horizontal bonds, and $-\Delta$ on vertical bonds while $\chi_{rr'} = t$ on all bonds. This describes fermionic spin-1/2 spinons on the square lattice with complex hopping amplitudes such that there is a non-zero flux that is staggered from plaquette to plaquette. Despite appearances, this saddle point possesses the full symmetry of the microscopic model including all lattice symmetries. (The apparent breaking of translational symmetry is a gauge artifact). Recent work has clarified the nature of fluctuations

about this mean field state. But in this present section, we will stick to the mean field description and see how a transition to a Neel ordered state may be described.

To access a Neel state we modify the dRVB mean field Hamiltonian by adding a nearest neighbour antiferromagnetic interaction between the spinons. Such an interaction will anyway be induced once fluctuations beyond the mean field theory are considered. By including it explicitly, we can induce a spin density wave ordering of the fermionic spinons. We therefore consider

$$H = -\sum_{\langle rr' \rangle} (T_{rr'} f_r^\dagger f_{r'} + T_{rr'}^* f_{r'}^\dagger f_r) + \frac{1}{g} \sum_{\langle rr' \rangle} \vec{S}_r . \vec{S}_{r'} \tag{4.4}$$

Here $T_{rr'} = T = t + i\Delta$ on bonds as shown in Fig. 4-2 and equals $T^* = t - i\Delta$ on other bonds as also shown in Fig 4-2. We now treat the $\frac{1}{g}$ term in a mean field approximation. We look for a solution where $< \vec{S}_r >= \epsilon_r N \hat{z}$ is non-zero (In mean field theory, $\vec{N} = \langle \epsilon_r \vec{S}_r \rangle$ is constant. So we can choose it's direction as z direction). Here $\epsilon_r = (-1)^{x+y}$ is $+1$ on the A sublattice and -1 on the B sublattice. The mean field Hamiltonian reads

$$H_{MF} = -\sum_{\langle rr' \rangle} (T f_r^\dagger f_{r'} + T^* f_{r'}^\dagger f_r) - \frac{4N}{g} \sum_r \epsilon_r f_r^\dagger \frac{\sigma^z}{2} f_r \tag{4.5}$$

The value of N is to be determined self-consistently. We can diagonalize this Hamiltonian using a two site unit cell as plotted in figure 4-2. This

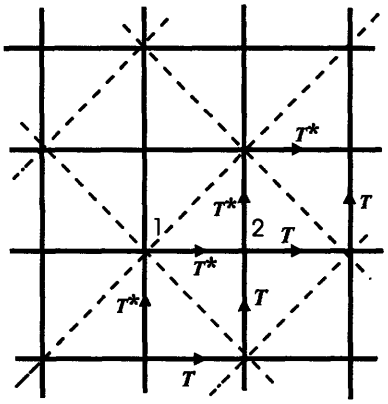

Figure 4-2: Two-site unit cells (indicated by dashed lines) used to diagonalize mean field Hamiltonian.

gives the following equation for energy eigenvalues and eigenstates:

$$\begin{bmatrix} -\frac{4}{g}N\frac{\sigma^z}{2} & \varepsilon(\mathbf{k}) - i\Delta(\mathbf{k}) \\ \varepsilon(\mathbf{k}) + i\Delta(\mathbf{k}) & \frac{4}{g}N\frac{\sigma^z}{2} \end{bmatrix} \begin{bmatrix} f_1 \\ f_2 \end{bmatrix} = E_{\mathbf{k}} \begin{bmatrix} f_1 \\ f_2 \end{bmatrix} \tag{4.6}$$

Heres, f_1 belongs to one sublattice and f_2 to the other one. We have decomposed T as $t - i\Delta$. $\varepsilon(\mathbf{k})$ and $\Delta(\mathbf{k})$ are then defined as:

$$\varepsilon(\mathbf{k}) = -2t(\cos(k_y) + \cos(k_x))$$

$$\Delta(\mathbf{k}) = 2\Delta(\cos(k_x) - \cos(k_y))$$

This gives spectrum of the two bands:

$$E_{\mathbf{k}}^{\pm} = \pm\sqrt{(\frac{2N}{g})^2 + \varepsilon(\mathbf{k})^2 + \Delta(\mathbf{k})^2} \tag{4.7}$$

Now with this in hand we can derive the self-consistency equation for N:

$$\langle -\frac{\partial H_{MF}}{\partial(\frac{4N}{g})}\rangle = \sum_r \langle \epsilon_r f_r^\dagger \frac{\sigma^z}{2} f_r\rangle = L^2 N \tag{4.8}$$

Where L is the linear system size. Using the spectral function of the

lower band (we consider $T = 0$) this gives:

$$g\ N = \frac{N}{L^2} \sum_{\mathbf{k}} \frac{1}{\sqrt{(\frac{2N}{g})^2 + \varepsilon(\mathbf{k})^2 + \Delta(\mathbf{k})^2}} \tag{4.9}$$

This equation has a trivial solution $N = 0$, but it is obvious from (4.7) that non-zero solution, if it exists, has lower energy. So the system has two phases, achieved by tuning the value of g. The critical value, g_c is given by:

$$g_c = \frac{1}{L^2} \sum_{\mathbf{k}} \frac{1}{\sqrt{\varepsilon(\mathbf{k})^2 + \Delta(\mathbf{k})^2}} \tag{4.10}$$

for $g > g_c$ there is no non-zero solution and so $N = 0$. But for $g < g_c$ we have $N \neq 0$. From (4.9) we can also derive the behavior of N at critical point within mean-field:

$$N \propto \begin{cases} 0 & for \quad g > g_c \\ g_c - g & for \quad g < g_c \end{cases} \tag{4.11}$$

Note that in the magnetic phase the non-zero N induces a gap to the spinons.

To study low energy properties, we will set up a continuum effective theory. In the next section we will include fluctuations in this continuum field theory. In the spin liquid state, the spectrum consists of two fermi points, located at $k_x = k_y = \frac{\pi}{2}$ and $k_x = -k_y = -\frac{\pi}{2}$ (at these points $\varepsilon(\mathbf{k}) = \Delta(\mathbf{k}) = 0$), in the reduced Brillouin zone. There are gapless spinon excitations near these nodes with a Dirac-like linear dispersion. A low energy description of the spin liquid is then possible

in terms of a continuum field theory of massless Dirac spinons (a brief review that helps fix notation is in appendix F). To study the magnetic transition described above within this continuum field theory, we need to introduce a 'mean field' that couples to the (π, π) component of the physical spin density. The resulting action takes the form

$$S_m = \int d^2x d\tau \bar{\psi}(-i\gamma^\mu \partial_\mu + i\lambda \ \mu^z N. \frac{\sigma^z}{2})\psi \tag{4.12}$$

In this representation, ψ consists of four two-component Dirac fields. The four Dirac fields arise from the presence of two physical spin species together with two pairs of nodes. The Pauli matrices $\vec{\sigma}$ act on the spin index while the $\vec{\mu}$ are Pauli matrices acting on the node index. It is readily seem that the combination $\frac{i}{2}\bar{\psi}\mu^z\vec{\sigma}\psi$ is precisely the continuum form of the physical spin density near (π, π). In the mean field theory N is to be determined self-consistently. The coupling λ is proportional to coupling $\frac{1}{g}$ and from now on the momenta are considered with respect to the nodes. As expected a non-zero N gaps out the Dirac spinons. This gap vanishes upon approaching the phase transition to the spin liquid. The inverse of this gap determines a diverging length scale - within the mean field theory this length scale describes the decay of the *connected* part of the spin correlations near (π, π). This may be seen by a direct calculation (described in appendix G.1) which gives:

$$e^{i\vec{Q}.\vec{r}}\langle S_i(0)S_j(r)\rangle_c \propto \frac{e^{-\frac{r}{\xi}}}{r^4}(1 + \frac{r}{\xi})\ \delta_{ij} \tag{4.13}$$

So the connected correlation for $r \ll \xi$ is a power-law decaying function with fourth power of r. For $r \gg \xi$ it is a exponential decaying function, with correlation length ξ and a pre-factor which decays as the third power of r. The correlation length at critical point diverges as:

$$\xi \propto \frac{1}{|\lambda - \lambda_c|} \sim \frac{1}{|g - g_c|} \tag{4.14}$$

4.2 Beyond mean field theory

In this Section we consider the effects of fluctuations beyond the mean field theory described above. In the spin liquid phase far from the magnetic transition the crucial fluctuations are those associated with the phase of the spinon hopping parameter. These are to be thought of as gauge fluctuations associated with a (compact) $U(1)$ gauge field that is coupled minimally to the spinons. Recent work has shown that the dRVB spin liquid is stable to such gauge fluctuations[88] (at least within a systematic large-N expansion where N is the number of Dirac spinons). We will assume that this stability persists to the physically relevant case $N = 4$. The low energy theory of the resulting phase is described by massless QED in three space-time dimensions:

$$S = \int d^2x d\tau \; \{-\bar{\psi}[i\gamma^\mu(\partial_\mu + i\ e\ a_\mu)]\psi + (\epsilon_{\mu\nu\kappa}\partial_\nu a_\kappa)^2\} \tag{4.15}$$

Here a_μ is a fluctuating $U(1)$ gauge field which may be taken to be non-compact at the low energies. This theory flows to a conformally invariant fixed point. Various physical quantities have non-trivial power

law correlations at the resultant spin liquid fixed point[96]. In particular the (π, π) spin correlator decays as a power law:

$$e^{i\vec{Q}.\vec{r}}\langle\vec{S}(0).\vec{S}(r) \sim \frac{1}{r^{2\Delta}} \tag{4.16}$$

The exponent Δ is not known - a rough estimate from projected wavefunctions[97, 98] gives $\Delta \approx 0.75$. The dynamical spin correlations at (π, π) in the scaling limit follow straighforwardly from the relativistic invariance of the field theory above. For the full zero temperature dynamical spin susceptibility, we have

$$\chi''_{SL}(q, \omega) \sim \frac{1}{\omega^{2-\eta}} F\left(\frac{\omega}{vq}\right) \tag{4.17}$$

Here $\vec{q}$ is the deviation of the wavevector from $\vec{Q} = (\pi, \pi)$, F is a universal scaling function, and v is a non-universal spinon velocity associated with the nodal Dirac dispersion. The exponent η is the anamolous dimension of the staggered spin and is related to Δ through $2\Delta = 1 + \eta$. Due to the power law spin correlations, this spin liquid phase has been dubbed as "algebraic spin liquid" (ASL)[96]. Note that the spinons are not good quasiparticles at low energies in the spin liquid phase. Indeed there presumably is no quasiparticle description of the spectrum (rather like at interacting quantum critical points). Nevertheless the field theory above in terms of spinons provides a useful description of the system.

A remarkable feature of the dRVB algebraic spin liquid phase is

the emergence of a huge global symmetry group characterizing the low energy fixed point. The low energy theory has an $SU(4)$ symmetry corresponding to free unitary rotations between the four Dirac species. In addition the irrelevance of space-time monopoles at low energies implies a non-trivial global $U(1)$ symmetry associated physically with the conservation of internal magnetic flux. Ref. [95] studied a number of consequences of the $SU(4)$ symmetry. In particular it showed that several other competing order parameters had the same power law correlators as the Neel vector - these include the order parameter associated with the columnar/plaquette VBS orders.

Near the transition to the antiferromagnetic state, we must treat the Neel field introduced in the previous section as a fluctuating vector $\vec{N}$. Further upon integrating out high energy spinons (*i.e.* ones far away from the nodes), this $\vec{N}$ field will develop some dynamics of its own. The resulting action takes the form

$$\begin{aligned} S = \int d^2x d\tau \; \{ & -\bar{\psi}[i\gamma^\mu(\partial_\mu + ie\, a_\mu)]\psi + i\lambda\bar{\psi}(\mu^z\, \vec{N}.\frac{\vec{\sigma}}{2})\psi + \\ & (\epsilon_{\mu\nu\kappa}\partial_\nu a_\kappa)^2 + \frac{(\partial_\mu \vec{N})^2}{2} + r\frac{(\vec{N})^2}{2} + \frac{u}{4!}((\vec{N})^2)^2\} \end{aligned} \tag{4.18}$$

In writing this action we have ignored anisotropies in the spinon velocities at the Dirac node and any difference between the velocities of spinon and N fields. Later we will show that all of these velocity anisotropies are irrelevant (if small) at the critical fixed point between the dRVB ASL and Neel states (see H.0.4).

In the presence of the coupling to the $\vec{N}$ field, the action no longer

has full $SU(4)$ global symmetry. An $SU(2)$ subgroup - corresponding to physical spin rotations - is still obviously a symmetry. This involves an $SU(2)$ spin rotation of the ψ field together with an $O(3)$ rotation of the $\vec{N}$ vector. In addition, the global transformation

$$\psi \to e^{i\theta\mu^z}\psi \tag{4.19}$$

with θ a constant is also a symmetry. This is a $U(1)$ subgroup of the full $SU(4)$ symmetry. Thus the action has a global $SU(2) \times U(1)$ symmetry apart from the $U_{flux}(1)$ associated with the gauge flux conservation. The extra $U(1)$ symmetry that survives from the full $SU(4)$ has the consequence that fermion bilinears such as $\bar{\psi}\mu_x\psi, \bar{\psi}\mu_y\psi$ can be freely rotated into another. In the original spin model, these operators transform identically to the VBS order parameter. The $U(1)$ symmetry then implies that the columnar and plaquette order parameters can be rotated into one another, and hence will have identical correlations.

Let us now study some general aspects of the two phases, near the phase transition.

4.2.1 Precursor fluctuations in the spin liquid

We will first consider the precursor fluctuations of the magnetic ordering in the spin liquid side.

First consider the limit $\lambda = 0$. Then the $\vec{N}$ field decouples from the spinon-gauge sector. It is instructive to think about the spectral function for the (π, π) spin correlations in the spin liquid phase in this

limit. It is simply a sum of two pieces as shown in Fig. 4-3 - a diverging power law coming from the ASL, and a sharp delta function peak coming from the N fluctuations. Now consider turning on a small non-zero λ. The low frequency divergence of the spin susceptibility will be unaffected by the coupling to the fluctuating $\vec{N}$ field (this follows from the assumed stability of the ASL fixed point). However the delta function peak coming from the $\vec{N}$ field will now be broadened due to decay into two spinons. The broadening may be described within a simple RPA approximation (for details see appendix G).

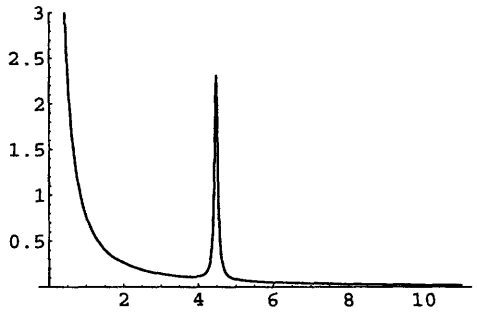

Figure 4-3: Dynamical spin susceptibility at (π,π) in the spin liquid phase in λ=0 limit

In Fig 4-4 we plot the dynamical spin susceptibility at (π, π) as the phase transition is approached (by decreasing r). Note that as expected, the peak coming from the $\vec{N}$ fluctuations "softens" on approaching the transition.

4.2.2 Magnetic state

When the parameter r is sufficiently negative the $\vec{N}$ field will condense leading to magnetic long range order. In the continuum field theory this may be viewed as a spin density wave state that arises out of the

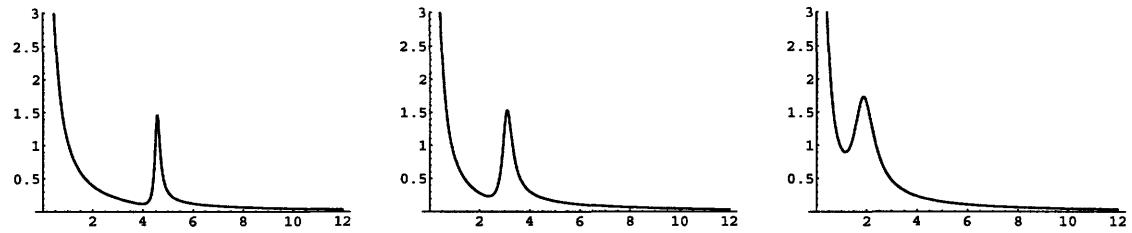

Figure 4-4: Dynamical spin susceptibility at (π, π) after turning on a nonzero value for λ. The plot shows the change upon approaching the transition from 4-4(a) to 4-4(c). Note the softening of the $\vec{N}$ peak, as the transition occurs.

dRVB ASL. In this subsection we will argue that contrary to naive expectations, it is in fact a different state from a conventional Neel state - rather it is a fractionalized antiferromagnet in the same spirit as that studied in Refs. [99, 53]. This apparent problem will be cured once we include the effects of monopole fluctuations (ignored so far). We will show that this fractionalized antiferromagnet evolves at long length/time scales into the conventional Neel antiferromagnet.

Consider first the description of the Neel ordered state within the mean field theory developed in Section 4.1. The mean field spectrum consists of *gapped* spin-1/2 spinons[1]. It is important to realize that the spinons are merely gapped - they however have not disappeared from the spectrum. Now consider including fluctuations as in Section 4.2. The important fluctuations are those associated with slow rotation of the direction of the Neel order parameter $\vec{N}$ (spin waves) and those asociated with the phase of the fermion hopping T (gauge fluctuations). These are both conveniently discussed within the continuum theory in

[1]Note that if $\vec{N} = N_0 \hat{z}$, then S^z is a good quantum number and can be used to label the states. The spinons have $S^z = \pm 1/2$.

Eqn. 4.18, that obtains close to the critical point. Integrating out the gapped spinons, we may obtain an effective action for the spin waves and the gauge fluctuations. To quadratic order in both the transverse component of the Neel vector $\vec{N}_\perp$ and the gauge field a, we get

$$S_{eff} = \int d^3x \frac{\rho_s}{2} \left(\partial_\mu \vec{N}_\perp\right)^2 + \frac{g}{2} \left(\epsilon_{\mu\nu\kappa}\partial_\nu a_\kappa\right)^2 + ... \tag{4.20}$$

where the ellipses refer to higher order terms that are unimportant at low energies. The first term describes the expected gapless spin wave excitations. The second term describes a gapless linear dispersing "photon" associated with the gauge fluctuations. This extra gapless mode provides a sharp low energy distinction between this Neel state (as described so far) and the conventional one. The gapless photon mode is minimally coupled to the gapped spinons - the presence of gapped spinons serves as another distinction with the conventional Neel state. Thus the antiferromagnet state is to be characterized as a "fractionalized antiferromagnet" with a $U(1)$ gauge structure. Following the notation of Ref. [99], we will dub it $U(1)$ AF^*.

Let us now include monopole fluctuations. In this magneticaly ordered phase, the low energy gauge action is that of free Maxwell theory in 2+1 dimensions. Then standard arguments show that the monopoles are strongly *relevant*. Thus the $U(1)$ AF^* state (in two dimensions) is ultimately unstable to monopole proliferation. The result is to gap out the photon mode and cause confinement of all objects that carry non-zero gauge charge. In particular it implies that the spinons (which

survived as gapped excitations when monopoles were ignored) will now be confined and disappear from the spectrum. The resulting state is thus simply smoothly connected to the conventional Neel state. Thus including monopole fluctuations cause an instability of the unconventional $U(1)$ AF^* state toward the conventional Neel state.

4.2.3 Projected wavefunctions

Before continuing we digress briefly to make contact with the large body of work on Gutzwiller projected superconducting wavefunctions (see Ref. [98] and references therein), as a route to implementing RVB ideas. Of interest to us, will be studies on projected d-wave BCS states and their variants. In the slave particle description, a useful guess for a prototypical wavefunction for a state is obtained by taking the mean field state and projecting it onto the space of physical states. At half-filling this is equivalent to doing a Gutzwiller projection on the mean field state. According to this prescription, a guess for the wavefunction of the dRVB algebraic spin liquid will simply be

$$|dRVB>=P_G|dBCS> \tag{4.21}$$

where $|dBCS>$ is the mean field ground state of a d-wave superconductor at half-filling with just nearest neighbour hopping and pairing on the square lattice. Correspondingly, a guess for the wavefunction of

the magnetic state, as we have obtained it, would simply be

$$|AF>= P_G|dBCS + SDW> \tag{4.22}$$

The preprojected state on the right simply has spin density wave order at (π, π) coexisting with the d-wave superconductivity. Such wavefunctions have been studied numerically[100] and are known to have excellent energy for the nearest neighbour Heisenberg model. From our considerations in the previous section, we would expect that this wavefunction is a prototype for a *confined* antiferromagnet with no finite energy spinons. Some support for this expectation comes from the work of Ref. [101] which studied the properties of a single hole in that state. The quasiparticle residue was found to be non-zero consistent with that expected in a confined antiferromagnet.

4.3 Phase transition: Generalities

Let us now consider the phase transition between the dRVB ASL and the Neel state. In the limit $\lambda = 0$, the $\vec{N}$ vector fluctuations are decoupled from the ASL and the magnetic transition is simply in the universality class of the usual $O(3)$ fixed point in $D = 3$ space-time dimensions. Note that in this limit mean field theory predicts that the Neel order parameter vanishes with exponent $\beta = 1/2$ on approaching the transition. What is the effect of turning on a weak λ at this decoupled transition? First note that in the mean field theory of Section

4.1 we found that the Neel order parameter vanished with exponent $\beta = 1$ clearly different from the $\lambda = 0$ limit. Thus a non-zero λ already changes the answers within mean field theory. More generally the effects of a weak λ may be assessed by considering the renormalization group flow of λ at the decoupled fixed point. We have

$$\frac{d\lambda}{dl} = (D - \Delta_N - \Delta)\lambda \tag{4.23}$$

where $D = 3$ is the space-time dimension, Δ_N is the scaling dimension of the N field at the $D = 3$ $O(3)$ fixed point, and Δ is the scaling dimension of the spin operator near (π, π) at the dRVB ASL fixed point. Here l is the usual logarithmic renormalization scale. We have $\Delta_N = \frac{1+\eta_N}{2} \approx \frac{1}{2}$, and $\Delta = \frac{1+\eta}{2}$. Thus $D - \Delta_N - \Delta \approx 2 - \frac{\eta}{2}$. With the rough estimate $\eta \approx 0.5$, we find that λ is strongly relevant at the decoupled fixed point. Thus the true critical behavior will involve strong coupling between the $\vec{N}$ field and the spinons of the ASL. In Section 4.4, we will study this critical behavior in a controlled $3 - \epsilon$ dimension. A very similar field theory where a fluctuating $O(3)$ vector field was coupled to massless Dirac fermions was studied many years ago by Balents et al[102] in a different physical context. The main difference between the theory of Balents et al and the action in Eqn. 4.18 is the presence of the gapless gauge fields in the latter. We will see that this modifies the universality class of the transition from that in Ref. [102].

What about monopole fluctuations at this critical point? Let us first

review the situation in the paramagnetic algebraic spin liquid state. Recent work has argued[88] that when the number of Dirac species N is sufficiently large (*i.e.* bigger than some N_c) the monopoles are formally irrelevant at the ASL fixed point[2]. In the large-N expansion, the monopole scaling dimension will be $o(N)$ both at the ASL fixed point and at the critical fixed point - thus at least for large enough N the monopoles are irrelevant at the critical fixed point as well. Here we will make the crucial assumption that this irrelevance continues to hold at $N = 4$, *i.e.* for $SU(2)$ spin models (see figure 4-5).

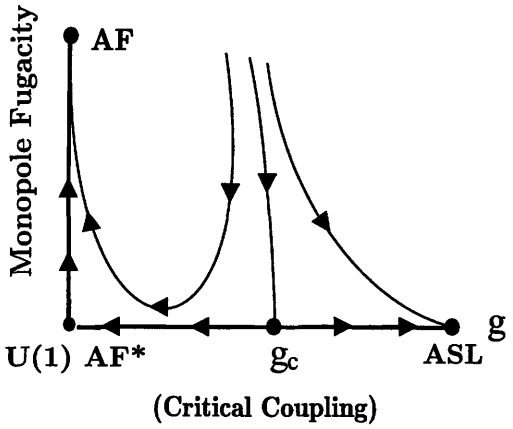

Figure 4-5: Renormalization flow diagram near the critical fixed point. The vertical axis is the monopole fugacity; the horizontal axis is a coupling g which describes the strength of the short range part of the spinon interaction.

With this assumption the monopole fugacity is irrelevant at the critical fixed point (and the paramagnetic ASL fixed point) but relevant at the ordered fixed point of the continuum field theory in Eqn. 4.18. In renormalization group language, the monopole fugacity is a dangerously irrelevant coupling. The length scale ξ_m at which the photon gets

[2]It is at present not known what the value of N_c is though existing numerical work suggests the bound $N_c < 8$. For the $SU(2)$ magnet we have $N = 4$ and have simply assumed that $N_c < 4$.

gapped (which may loosely be dubbed the "confinement scale") in the magnetic side may be estimated as follows. Let the monopole scaling dimension at the critical point be $\Delta_m > 3$. Upon scaling out of the critical region in the ordered state to the correlation length scale ξ, the monopole fugacity will renormalize to $z_\xi \sim \xi^{3-\Delta_m}$. It is beyond this scale ξ that the action in Eqn. 4.20 starts applying. In the free Maxwell theory that obtains beyond ξ, the monopole fugacity grows. A standard matching argument now gives $\xi_m \sim \xi^{(\Delta_m-1)/2}$. Thus ξ_m diverges faster than ξ. The physics on scales $\xi \ll L \ll \xi_m$ is that of the fractionalized antiferromagnet $U(1)$ AF^*. It is only at the longest scales $L \gg \xi_m$ that the conventional Neel behavior is obtained (fig. 4-6).

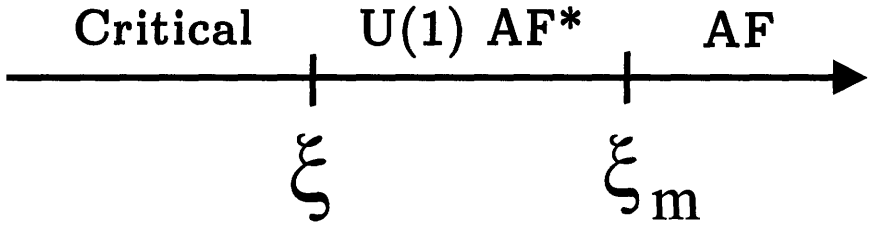

Figure 4-6: Crossover length scales in the magnetic state close to the transition to the spin liquid. The shorter length scale ξ describes the crossover from the critical state to the fractionalized antiferromagnet. The longer scale ξ_m is where this exotic antiferromagnet crosses over to the conventional Neel state through confinement. Both scales diverge near the critical point but ξ_m diverges faster than ξ.

4.4 ϵ expansion for critical properties

In this section we will show how the structure of the critical fixed point can be studied in a formal expansion near three space dimensions. Some care is necessary in dealing with the Dirac matrices in arbitrary dimen-

sion. But here following Ref. [102], we will sidestep this issue. We will perform calculations in a perturbative expansion of the coupling constants in $d = 2$, take the traces over the Dirac matrices and then finally, in evaluating momentum integrals, set $d = 3 - \epsilon$. As a warm-up we first describe the ASL fixed point within this ϵ expansion.

4.4.1 ASL in the ϵ expansion

Before starting the ϵ expansion studies for the full theory, we study ASL phase with this approach. To do that we consider action (4.18) and assume $N = 0$. Then it reduces to the usual QED_3 action. The flow equation for this theory is well known[103] (and also calculated in appendix G.1):

$$\beta_{e^2} = \epsilon e^2 - \frac{16}{3}\frac{e^4}{(4\pi)^2} \tag{4.24}$$

Here $\epsilon = 3 - d$. This flow equation indicates the presence of nontrivial fixed point of order ϵ at:

$$e^{*2} = 3\pi^2\epsilon \tag{4.25}$$

This is the pure ASL fixed point. The microscopic derivation of the continuum field theory for the spin liquid allows for a velocity anisotropy between the two spinon nodes. This anisotropy was found to be irrelevant in the large-N limit of QED_3[104, 105, 95]. Here we examine its fate within the ϵ expansion. Direct calculation (appendix H.0.4) shows that $\beta_\delta = -\delta\frac{14}{3(4\pi)^2}\, e^{*2} = -\frac{7}{8}\,\delta\,\epsilon$, where δ measures the velocity anisotropy (*i.e.* $\delta = 0$ corresponds to isotropic QED_3). So that it is

irrelevant at $o(\epsilon)$. Combined with the large-N result, this is strong evidence for its irrelevance at the physically relevant ASL fixed point for $N = 4$ in two space dimensions. As noted in previous papers[95] this irrelevance implies that the $N = 4$ ASL fixed point has global $SU(4)$ symmetry corresponding to free unitary rotation between the four Dirac species.

Finally we can examine the scaling of gauge neutral fermion bilinears (such as the Neel vector) in the ϵ-expansion. This is conveniently done by adding a source term that couples to such a bilinear, and calculating the one loop correction to the corresponding vertex (see appendix G.1). We find that the (π, π) component of the spin has scaling dimension $\Delta = 3 - 1.94\epsilon$. Setting $\epsilon = 1$ gives the estimate $\Delta \approx 1.06$. This implies extremely slow decay of the corresponding correlator. This estimate may be compared with that from the $1/N$ expansion directly in $d = 2$ which gives $\Delta \approx 1.54$. Thus both expansions give slow decay for the Neel correlations that are strongly enhanced compared to the mean field results.

4.4.2 Critical fixed point

In this section we study the critical point within the ϵ expansion by including the fluctuating $\vec{N}$ field. ¿From the action (4.18) we have three types of vertices and eleven different one loop diagrams. At one loop level, as derived in appendix G.1, we get the following set of flow

equations:

$$\beta_{e^2} = \epsilon e^2 - \frac{16}{3}\frac{e^4}{(4\pi)^2} \tag{4.26}$$

$$\beta_{\lambda^2} = \epsilon\lambda^2 - \frac{10}{(4\pi)^2}\lambda^4 + \frac{10}{(4\pi)^2}e^2\lambda^2 \tag{4.27}$$

$$\beta_u = \epsilon u - \frac{11}{3}\frac{u^2}{(4\pi)^2} - 16\frac{\lambda^2 u}{(4\pi)^2} + 96\frac{\lambda^4}{(4\pi)^2} \tag{4.28}$$

$$\beta_r = (2 - \frac{5}{3}\frac{u}{(4\pi)^2} - 8\frac{\lambda^2}{(4\pi)^2})r \tag{4.29}$$

Note that flow equation for electric charge is the same as usual quantum electrodynamics. In fact, gauge invariance dictates this form[106, 103] (to keep the form $e\ a_\mu$ invariant under RG flow we need to have $Z_e/\sqrt{Z_a} = 1$). From these we can get the following fixed points:

$$e^{*2} = 0 \tag{4.30}$$

$$\lambda^{*2} = \frac{8\pi^2}{5}\epsilon \tag{4.31}$$

$$u^* = \frac{384\pi^2}{55}\epsilon \tag{4.32}$$

This fixed point describes the transition in the absence of the gauge field and was first discussed by Balents et al[102]. Our calculations at this fixed point matches this previous work which therefore provides a useful check. As another check at this fixed point, if we consider our theory, with the three component $\vec{N}$ field replaced by a scalar field ϕ, it represent a Yukawa like theory, which has been studied in Ref. [103]. Our results then can be partially checked against these previous calculations. The full flow equations admit another fixed point located

at:

$$e^{*2} = 3\pi^2\epsilon \tag{4.33}$$

$$\lambda^{*2} = \frac{23\pi^2}{5}\epsilon \tag{4.34}$$

$$u^* = \frac{12\pi^2}{55}(-36+\sqrt{12934})\epsilon \tag{4.35}$$

It is readily checked that the $e^2 = 0$ fixed point is unstable towards this one. Thus the presence of the gauge field has changed the universality class of the transition. Here we should also note that the at the one loop level, calculation in appendix H.0.4 shows that at this fixed point, the velocity anisotropy is irrelevant at $o(\epsilon)$. So this fixed point is also stable against small velocity anisotropy. Now using the flow equation for r (Eqn. 4.29), it is easy to extract exponent ν for this fixed point:

$$\frac{1}{\nu} = 2 - 4.07\epsilon \tag{4.36}$$

Note that simply setting $\epsilon = 1$ gives an unphysical answer. This is a signal that the leading order ϵ expansion is not quantitatively very accurate in estimating scaling dimensions in two space dimensions. Despite this the ϵ expansion is useful to describe the structure of the fixed points and the trends of the various exponents.

It is very interesting to ask about the behavior of the staggered spin correlations (*i.e.* near (π, π)) at this critical point. Naively there are two different physical operators that have the same symmetries as the staggered spin: the vector $\vec{N}$ and the fermion bilinear $\vec{N}^z_A = \bar{\psi}\mu_z\vec{\sigma}\psi$.

Thus in writing down an expression for the staggered spin in terms of the fields of the continuum theory, we must include both contributions:

$$e^{i\vec{Q}.\vec{x}}\vec{S}(\vec{x}) \sim c_1\vec{N} + c_2\vec{N}_A^z + ... \tag{4.37}$$

The ellipses refer to other operators with larger scaling dimension that also have the same symmetries as the staggered spin. The coefficients $c_{1,2}$ are non-universal. Now consider the scaling of the staggered spin. If $\lambda = 0$, then the fermion bilinear and $\vec{N}$ scale independently. Near $d = 3$, and with the available estimate of the scaling dimension of the fermion bilinear at the ASL, it is readily checked that $\vec{N}$ has the lower scaling dimension. Hence the long distance decay of the staggered spin correlations will be determined by $\vec{N}$ in the $\lambda = 0$ limit. What happens when λ is non-zero as at the non-trivial fixed point above in the ϵ expansion? It is expected that the true scaling fields will be some linear combinations of $\vec{N}$ and $\vec{N}_A^z$ which will have the form

$$\vec{\phi}_1 \sim A_1\vec{N} + A_2\vec{N}_A^z \tag{4.38}$$

$$\vec{\phi}_2 \sim B_1\vec{N} + B_2\vec{N}_A^z \tag{4.39}$$

These fields will have scaling dimension $\Delta_{1,2}$ with (by definition) $\Delta_1 < \Delta_2$ so that the long distance decay will be dominated by $\vec{\phi}_1$. The coefficients $A_{1,2}$ and $B_{1,2}$ will be determined by the fixed point theory. At $o(\epsilon)$ we expect $A_1 \sim o(1), A_2 \sim o(\epsilon), B_1 \sim o(\epsilon), B_2 \sim o(1)$. Thus to obtain the scaling dimensions $\Delta_{1,2}$ to $o(\epsilon)$ we can ignore the 'mixing'

terms A_2, B_1, and simply calculate the anamolous dimension of $\vec{N}$ and $\vec{N}_A^z$.

The exponent η for N field (which determines the scaling dimension) is easily calculated from the field renormalization coefficient Z_N:

$$Z_N = 1 - \frac{8}{(4\pi)^2}\frac{\lambda^2}{\epsilon} \tag{4.40}$$

η is then given by coefficient of $\frac{1}{\epsilon}$ in Z_N:

$$\eta = 2.3\epsilon \tag{4.41}$$

so that $\Delta_1 = 1 + 0.65\epsilon$. The dimension Δ_2 is readily calculated as in our discussion of the ASL above. We find $\Delta_2 = 3 - 1.65\epsilon$.

It is straightforward to determine the scaling dimension of all the fermion bilinears related to $\vec{N}_A^z$ by $SU(4)$ rotations. These are listed in Table 4.1; the corresponding Feynman diagrams are in Appendix G.1. The absence of $SU(4)$ symmetry at the critical fixed point implies that these bilinears mostly all have different scaling dimensions. Some weak constraints follows from the $U(1)$ subgroup of the $SU(4)$ that remains unbroken. For instance it implies that N_A^x, N_A^y have the same scaling dimension. As emphasized before physically this implies identical scaling of the plaquette and columnar VBS order parameters at this critical point.

Field theory	Spin Model	Scaling dimension
$\vec{N}_A^x$, $\vec{N}_A^y$	$(-1)^{r_x+1}\vec{S}_r \times \vec{S}_{r+\vec{y}}$, $(-1)^{r_y}\vec{S}_r \times \vec{S}_{r+\vec{x}}$	3-0.5ϵ
$\vec{N}_A^z$	$(-1)^{r_x+r_y}\vec{S}_r$	3-1.65ϵ
$\vec{N}_B$	$(-1)^{r_x+r_y}[(\vec{S}_1+\vec{S}_3)(\vec{S}_2\cdot\vec{S}_4)$ $+(\vec{S}_2+\vec{S}_4)(\vec{S}_1\cdot\vec{S}_3)]$	3-1.65ϵ
N_C^x , N_C^y	$(-1)^{r_y}\vec{S}_r\cdot\vec{S}_{r+y}$, $(-1)^{r_x}\vec{S}_r\cdot\vec{S}_{r+x}$	3-2.8ϵ
N_C^z	$[\vec{S}_1\cdot(\vec{S}_2\times\vec{S}_4)-\vec{S}_2\cdot(\vec{S}_3\times\vec{S}_1)$ $+\vec{S}_3\cdot(\vec{S}_4\times\vec{S}_2)-\vec{S}_4\cdot(\vec{S}_1\times\vec{S}_3)]$	3+0.65ϵ

Table 4.1: List of observable in the spin model that are symmetry-equivalent to the N^a and M fermion bilinears. For some of these we label the sites around the plaquette with lower-left corner at $\vec{r}$ by the numbers $1,\ldots,4$. Precisely, $\vec{S}_1 = \vec{S}_r$, $\vec{S}_2 = \vec{S}_{r+x}$, $\vec{S}_3 = \vec{S}_{r+x+y}$ and $\vec{S}_4 = \vec{S}_{r+y}$.

Here we have defined the observable as:

$$\vec{N_A}^i = -i\bar{\psi}\mu^i\vec{\sigma}\psi \tag{4.42}$$

$$\vec{N_B} = -i\bar{\psi}\vec{\sigma}\psi \tag{4.43}$$

$$N_C{}^i = -i\bar{\psi}\mu^i\psi \tag{4.44}$$

We see that $\vec{N_A}^z$ corresponds to Neel vector and $iN_c^x + N_c^y$ corresponds to VBS order parameter.

4.4.3 Discussion

Now let us examine the trends shown by the exponents calculated in table 4.1. Note that the scaling dimension of these gauge invariant bilinears are the same in ASL phase due to the $SU(4)$ symmetry. So for all of them we have $\Delta = 3-1.94\epsilon$. Remarkably the scaling dimension of the VBS order parameter (N_C^x, N_C^y) is *smaller* at the critical point than it is in the ASL phase. Thus the VBS fluctuations are *enhanced* by the

critical $\vec{N}$ vector fluctuations. All other fermion bilinears decay faster at the critical point as their scaling dimension is increased. This includes the vector $\vec{N_A}^z$ which is the contribution from the gapless fermions to the Neel vector. It is at present not clear whether in $d = 2$ the susceptibilities of these other operators (such as $\vec{N}_A^x$, etc) will diverge at the critical point (though they apparently do in the ASL phase). In contrast the VBS susceptibility will presumably diverge at the critical point. The divergence will be faster at the critical point (as say a function of temperature) than in the ASL phase. On the magnetic side the VBS susceptibility will of course be finite in the ground state. However it will diverge as the transition is approached and will thus be large if the antiferromagnet is to be regarded as being close to this critical point. Thus a qualitative conclusion from our calculations is that in the limit that the Neel state can be usefully regarded as being born out of the dRVB spin liquid, it will also have enhanced VBS susceptibility.

The diverging VBS susceptibility also provides an interesting way to define the corelation length ξ in terms of directly measurable quantities. Consider the VBS corelations in the magnetic side as a function of length scale. At scales smaller than ξ they will decay as a power law. However at scales larger a length set by ξ, they will decay exponentially. Thus ξ may be usefully defined as the correlation length for VBS fluctuations in the ordered antiferromagnet.

4.5 Implications for cuprate theory

We now discuss some of the implications of our results for theories of the cuprates. As we emphasized in the introduction, a second order transition between a collinear Neel state and a gapless spin liquid is attractive for a number of reasons. Here we explore this in some greater detail. Our thinking on the cuprates is guided by Fig 4-1. We suppose that increasing magnetic frustration (the parameter g) at zero doping can induce a transition out of the collinear Neel state to a spin liquid. Theoretically the spin liquid is expected to evolve rather naturally into a superconductor when it is doped. The real material starts off in the antiferromagnetic state at zero doping. The idea is that doping (apart from introducing holes) also has the effect of increasing g. Then we can hope that the intermediate and long scale physics of the resulting doped superconductor may be fruitfully described as a doped spin liquid. This is the rationale behind the spin liquid based approach to the cuprates.

With this point of view in mind let us consider the effects of doping the dRVB algebraic spin liquid. Previous papers (for a review see Ref. [21]) have shown how a d-wave superconductor with gapless nodal quasiparticles emerges quite naturally upon doping this spin liquid. Now consider reducing the doping in the real material. According to Fig 4-1 this also has the effect of reducing the magnetic frustration g. This pushes the "parent" spin liquid state closer to the transition to antiferromagnetism. The magnetic response of the parent spin liquid at wave vector (π, π) then evolves in the manner shown in Fig 4-4. Note

in particular that if the transition to the magnetic state is second order then the "resonance" due to the $\vec{N}$ fluctuations softens. How does this impact the magnetic response in the doped superconductor?

The doping of the spin liquid is incorporated theoretically by the introduction of two species of charged spinless bosons b_1 and b_2. These bosons also carry gauge charges $+1$ and -1 respectively. Superconductivity is achieved when both b_1 and b_2 condense with equal amplitude. This route from the dRVB spin liquid to the dSC has two important features. First the gauge charge carried by the bosons implies that the gapless gauge fluctuations of the spin liquid are quenched in the superconducting state (by the Anderson Higgs mechanism). The spinons evolve naturally into the fermionic quasiparticle excitations of the dSC. The nodal structure of the spinons is retained - however coupling between the b and f fields moves the nodes of the quasiparticles away from $(\pi/2, \pi/2)$ by an amount proportional to the doping x.

For the magnetic response this has some crucial implications. First when compared with Fig 4-4, the diverging low frequency response is killed as it comes entirely due to the gapless gauge fluctuations of the spin liquid. The resonance due to the triplon $\vec{N}$ mode then becomes the most prominent feature in the (π, π) response. Further its frequency will soften as the doping is reduced. Second as the fermionic quasiparticles no longer have nodes at (π, π) they only weakly damp out this reonance. Finally the fermionic quasiparticles will still contribute some background magnetic response which can now be usefully addressed in a

standard RPA calculation. Such calculations have been reported before in the literature, and give rise to incommensurate continuum scattering at frequencies below the resonance that appear to be consistent with experiment.

Since the original discovery of the neutron resonance peak, there have been two more or less independent interpretations. One view is to describe it as a soft mode associated with the magnetism of the undoped Mott insulator. This view has the advantage that it provides a natural explanation of the softening of the resonance frequency with underdoping. The other view has been to simply regard it as a $S = 1$ collective mode of weakly correlated fermionic quasiparticles in the superconducting state. The description given above unifies these two different interpretations. Indeed in the parent spin liquid the triplon $\vec{N}$ mode may be viewed as a particle-hole triplet exciton made out of *spinons* - rather than electrons. This mode appears naturally as a recognizable peak in the magnetic response upon approaching the AF state. Doping this spin liquid then leads to a superconductor with gapless fermionic quasiparticles and a sharp gapped $S = 1$ triplon.

Chapter 5

Conclusions

In this thesis I tried to address some of the challenges in correlated electron systems. Although the title is much broader than what covered in this thesis, I hope that I could have at least developed new insight into some interesting phases and phase transitions in strongly correlated systems during my PhD.

My main focus here was on two important strongly correlated systems, cuprate superconductors and heavy fermions. But the ideas developed here might be used in correlated electron systems in general.

The example of the cuprate materials shows that correlation effects may not uniformly affect all regions of the fermi surface. The result is strong correlation induced anisotropy along the fermi surface. Theoretical approaches to addressing such effects are hampered by the difficulty that correlation effects are easiest to handle in real space and not in momentum space. In this thesis in the specific case of Kondo lattices, we have shown how to incorporate momentum space information into the Kondo singlet formation that determines the fate of the local

moments at low temperature. We explored the properties of metallic 'fermi liquid' states driven by Kondo singlet formation in a channel with non-zero internal angular momentum. Through out chapter 2.2 we focused on two dimensional systems. We showed that such metallic states naturally have strong anisotropy of the quasiparticle effective mass and residue on moving around the fermi surface. In some cases the quasiparticle residue even vanishes at four isolated points on the fermi surface. The excitations at such points may be thought of as neutral spin-1/2 spinons that occur without any residual 'gauge' interactions. Thus these states provide interesting examples where strongly anisotropic quasiparticle residues are naturally built into the symmetry of the states. We also studied two dimensional Kondo *insulators* driven by Kondo singlet formation with complex internal angular momentum and showed that they have a quantized non-trivial electrical Hall conductivity. Such Kondo insulators thus present an interesting situation where a quantum Hall effect occurs due to the Kondo effect. Exploiting the ideas of this thesis to develop techniques for thinking about the angle dependence of correlation effects in momentum space is an interesting challenge for the future.

We also noted that anisotropic hybridization is directly relevant for real Kondo lattices. In these systems a singlet is formed between conduction electrons and local moments which are in d or f orbital. The singlet then naturally have non-zero angular momentum. We mentioned that this might have observable effects in ARPES experiments

which is starting to be done on heavy fermion compounds[35]. It remains as an open problem to find other experimental methods to observe this effect. STM experiments to detect the density profile of an external impurity might be one possibility.

We also explored the possibility that the pseudogap state of the underdoped cuprates may be a large surface fermi liquid state with a strongly angle dependent Z. While such a picture has some very appealing features it has enough difficulties with experiments that it is unlikely to directly be a relevant theory of the pseudogap state.

In this thesis studies on Kondo lattices were done in heavy fermi liquid phase. Experiments on heavy fermion compounds have shown, within the accuracy of experiments, direct transition between this heavy fermi liquid phase and a phase where local moments have antiferromagnetic order. Although scenarios for transition between heavy Ferm liquid phase and a phase with local moments in spin liquid state have been developed (see [46]), the full transition is still a big challenge. In the last chapter, we examined a transition between two insulating states of correlated electron systems. This transition between Neel and spin liquid phases, might be enlightening to describe the full heavy fermions phase transition transition, although we highlighted the differences between the two models. But the main motivation for this chapter was observations in cuprates.

In chapter 4 we have revisited the issue of possible second order phase transitions out of the collinear Neel state into paramagnetic spin

liquid states in two dimensional quantum antiferromagnets. The particular spin liquid we considered is a $dRVB$ state which has gapless spin excitations. Correspondingly there are non-trivial power law corelations in the spin and other quantities. A useful description is provided in terms of gapless Dirac-like spinons that are coupled to a fluctuating $U(1)$ gauge field. However there is possibly no true quasiparticle description of the spectrum. Indeed this state is in a critical phase that is the two dimensional analog of the one dimensional spin-1/2 chain. In contrast to other simpler spin liquids which have a spin gap, a direct second order transition to the collinear Neel state appears to be possible for such a two dimensional algebraic spin liquid. We developed in some detail a theory for such a transition. Magnetic long range order was obtained as a spin density wave transition of spinons.

We argued that gauge fluctuations convert the resulting magnetic state into a conventional one that is smoothly connected to the usual Neel state. Thus the spinons disappear from the spectrum in the magnetic state. The theory for the transition shares a number of similarities with the deconfined critical points studied recently [11]. Most importantly, there are two diverging length/time scales as the transition is approached from the magnetic side. The shorter of the two scales is associated with the onset of magnetic order from a critical soup of spinons. The second longer scale is associated with confinement of the spinons. It is in the intermediate length/time scale regime (*i.e.* between the two diverging lengths) that the magnetic ordering is correctly described as

a spin density wave formed out of spinons. This intermediate scale regime may also be characterized as a fractionalized antiferromagnet.

We noted several implications of our results for theories of the cuprates that regard them as doped spin liquids. First it allows us to develop a qualitative picture of the resonance mode seen in neutron experiments. Our picture unifies the existing descriptions as a soft mode associated with the magnetic ordering in the insulator and as a triplet excition formed from a particle-hole pair of fermionic BCS quasiparticles. Indeed in our description the resonance is a soft mode of the magnetic ordering that is formed as a particle-hole triplet exciton of *spinons*. This picture is closest to that in Ref. [86].

We have shown how magnetism may be incorporated into the spin liquid based approach to the cuprates. Central to this is the description of magnetism as a spin density wave ordering of spinons. Such a description has been explored before in a number of publications. As summarized in the first paragraph of this section, our work clarifies the range of validity of such a description. Indeed should experiments reveal clear signatures for a fermionic spinon description of the intermediate scale spin physics of the undoped cuprates then we could take that to be a signature of proximity to the quantum transition to the dRVB algebraic spin liquid.

The ideas in this thesis were presented in one band and two band correlated models relevant to theories of cuprates and heavy fermions respectively. But I hope that the general frame work could be extended

to other cases and open new research directions in Physics of strongly correlated systems.

Appendix A

Maximum energy of d-wave Kondo in Brillouin zone

As derived before, lower band energy at each point of Brillouin zone (BZ) is given by

$$E_{\mathbf{k}}^{-} = \frac{\epsilon_{\mathbf{k}} + \mu_f}{2} - \sqrt{(\frac{\epsilon_{\mathbf{k}} - \mu_f}{2})^2 + V_{\mathbf{k}}^2} \tag{A.1}$$

where $V_{\mathbf{k}} = V(\cos(k_x) - \cos(k_y))$. So $V_{\mathbf{k}} = 0$ only along diagonal directions. From A.1, we see for all points in BZ:

$$E_{\mathbf{k}}^{-} \leq \frac{\epsilon_{\mathbf{k}} + \mu_f}{2} - \sqrt{(\frac{\epsilon_{\mathbf{k}} - \mu_f}{2})^2} \tag{A.2}$$

Right hand side of the above equation is equal to μ_f for $\mu_f < \epsilon_{\mathbf{k}}$ and $\epsilon_{\mathbf{k}}$ for $\epsilon_{\mathbf{k}} < \mu_f$. Putting these together we get:

$$\begin{cases} E_{\mathbf{k}}^{-} \leq \epsilon_{\mathbf{k}} & for \quad \epsilon_{\mathbf{k}} \leq \mu_f \\ E_{\mathbf{k}}^{-} \leq \mu_f & for \quad \epsilon_{\mathbf{k}} > \mu_f \end{cases} \tag{A.3}$$

You see that all points in BZ, obviously, satisfy one the two conditions ($\epsilon_{\mathbf{k}} \leq \mu_f$ or $\epsilon_{\mathbf{k}} > \mu_f$). So we get for any point in the BZ:

$$E_{\mathbf{k}}^{-} \leq \mu_f \tag{A.4}$$

A closer look at equations A.1 and A.2, shows that equality in equation A.4, could be only for the points along diagonal direction with $\epsilon_{\mathbf{k}} > \mu_f$. Such points cover a region with zero volume in the BZ. So that for any finite doping $E_f < \mu_f$ (see section 2.2).

Appendix B

Self consistency equation for d-wave Kondo

Analytic treatment of self consistency relation is easier and much more clear at zero doping ($\mu_f = 0$). So we start with this case and later, we can argue if our result might be modified at finite, but small, doping. In continuum limit, self consistency relation (at zero doping) have the form:

$$\frac{1}{J_k} = \frac{1}{2n} \int \frac{d^2k}{(2\pi)^2} \frac{(\cos(k_x) - \cos(k_y))^2}{\sqrt{(\frac{\epsilon_\mathbf{k}}{2})^2 + V^2(\cos(k_x) - \cos(k_y))^2}} \tag{B.1}$$

where n is density of lattice sites. We saw before that, this equation for V has a solution, no matter how small J_k is (see section 2.1). This was because, the integral is divergent at $V = 0$. The divergence comes from the region where $\epsilon_\mathbf{k}$ is small. So to study the behavior of this integral, it is enough to look at the points where $\epsilon_\mathbf{k}$ is small. Because of the symmetry of BZ with respect to 90° rotation, it is enough to consider region with $k_x, k_y \geq 0$. The point with $\epsilon_\mathbf{k} = 0$ in this region, are points

with $k_x = \pi - k_y$. We want to look around such points so if we change the variables to $k_y \to k_y$ and $k_x \to q = k_y + k_x - \pi$, we just want to look at region with small q. Putting these variables in to in to B.1 and expanding up to first non-zero order in q, we get:

$$\frac{1}{J_k} = \frac{1}{2n} \int \frac{dk_y dq}{(2\pi)^2} \frac{(\sin(k_y)q + 2\cos(k_y))^2}{\sqrt{(t\sin(k_y)q)^2 + V^2(\sin(k_y)q + 2\cos(k_y))^2}} \tag{B.2}$$

As discussed before, we like to study the singular behavior around $q = 0$ so we can ignore the q dependence in non-singular terms. The relation simplifies to:

$$\frac{1}{J_k} = \frac{1}{2n} \int \frac{dk_y dq}{(2\pi)^2} \frac{(2\cos(k_y))^2}{\sqrt{(t\sin(k_y)q)^2 + V^2(2\cos(k_y))^2}} \tag{B.3}$$

Now we first perform the integral over k_y. Note that the limits for this is q dependent (i.e. $0 + O(q^2)$ and $\pi + O(q^2)$) but these also could be ignored since they have no effect on singular behavior:

$$\frac{1}{J_k} = \frac{1}{2n} \int \frac{dq}{2\pi} \int_0^\pi \frac{dk_y}{(2\pi)} \frac{(2\cos(k_y))^2}{\sqrt{(t\sin(k_y)q)^2 + V^2(2\cos(k_y))^2}} \tag{B.4}$$

Integral over k_y could be perform exactly which gives:

$$\frac{2}{|q|} \, {}_2F_1(\frac{1}{2}, \frac{3}{2}; 2; 1 - \frac{V^2}{q^2}) \tag{B.5}$$

here, ${}_2F_1$ is Hypergeometric Function. We are in interested in small q behavior so $1 - \frac{V^2}{q^2} \approx -\frac{V^2}{q^2}$. The expression could be simplified using

the identity[107]:

$$ {}_2F_1(a,b;c;z) = (1-z)^{-a}\ {}_2F_1(a,c-b;c;\frac{z}{z-1}) $$

Using this for the result of integral we get:

$$ \frac{1}{J_k} \approx \frac{1}{2n}\int \frac{dq}{2\pi}\frac{2}{\sqrt{q^2+V^2}}\ {}_2F_1(\frac{1}{2},\frac{1}{2};2;1) \tag{B.6} $$

where we used the fact $\frac{-\frac{V^2}{q^2}}{-\frac{V^2}{q^2}-1} \approx 1$. Since ${}_2F_1(\frac{1}{2},\frac{1}{2};2;1)$ is convergent[107] we get:

$$ \frac{1}{J_k} = A\int \frac{dq}{\sqrt{q^2+V^2}} \tag{B.7} $$

where A is a finite constant. Integral over q is now trivial and leads to result mentioned before (see section 2.2):

$$ V \propto e^{-\frac{C}{J_k}} \tag{B.8} $$

After dopinping, continuum form of self consistency relation changes:

$$ \frac{1}{J_k} = \frac{1}{2n}\int \frac{d^2k}{(2\pi)^2}\ \Theta(E_f - E^-\mathbf{k}) \frac{(\cos(k_x)-\cos(k_y))^2}{\sqrt{(\frac{\epsilon_\mathbf{k}-\mu_f}{2})^2 + V^2(\cos(k_x)-\cos(k_y))^2}} \tag{B.9} $$

Again dominant contribution comes from the region where $|\epsilon_\mathbf{k} - \mu_f|$ is small. Similar expansion could be carried out but this time the points we look at are close to different curve (defined by $\cos(k_x)+\cos(k_y) = \frac{\mu_f}{2t}$ which is slightly away from $k_x = \pi - k_y$ for small μ_f). We don't expect

(and in fact the resulting integral shows) that there is not much change in singular behavior as V goes to zero. So we expect that behavior seen in B.8 holds and in fact this is confirmed with numerical studies.

Appendix C

Density of states of d-wave Kondo liquid

To get density of states we use the general formula[108]:

$$\rho(E_f) = \int \frac{d^2k}{(2\pi)^2}\, \delta(E_f - E^-_{\mathbf{k}}) \tag{C.1}$$

Again symmetries in BZ are helpful. First of all we can do the calculation on one patch of Fermi surface (in $k_x \leq 0$ and $k_y \leq 0$ quarter). Also because of reflection symmetry respect to diagonal, we can do the calculation for the points on Fermi surface which are above the diagonal and double the result. Now in this region we can safely (since $\epsilon_{\mathbf{k}}$ is one to one function of (k_x, k_y)) do the change of variable, and work with k_y and $\epsilon_{\mathbf{k}}$:

$$\rho(E_f) = \int \frac{dk_y}{(2\pi)^2} \frac{d\epsilon_{\mathbf{k}}}{2t\sqrt{1-(\frac{\epsilon_{\mathbf{k}}}{2t} - \cos(k_y))^2}}\, \delta(E_f - E^-_{\mathbf{k}}) \tag{C.2}$$

Note that $\sqrt{1-(\frac{\epsilon_{\mathbf{k}}}{2t} - \cos(k_y))^2} = \sin(k_x)$ is never zero in the part of

BZ we are integrating over. In terms of new variables:

$$E_{\mathbf{k}}^{-} = \frac{\epsilon_{\mathbf{k}} + \mu_f}{2} - \sqrt{(\frac{\epsilon_{\mathbf{k}} - \mu_f}{2})^2 + V^2(\frac{\epsilon_{\mathbf{k}}}{2t} - 2\cos(k_y))^2} \tag{C.3}$$

Using this we first do the integration over $\epsilon_{\mathbf{k}}$ which leads to:

$$\rho(E_f) = \int \frac{dk_y}{(2\pi)^2} \frac{1}{2t\sqrt{1 - (\frac{\epsilon}{2t} - \cos(k_y))^2}} \left(\frac{1}{2} - \frac{\frac{\epsilon - \mu_f}{4} + (V^2/2t)(\frac{\epsilon}{2t} - 2\cos(k_y))}{\sqrt{(\frac{\epsilon - \mu_f}{2})^2 + V^2(\frac{\epsilon_{\mathbf{k}}}{2t} - 2\cos(k_y))^2}} \right)^{-1} \tag{C.4}$$

here, ϵ is solution of equation:

$$E_{\mathbf{k}}^{-} = E_f$$

for $\epsilon_{\mathbf{k}}$, which is a simple second order equation but we avoid presenting the answer which is not necessary for the rest of calculation. Now to proceed we need to divide to points in three different regions. The first region is defined by the points where:

$$(\frac{\epsilon_{\mathbf{k}} - \mu_f}{2})^2 \sim V^2(\frac{\epsilon_{\mathbf{k}}}{2t} - 2\cos(k_y))^2$$

for these points contribution to C.4 is of order one.

The other regions are where:

$$(\frac{\epsilon_{\mathbf{k}} - \mu_f}{2})^2 \gg V^2(\frac{\epsilon_{\mathbf{k}}}{2t} - 2\cos(k_y))^2 \tag{C.5}$$

This contains most of the points on the Fermi surface, since from B.8

we know that V is small. Now we expand expression in prentices in C.4 up to first non-zero order in V^2:

$$\rho(E_f) = \int \frac{dk_y}{(2\pi)^2} \left(\frac{1}{2}(1 - Sign(\epsilon_{\mathbf{k}} - \mu_f)) + \frac{V^2}{t^2} f(\epsilon, k_y) \right)^{-1} \tag{C.6}$$

here $f(\epsilon, k_y)$ is convergent function. We don't need the detailed form of this function though. The important property of this integral is that for points with $\epsilon_{\mathbf{k}} < \mu_f$ (which corresponds to points near diagonal as discussed in A) contribution to integral is of order one. We expected this since in this region quasi-particles are more free electron like. However for points with $\epsilon_{\mathbf{k}} > \mu_f$ (which are away from diagonal) contribution is large and proportional to V^{-2}. Putting all these together we get a large density of state:

$$\rho(E_f) \propto e^{\frac{2C}{J_k}} \tag{C.7}$$

Appendix D

Kubo calculation

Using equation 2.35 we can write J_μ as:

$$J_\mu(\tau) = \sum_{\mathbf{k}} \psi^\dagger(\tau)(\partial_\mu a(\mathbf{k}) + \partial_\mu \vec{m}(\mathbf{k}).\vec{\sigma})\psi(\tau) \tag{D.1}$$

where $\vec{m(\mathbf{k})}$ is defined in 2.34 and $a(\mathbf{k}) = \frac{\epsilon_\mathbf{k}+\mu_f}{2}$. Also ∂_μ is the shorthand for $\frac{\partial}{\partial k_\mu}$. Putting this form in Kubo formula[57] we get:

$$\begin{aligned}\sigma_{\mu\nu}(\omega) = \int d\tau \frac{e^{-i\omega\tau}-1}{\omega} \times \\ \sum_{k,k'} \langle \psi^\dagger(\tau)(\partial_\mu a(\mathbf{k}) + \partial_\mu \vec{m}(\mathbf{k}).\vec{\sigma})\psi(\tau) \\ \psi^\dagger(0)(\partial_\nu a(k') + \partial_\nu \vec{m}(k').\vec{\sigma})\psi(0)\rangle\end{aligned} \tag{D.2}$$

Using the Hamiltonian given in 2.33 we get the green function for ψ fields:

$$G(i\omega, k) = \frac{1}{i\omega - a(\mathbf{k}) - \vec{m}(\mathbf{k}).\vec{\sigma}} \tag{D.3}$$

With this in hand, the Kubo equation reduces to the following form:

$$\omega\sigma_{xy}(\omega) = \sum_{\mathbf{k}} \int \frac{dE}{2\pi}$$
$$tr\left[\frac{(\partial_x a(\mathbf{k}) + \partial_x \vec{m}(\mathbf{k}).\vec{\sigma})(\partial_y a(\mathbf{k}) + \partial_y \vec{m}(\mathbf{k}).\vec{\sigma})}{(iE - a(\mathbf{k}) - \vec{m}(\mathbf{k}).\vec{\sigma})} \times \right. \tag{D.4}$$
$$\left.\left(\frac{1}{(i(\omega + E) - a(\mathbf{k}) - \vec{m}(\mathbf{k}).\vec{\sigma})} - \frac{1}{(iE - a(\mathbf{k}) - \vec{m}(\mathbf{k}).\vec{\sigma})}\right)\right]$$

We are interested in the limit of above equation as $\omega \longrightarrow 0$. In this limit we get the following expression for Hall conductivity:

$$\sigma_{xy} = -i \int \frac{d^2k}{(2\pi)^2} \frac{dE}{2\pi}$$
$$tr\left[(\partial_x a(\mathbf{k}) + \partial_x \vec{m}(\mathbf{k}).\vec{\sigma}) \frac{1}{(iE - a(\mathbf{k}) - \vec{m}(\mathbf{k}).\vec{\sigma})^2}\right. \tag{D.5}$$
$$\left.(\partial_y a(\mathbf{k}) + \partial_y \vec{m}(\mathbf{k}).\vec{\sigma}) \frac{1}{(iE - a(\mathbf{k}) - \vec{m}(\mathbf{k}).\vec{\sigma})}\right]$$

Expanding out the sums, we have several terms but taking the trace, cancel some of the terms. After integration over the E and dropping the terms which are zero under the trace gives:

$$\sigma_{xy} = -i \int \frac{d^2k}{(2\pi)^2} \frac{1}{8|\vec{m}(\mathbf{k})|^3} \tag{D.6}$$
$$tr\left(\partial_x \vec{m}(\mathbf{k})\ [\vec{m}(\mathbf{k}).\vec{\sigma}, \partial_y a(\mathbf{k}) + \partial_y \vec{m}(\mathbf{k}).\vec{\sigma}]\right)$$

After doing some algebra on the Pauli matrices and taking the trace, we get the relation given in 2.36.

Appendix E

Calculation of matrix element f-orbitals

To calculate $\langle \mathbf{k}, \sigma | k, M \rangle$, we use the known overlap of $|\mathbf{k}, \sigma\rangle$ and $|k, J_z\rangle$[109] for $l = 3$:

$$\langle \mathbf{k}, \sigma | k, J_z \rangle = 4\pi \left[\alpha_{J_z} Y_3^{J_z+\frac{1}{2}}(\Omega_{\mathbf{k}})\ \delta_{\sigma,-\frac{1}{2}} + \beta_{J_z} Y_3^{J_z-\frac{1}{2}}(\Omega_{\mathbf{k}})\ \delta_{\sigma,\frac{1}{2}} \right] \tag{E.1}$$

where $Y_l^m(\Omega_{\mathbf{k}})$ are associated Legender functions and $\alpha_{J_z} = [(7 + 2J_z)/14]^{1/2}$ and $\beta_{J_z} = [(7-2J_z)/14]^{1/2}$ are Clebsh-Gordan coefficients[109]. Now using the forms given in 3.1 we get the following for the two orbital

states:

$$\begin{aligned}
\langle \mathbf{k}, \sigma | \mathbf{1} \rangle &= \frac{1}{\sqrt{6}} \left[\frac{1}{\sqrt{7}} Y_3^{-2}(\Omega_\mathbf{k}) \; \delta_{\sigma,-\frac{1}{2}} + \sqrt{\frac{6}{7}} Y_3^{-3}(\Omega_\mathbf{k}) \; \delta_{\sigma,\frac{1}{2}} \right] \\
&- \sqrt{\frac{5}{6}} \left[\sqrt{\frac{5}{7}} Y_3^{2}(\Omega_\mathbf{k}) \; \delta_{\sigma,-\frac{1}{2}} + \sqrt{\frac{2}{7}} Y_3^{1}(\Omega_\mathbf{k}) \; \delta_{\sigma,\frac{1}{2}} \right] \\
\langle \mathbf{k}, \sigma | \mathbf{2} \rangle &= \frac{1}{\sqrt{6}} \left[\sqrt{\frac{6}{7}} Y_3^{3}(\Omega_\mathbf{k}) \; \delta_{\sigma,-\frac{1}{2}} + \frac{1}{\sqrt{7}} Y_3^{2}(\Omega_\mathbf{k}) \; \delta_{\sigma,\frac{1}{2}} \right] \\
&- \sqrt{\frac{5}{6}} \left[\sqrt{\frac{2}{7}} Y_3^{-1}(\Omega_\mathbf{k}) \; \delta_{\sigma,-\frac{1}{2}} + \sqrt{\frac{5}{7}} Y_3^{-2}(\Omega_\mathbf{k}) \; \delta_{\sigma,\frac{1}{2}} \right]
\end{aligned}$$

It is more convenient to work with a simplified version of these relations as:

$$\begin{aligned}
\langle \mathbf{k}, \sigma | \mathbf{1} \rangle &= \frac{1}{\sqrt{42}} \left[Y_3^{-2}(\Omega_\mathbf{k}) - 5 \; Y_3^{2}(\Omega_\mathbf{k}) \right] \delta_{\sigma,-\frac{1}{2}} \\
&+ \frac{1}{\sqrt{42}} \left[\sqrt{6} Y_3^{-3}(\Omega_\mathbf{k}) - \sqrt{10} \; Y_3^{1}(\Omega_\mathbf{k}) \right] \delta_{\sigma,\frac{1}{2}} \\
\langle \mathbf{k}, \sigma | \mathbf{2} \rangle &= \frac{1}{\sqrt{42}} \left[\sqrt{6} Y_3^{3}(\Omega_\mathbf{k}) - \sqrt{10} \; Y_3^{-1}(\Omega_\mathbf{k}) \right] \delta_{\sigma,-\frac{1}{2}} \\
&+ \frac{1}{\sqrt{42}} \left[Y_3^{2}(\Omega_\mathbf{k}) - 5 \; Y_3^{-2}(\Omega_\mathbf{k}) \right] \delta_{\sigma,\frac{1}{2}}
\end{aligned}$$

If we introduce new functions $A(\Omega_\mathbf{k})$ and $B(\Omega_\mathbf{k})$:

$$\begin{aligned}
\langle \mathbf{k}, \sigma | \mathbf{1} \rangle &= A(\Omega_\mathbf{k}) \; \delta_{\sigma,-\frac{1}{2}} + B(\Omega_\mathbf{k}) \; \delta_{\sigma,\frac{1}{2}} \\
\langle \mathbf{k}, \sigma | \mathbf{2} \rangle &= -B^*(\Omega_\mathbf{k}) \; \delta_{\sigma,-\frac{1}{2}} + A^*(\Omega_\mathbf{k}) \; \delta_{\sigma,\frac{1}{2}} \qquad \text{(E.2)}
\end{aligned}$$

where $A(\Omega_\mathbf{k}) = \frac{4\pi}{\sqrt{42}} \left[Y_3^{-2}(\Omega_\mathbf{k}) - 5 \; Y_3^{2}(\Omega_\mathbf{k}) \right]$ and $B(\Omega_\mathbf{k}) = \frac{4\pi}{\sqrt{42}} \left[\sqrt{6} Y_3^{-3}(\Omega_\mathbf{k}) - \sqrt{10} \; Y_3^{1} \right.$

Appendix F

Dirac Action

Here we show that low energy effective action is described by a continuum theory of fermionc spinons with Dirac dispersion. As mentioned before, we need to expand the Hamiltonian close to nodes at $(\frac{\pi}{2}, \frac{\pi}{2})$ and $(-\frac{\pi}{2}, \frac{\pi}{2})$. From now on (k_x, k_y) refer to deviation from $(\frac{\pi}{2}, \frac{\pi}{2})$ or $(-\frac{\pi}{2}, \frac{\pi}{2})$ points. Here we explicitly derive the Hamiltonian near $(\frac{\pi}{2}, \frac{\pi}{2})$. The other node is similar:

$$H = \begin{bmatrix} -\frac{4}{g}\vec{N}.\frac{\vec{\sigma}}{2} & 2t\ k_+ - 2i\Delta\ k_- \\ 2t\ k_+ + 2i\Delta\ k_- & \frac{4}{g}\vec{N}.\frac{\vec{\sigma}}{2} \end{bmatrix} \tag{F.1}$$

where $k_+ = k_x + k_y$ and $k_- = k_x - k_y$. This Hamiltonian could be written in terms of two by two Pauli matrices which are defined as:

$$\tau^x = \begin{bmatrix} 0 & 1 \\ 1 & 0 \end{bmatrix} \quad \tau^y = \begin{bmatrix} 0 & -i \\ i & 0 \end{bmatrix} \quad \tau^z = \begin{bmatrix} 1 & 0 \\ 0 & -1 \end{bmatrix}$$

Using this notation and also adding the contribution from $(-\frac{\pi}{2}, \frac{\pi}{2})$ node we get the following form for low energy Hamiltonian:

$$\begin{aligned} H = \sum_{k_+,k_-} & c_1^\dagger \ (2t \ k_+\tau^x + 2\Delta \ k_-\tau^y - \frac{4}{g} \ \tau^z \ \vec{N}.\frac{\vec{\sigma}}{2}) \ c_1 \\ & - c_2^\dagger \ (2t \ k_-\tau^x + 2\Delta \ k_+\tau^y + \frac{4}{g} \ \tau^z \ \vec{N}.\frac{\vec{\sigma}}{2}) \ c_2 \end{aligned} \tag{F.2}$$

Here c_1 and c_2 refer to $(\frac{\pi}{2}, \frac{\pi}{2})$ and $(-\frac{\pi}{2}, \frac{\pi}{2})$ nodes, respectively. They are two component fermionic operators, each component representing one of the sites in the unit cell. The τ^i matrices operate in the space of these two components. Each component has a $SU(2)$ spin index, where σ matrices operates. Now assume $t = \Delta$ (i.e. ignore the velocity un-isotropy which is irrelevant in renormaliztion group language) and we rename k_+ as k_y and k_- as k_x. Then introduce the new fermionic operators:

$$\psi_1 = -i\tau^x \ c_1 \tag{F.3}$$

$$\psi_2 = e^{i\frac{\pi}{4}\tau^z} \ c_2 \tag{F.4}$$

and subsequently:

$$\bar{\psi}_{1,2} = \psi_{1,2}^\dagger(i\tau^z) \tag{F.5}$$

With these new variables, the Hamiltonian (F.2) takes the following

simple form:

$$H = \sum_{k_x,k_y} \bar{\psi}_1 (k_x \tau^x + k_y \tau^y + J\vec{N}.\frac{\vec{\sigma}}{2})\ \psi_1 + \bar{\psi}_2 (k_x \tau^x + k_y \tau^y - J\vec{N}.\frac{\vec{\sigma}}{2})\ \psi_2 \tag{F.6}$$

Then using μ matrices that operates in the space, made by presence of two different nodes, we can put but nodes contribution (ψ_1 and ψ_2) as a single vector, ψ. Then the Hamiltonian takes the form:

$$H = \sum_{k_x,k_y} \bar{\psi} (k_x \tau^x + k_y \tau^y + iJ\mu^z\ \vec{N}.\frac{\vec{\sigma}}{2})\ \psi \tag{F.7}$$

This form in continuum limit and in real space leads to action given in 4.12.

Appendix G

Random Phase Calculation

We start with the partition function with an external magnetic field h that couples to the Neel vector:

$$Z = \int [D\psi][D\bar{\psi}][Da][DN]\ e^{-S} \tag{G.1}$$

$$S = S_N + S_{\psi,a} + S_{mixing} + S_h \tag{G.2}$$

$$S_N = \int d^2x d\tau \{\frac{1}{2}(\partial_\mu N)^2 + \frac{r}{2}N^2\} \tag{G.3}$$

$$S_{\psi,a} = \int d^2x d\tau \bar{\psi}[-i\gamma^\mu(\partial_\mu + iea_\mu)]\psi \tag{G.4}$$

$$S_{mixing} = \int d^2x d\tau\ \ i\bar{\psi}\vec{\sigma}\mu^z\psi.(\lambda\vec{N}) \tag{G.5}$$

$$S_h = \int d^2x d\tau \vec{h}.(a\ i\bar{\psi}\vec{\sigma}\mu^z\psi + b\vec{N}) \tag{G.6}$$

Here a and b are non-universal constants that depend on details of the microscopic physics.

Now by expanding the the terms which contain $i\bar{\psi}\mu^z\vec{\sigma}\psi$ (one coming from S_{mixing} and one from coupling to $\vec{h}$ field.) up to quadratic order, and performing the integral over ψ and a fields we get the following

form for the partition function:

$$Z = \int [DN] e^{-S_N - b\int d^2x d\tau \vec{h}.\vec{N}} \int d^2q d\omega \frac{\chi(q,\omega)}{2} |\vec{h} + \lambda \vec{N}|^2 \qquad \text{(G.7)}$$

Where $\chi(q,\omega)$ is the susceptibility of $i\bar{\psi}\vec{\sigma}\mu^z\psi$ operator calculated using the action $S_{\psi,a}$. We can rewrite the $\frac{\chi(q,\omega)}{2}|\vec{h} + \lambda\vec{N}|^2$ up to quadratic order in N as an exponential. Putting this form in G.7 we get the following for the partition function:

$$\begin{aligned} Z &= \int [DN] e^{-S_N^{eff}} && \text{(G.8)} \\ S_N^{eff} &= S_N + \int d^2q d\omega \{ b\ \vec{h_q}.\vec{N_{-q}} - \frac{\chi(q,\omega)}{2} |a\ \vec{h_q} + \lambda \vec{N_q}|^2 \} \\ &= \int d^2q d\omega \{ \frac{\chi_N(\omega,q)^{-1}}{2} |\vec{N_q}|^2 + \vec{h_q}.\vec{N_{-q}} \\ &\quad - \frac{\chi(q,\omega)}{2} |\vec{h} + \lambda \vec{N}|^2 \} && \text{(G.9)} \end{aligned}$$

Now to get the quadratic action for $\vec{h}$ field we should integrate out $\vec{N}$ field, which is a simple Gaussian integral now. This leads to the following value for effective susceptibility:

$$\chi_{eff} = \frac{a^2\ \chi + b^2\ \chi_N - 2\lambda a\ b\ \chi\ \chi_N}{1 - \lambda^2 \chi\ \chi_N} \qquad \text{(G.10)}$$

You can see that as one expects, for $\lambda = 0$, this reduces to some of susceptibilities for $\vec{N}$ and $i\bar{\psi}\mu^z\frac{\vec{\sigma}}{2}\psi$ fields. Also note that, this is valid only for the frequencies where $\lambda^2\chi\ \chi_N$ is not of order one (*i.e.* it is not valid for small frequencies). Now by analytic continuation to real frequencies and taking the imaginary part, we get the spectral functions

plotted in section 4.2.1.

G.1 Feynman diagrams

G.1.1 Spin-Spin correlation in mean-field theory

For spin-spin correlation we need to calculate the following diagram which consists of two fermionic propagators. The fermionic propagator in mean field is derived from the action 4.12:

$$\underset{p}{\longrightarrow} = \frac{1}{\not{p} - i\lambda\vec{N}.\vec{\sigma}} \tag{G.11}$$

This diagram, in the real space, corresponds to the following integral:

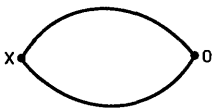

Figure G-1: Spin-Spin correlation in mean field

$$\langle S_i S_j \rangle = -\delta_{ij} \int \frac{d^3p}{(2\pi)^3} \frac{d^3q}{(2\pi)^3} e^{-i\vec{p}.\vec{r}} \frac{tr[(\not{p}+\not{q}-i\lambda\vec{N}.\vec{\sigma})(\not{q}-i\lambda\vec{N}\vec{\sigma})]}{((p+q)^2+\lambda^2N^2)(q^2+\lambda^2N^2)} \tag{G.12}$$

After integrating over q this gives:

$$\langle S_i S_j \rangle \propto -\frac{\delta_{ij}}{r} \int p\, dp\, sin(pr)[4\lambda N + \frac{2}{p}\arctan(\frac{p}{2\lambda N})(4\lambda^2N^2+p^2)] \tag{G.13}$$

The first term is proportional to $\delta(r)$. Since we are interested in the case where $r \neq 0$, we can ignore that term. The second term gives:

$$\frac{e^{-2\lambda N r}}{r^4}(1 + 2\lambda N r) \tag{G.14}$$

We already saw that N goes to zero as g approaches g_c like $g_c - g$. So if we define correlation length as $\xi = \frac{1}{2\lambda N}$ we get the equations 4.13 and 4.14.

Appendix H

Beyond mean field: ϵ-expansion

Now to do the ϵ-expansion we need to study the action given in 4.18. We can see that there are three different types of vertices present in the theory and eleven different one loop diagrams which cause field renormalizations, vertex corrections and mass renormalization. we use the following diagrammatic representation for the propagators of the fields, in the theory:

$$\begin{aligned} \overset{a}{\text{-----}}\overset{b}{\text{-----}} \;(p) &= \frac{\delta^{ab}}{p^2 + r} \\ \text{————} \;(p) &= \frac{1}{\not{p}} \\ \overset{\mu}{\sim\!\sim\!\sim}\overset{\nu}{\sim\!\sim\!\sim} \;(p) &= \frac{\delta^{\mu\nu}}{p^2} \end{aligned} \tag{H.1}$$

Here we have used Feynman gauge for the gauge field propagator, and Euclidian metric. Now we start to calculat the one loop diagrams.

Fermion self energy

There are two, one loop diagrams which will generated fermions self energy. Diagram H-1(a) represent N field contribution to fermion self

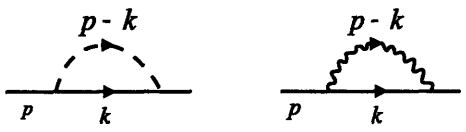

Figure H-1: fermion self energy

energy:

$$\begin{aligned}\Sigma_N^{\psi}\ \not{p} &= (i\lambda)^2 \int \frac{d^dk}{(2\pi)^d}\sigma^i \frac{\delta^{ij}\ \not{k}}{k^2(k+p)^2}\sigma^j \\ &= -\frac{3}{(4\pi)^2}\frac{\lambda^2}{\epsilon}\ \not{p}\end{aligned} \tag{H.2}$$

Diagram H-1(b) represents gauge field contribution to fermion self energy:

$$\begin{aligned}\Sigma_a^{\psi}\ \not{p} &= e^2 \int \frac{d^dk}{(2\pi)^d}\gamma^\mu \frac{\delta^{\mu\nu}\ \not{k}}{k^2(k+p)^2}\gamma^\nu \\ &= -\frac{1}{(4\pi)^2}\frac{e^2}{\epsilon}\ \not{p}\end{aligned} \tag{H.3}$$

N Field Self Energy

Since N field is coupled to fermion field only, there is just one diagram contributing to its self energy.

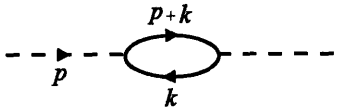

Figure H-2: N field self energy

This has the following contribution:

$$\begin{aligned}\Sigma_{\psi}^{N} p^2 \delta^{ij} &= (-1)(i\lambda)^2 \int \frac{d^d k}{(2\pi)^d} \frac{tr(\sigma^i \sigma^j) tr(\not{k}(\not{k}+\not{p}))}{k^2 (k+p)^2} \\ &= -\frac{8}{(4\pi)^2} \frac{\lambda^2}{\epsilon} p^2 \delta^{ij}\end{aligned} \tag{H.4}$$

Here the minus sign appears because of presence of a fermionic loop in the diagram [106].

Gauge field self energy

Gauge field is only coupled to fermion field as well, so there is only one diagram generates gauge field self energy:

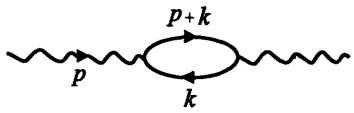

Figure H-3: Gauge Field Self Energy

This diagram has the following contribution:

$$\begin{aligned}\Sigma_{\psi}^{a} [p^\mu p^\nu - p^2 \delta^{\mu\nu}] &= (-1) e^2 \int \frac{d^d k}{(2\pi)^d} \frac{tr(\gamma^\mu \not{k} \gamma^\nu (\not{k}+\not{p}))}{k^2 (k+p)^2} \\ &= -\frac{16}{(4\pi)^2} \frac{e^2}{3\epsilon} p^2 [\delta^{\mu\nu} - \frac{p^\mu p^\nu}{p^2}]\end{aligned} \tag{H.5}$$

Note that in this relation the term proportional to $p^\mu p^\nu$ dose not contribute to physical observables (S-matrix elements). This is guarantied

by Ward identity[106].

$u((\vec{N})^2)^2$ vertex correction

There are two diagrams contributing to this vertex renormalization at one loop level. Note that up to one loop order, it is enough to

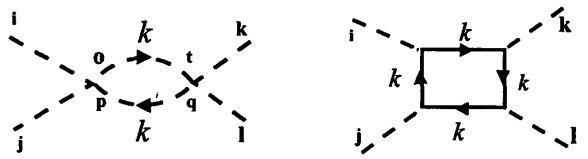

Figure H-4: u renormalization

calculate vertex corrections with zero external momentum. Diagram H-4(a) gives:

$$\begin{aligned}
&\Delta_N^u(\delta^{ij}\delta^{kl}+\delta^{ik}\delta^{jl}+\delta^{il}\delta^{jk}) \\
&= -\frac{u^2}{6}(\delta^{ij}\delta^{op}+\delta^{io}\delta^{jp}+\delta^{ip}\delta^{jo})\int\frac{d^dk}{(2\pi)^2}\frac{\delta^{oq}\delta^{pt}}{(k^2+r)^2} \\
&\qquad\qquad (\delta^{qt}\delta^{kl}+\delta^{qk}\delta^{tl}+\delta^{ql}\delta^{tk}) \\
&= -\frac{11}{(4\pi)^2}\frac{u^2}{3\epsilon}(\delta^{ij}\delta^{kl}+\delta^{ik}\delta^{jl}+\delta^{il}\delta^{jk})
\end{aligned} \tag{H.6}$$

The contribution of diagram H-4(b) is similarly calculated:

$$\begin{aligned}
&\Delta_\psi^u(\delta^{ij}\delta^{kl}+\delta^{ik}\delta^{jl}+\delta^{il}\delta^{jk}) \\
&= -3(-1)(i\lambda)^4\int\frac{d^dk}{(2\pi)^d}\frac{tr(\not{k}^4)}{k^8}tr(\sigma^i\sigma^j\sigma^k\sigma^l) \\
&= \frac{96}{(4\pi)^2}\frac{\lambda^4}{\epsilon}(\delta^{ij}\delta^{kl}+\delta^{ik}\delta^{jl}+\delta^{il}\delta^{jk})
\end{aligned} \tag{H.7}$$

Again one minus sign appears because of the fermionic loop [106].

N-ψ vertex correction

Again, there are two different diagrams associated with this correction at one-loop level:

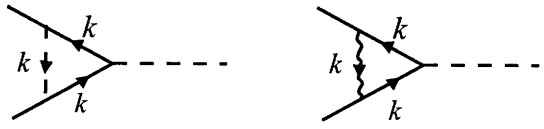

(a) (b)

Figure H-5: λ renormalization

As before we set the external momentums to zero. Then the contribution of diagram H-5(a) is:

$$\begin{aligned} i\Delta_N^\lambda \sigma^k =& (i\lambda)^3 \int \frac{d^d k}{(2\pi)^d} \frac{\not{k}}{k^2} \sigma^i \frac{\delta^{ij}\ \sigma^k}{k^2 + r}\ \sigma^j \frac{\not{k}}{k^2} \\ =& \ i \frac{2}{(4\pi)^2} \frac{\lambda^3}{\epsilon} \sigma^k \end{aligned} \tag{H.8}$$

and diagram H-5(b) gives:

$$\begin{aligned} i\Delta_a^\lambda =& i\lambda\ e^2 \int \frac{d^d k}{(2\pi)^d} \frac{\not{k}}{k^2} \gamma^\mu \frac{\delta^{\mu\nu}}{k^2 + r} \gamma^\nu \frac{\not{k}}{k^2} \\ =& i \frac{6}{(4\pi)^2} \frac{\lambda\ e^2}{\epsilon} \end{aligned} \tag{H.9}$$

a-ψ vertex correction

Similar to H there are two diagrams:

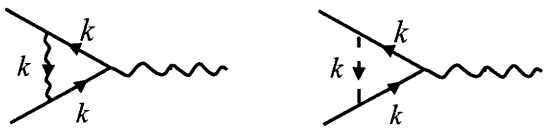

(a) (b)

Figure H-6: e renormalization

The first diagram (H-6(a)) gives:

$$\begin{aligned}\Delta_a^e\ \gamma^\alpha =& e^3 \int \frac{d^dk}{(2\pi)^d}\gamma^\mu \frac{\not k}{k^2}\frac{\gamma^\alpha \delta^{\mu\nu}}{k^2}\frac{\not k}{k^2}\gamma^\nu \\ =& \frac{1}{(4\pi)^2}\frac{e^3}{\epsilon}\gamma^\alpha\end{aligned} \tag{H.10}$$

and H-6(b) gives:

$$\begin{aligned}\Delta_N^e\ \gamma^\alpha =& e(i\lambda)^2 \int \frac{d^dk}{(2\pi)^d}\sigma^i \frac{\not k}{k^2}\frac{\gamma^\alpha \delta^{ij}}{k^2+r}\frac{\not k}{k^2}\sigma^j \\ =& \frac{3}{(4\pi)^2}\frac{e^3}{\epsilon}\gamma^\alpha\end{aligned} \tag{H.11}$$

Note that H.10 is minus the contribution of H.3 and H.11 has the minus contribution of H.2. This, in fact, should be the case to keep gauge invariance of the theory.

Mass renormalization

The last one loop diagram, we consider, generates mass renormalization:

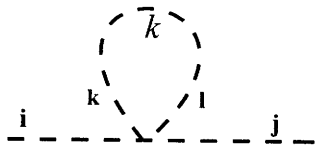

$$\begin{aligned}\Delta_r\ \delta^{ij} &= \frac{u}{6}(\delta^{ij}\delta^{kl}+\delta^{ik}\delta^{jl}+\delta^{il}\delta^{jk})\int\frac{d^dk}{(2\pi)^d}\frac{\delta^{lk}}{k^2+r} \\ &= -\frac{5}{(4\pi)^2}\frac{u}{3\epsilon}\ \delta^{ij}\end{aligned} \tag{H.12}$$

H.0.2 Renormalization conditions

Now with these in hand, we can proceed using minimal subtraction scheme. Introducing a mass scale $m \propto \sqrt{r}$ we can write the following set of renormalization conditions:

$$\begin{aligned}\not{p}\ (Z_\psi - (\Sigma_N^\psi + \Sigma_a^\psi)) &= finite\ O(2\ loops) \\ m^{-\frac{\epsilon}{2}} e_0 Z_\psi \sqrt{Z_a} + (\Delta_N^e + \Delta_a^e) &= finite\ O(2\ loops) \\ Z_N(p^2+r) + (r\Delta_r - \Sigma_\psi^N\ p^2) &= finite\ O(2\ loops) \\ m^{-\frac{\epsilon}{2}} \lambda_0 Z_\psi \sqrt{Z_N} + (\Delta_N^\lambda + \Delta_a^\lambda) &= finite\ O(2\ loops) \\ p^2(Z_a - \Sigma_\psi^a) &= finite\ O(2\ loops) \\ m^{-\epsilon} u_0 Z_N^2 + (\Delta_N^u + \Delta_\lambda^u) &= finite\ O(2\ loops)\end{aligned}$$

Here e_0, λ_0 and u_0 are bare coupling constants and so does not flow with mass scale. These relations give field renormalization coefficients directly, since the divergence part of self energy diagrams should cancel out with these field renormalization coefficients.

$$Z_\psi = 1 + \Sigma_\psi^N + \Sigma_\psi^a \tag{H.13}$$

$$Z_N = 1 + \Sigma_N^\psi \tag{H.14}$$

$$Z_a = 1 + \Sigma_a^\psi \tag{H.15}$$

Putting them back in renoemalization condition equations, and letting the mass scale flow [106], we get the equations given in section 4.4.

H.0.3 Renormalization of bilinear operatores

Here we introduce a new term in the Lagrangian with the general form:

$$v\ \bar{\psi}\mathcal{O}\psi, \tag{H.16}$$

where $\mathcal{O}$ is the combination of μ and σ matrices which are given in table 4.1. There are two new diagrams corresponding to this new vertex (H-7(a),H-7(b)) Diagram H-7(a) gives:

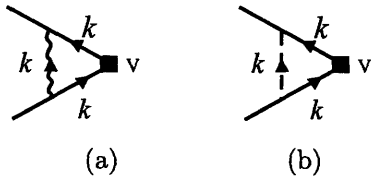

Figure H-7: bilinear operators scaling dimension

$$\begin{aligned}\Delta^N_{\mathcal{O}}\mathcal{O} =&(i\lambda)^2\int\frac{d^dk}{(2\pi)^d}\sigma^i\mu^z\frac{\not{k}}{k^2}\mathcal{O}\frac{\not{k}}{k^2}\frac{\delta^{ij}}{k^2+r}\mu^z\sigma^j\\ =&-\lambda^2\frac{2}{(4\pi)^2\,\epsilon}\,A_{\mathcal{O}}\mathcal{O},\quad A_{\mathcal{O}}\mathcal{O}=\sigma^i\mu^z\mathcal{O}\mu^z\sigma^i\end{aligned} \tag{H.17}$$

and diagram H-7(b) gives:

$$\begin{aligned}\Delta^a_{\mathcal{O}}\mathcal{O} =&e^2\int\frac{d^dk}{(2\pi)^d}\gamma^\mu\frac{\not{k}}{k^2}\mathcal{O}\frac{\not{k}}{k^2}\frac{\delta^{\mu\nu}}{k^2}\gamma^\nu\\ =&\,e^2\frac{6}{(4\pi)^2\,\epsilon}\,\mathcal{O}\end{aligned} \tag{H.18}$$

Whit these in hand we can get the scaling dimension of v:

$$\begin{aligned}\Delta_v = 1 + \delta_v &= [1 + (\Delta_{\mathcal{O}}^N + \Sigma_\psi^N)\lambda^2 + (\Delta_{\mathcal{O}}^a + \Sigma_\psi^a)e^2]v \\ &= [1 + (-2A_{\mathcal{O}} - 3)\frac{\lambda^2}{(4\pi)^2} + 5\frac{e^2}{(4\pi)^2}]v\end{aligned} \tag{H.19}$$

This gives the scaling dimension of v $(1 + \delta_v)$. Now to get the scaling dimension of $\mathcal{O}$ $(\Delta_{\mathcal{O}})$, note:

$$\Delta_{\mathcal{O}} = D - (1 + \delta_v) = 3 - \epsilon - \delta_v \tag{H.20}$$

Using the fixed point values for λ and e, we get the scaling dimensions mentioned in table 4.1.

H.0.4 Velocity anisotropy

In this section we assume a small velocity anisotropy and treat it as a perturbation to our QED_3 theory. Following the notation used in Ref. [95], this anisotropy is presented by:

$$K_a = -i\delta\bar{\psi}\mu^z\hat{\gamma}^\mu(\partial_\mu + ie\ a_\mu)\psi \tag{H.21}$$

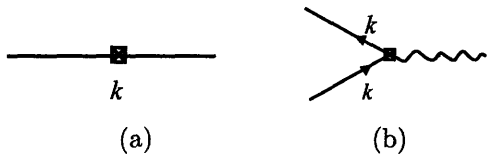

Figure H-8: Velocity anisotropy vertexes

Here, δ is the small perturbation parameter (we are essential inter-

ested in its behavior under renormalization) and $\hat{\gamma^\mu} = \gamma^x \delta_{x,\mu} - \gamma^y \delta_{y,\mu}$. There are two vertexes associated with this perturbation. One is correction in fermionic kinetic energy presented in figure H-8(a) and correction to the $a - \psi$ vertex presented in figure H-8(b):

$$-\delta\mu^z \hat{\not{k}} \tag{H.22}$$

$$-\delta\mu^z \hat{\gamma^\mu} \tag{H.23}$$

So there are there three different type of one-loop diagrams, in addition to field renormalization factors calculated before contributing renormalization of the anisotropy term in fermionic kinetic energy (*i.e.* δ). Diagram H-9(a) gives:

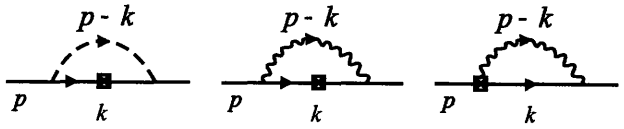

(a) (b) (c)

Figure H-9: Velocity anisotropy one-loop renormalization

$$\begin{aligned} -\delta\ \Sigma_\delta^N \hat{\not{p}} &= -\delta\ (i\lambda)^2 \int \frac{d^d k}{(2\pi)^d} \sigma^i \frac{1}{\not{k}} \hat{\not{k}} \frac{1}{\not{k}} \frac{\delta^{ij}}{(p-k)^2 + r} \sigma^j \\ &= -\frac{\delta}{(4\pi)^2} \frac{\lambda^2}{\epsilon} \hat{\not{p}} \end{aligned} \tag{H.24}$$

Diagram H-9(b) similarly gives:

$$\begin{aligned} -\delta\ \Sigma_\delta^a \delta \hat{\not{p}} &= -\delta\ e^2 \int \frac{d^d k}{(2\pi)^d} \gamma^\mu \frac{1}{\not{k}} \hat{\not{k}} \frac{1}{\not{k}} \frac{\delta^{\mu\nu}}{(p-k)^2} \gamma^\nu \\ &= -\frac{\delta}{3(4\pi)^2} \frac{e^2}{3\epsilon} \hat{\not{p}} \end{aligned} \tag{H.25}$$

Diagram H-9(c) and the similar one with the correction on the right vertex give:

$$\begin{aligned} -\delta\ \Delta_\delta^a \hat{\not{p}} &= \delta\ e^2 \int \frac{d^d k}{(2\pi)^d} \hat{\gamma}^\mu \frac{1}{\not{k}} \frac{\delta^{\mu\nu}}{(p-k)^2} \gamma^\nu \\ &= \frac{\delta}{(4\pi)^2} \frac{2e^2}{\epsilon} \hat{\not{p}} \end{aligned} \tag{H.26}$$

Now with these in and also the field renormalziation coefficients calculated perviously we can get the RG flow for δ:

$$\begin{aligned} \beta_\delta &= \delta\ (2\ \Delta_\delta^a + \Sigma_\delta^N + \Sigma_\delta^a + \Sigma_N^\psi + \Sigma_a^\psi) \\ &= -\delta\ (\frac{14}{3(4\pi)^2}\ e^2 + \frac{2}{(4\pi)^2}\ \lambda^2) \end{aligned} \tag{H.27}$$

This proves that the small velocity anisotropy is irrelevant.

Bibliography

[1] k. M. Shen et. al., science p. 901 (2005).

[2] Andres, Ott, and Grabner, Phys. Rev. Lett. **35,** 1775 (1975).

[3] J. C. et. al., Nature **424,** 524 (2003).

[4] P. Coleman, in *Handbook of Magnetism and Advanced Magnetic Materials. Vol 1: Fundamentals and Theory* (John Wiley and Sons, 2007), p. 95, edited by: Helmut Kronmuller and Stuart Parkin.

[5] P. W. Anderson, Science **177,** 393 (1986).

[6] H. A. Hertz, Phys. Rev. B **14,** 1165 (1976).

[7] S. Sachdev, *Quantum phase transitions* (Cambridge University Press, 1999).

[8] T. Senthil, Int. J. of Mod. Phys. **20,** 2603 (2006).

[9] P. Nozieres and D. Pines, *Theory Of Quantum Liquids* (Perseus Books Publishing L.L.C., 1999).

[10] R. Laughlin, Phys. Rev. Lett. **50,** 1395 (1983).

[11] T. Senthil, A. Vishwanath, L. Balents, S. Sachdev, and M. P. A. Fisher, Science **303,** 1490 (2004).

[12] T. Senthil (unpublished).

[13] A. Millis and P. Lee, Phys. Rev. B **35,** 3394 (1987).

[14] N. Read, D. M. Newns, and S. Doniach, Physical Review B **30,** 3841 (1984).

[15] J. G. Bednorz and K. A. Muller, Z. Phys. B **64,** 188 (1986).

[16] M. K. W. et. al., Phys. Rev. Lett. **58,** 908 (1987).

[17] P. A. Lee, Rep. Prog. Phys. **71,** 012501 (2008).

[18] P. W. Anderson, Science **235,** 1196 (1987).

[19] F. Zhang and T. Rice, Phys. Rev. B **37,** 3759 (1988).

[20] J. Orenstein and A. J. Millis, Science **288,** 468 (2000).

[21] P. A. Lee, N. Nagaosa, and X.-G. Wen, Rev. Mod. Phys. **78,** 17 (2006).

[22] A. M. Mook, M.Yehiraj and Armstrong, Phys. Rev. Lett **70,** 3490 (1993).

[23] D. Fong, Keimer and Aksay, Phys. Rev. Lett **78,** 713 (1997).

[24] R. S. He, Lin. and Keimer, Phys. Rev. Lett **86,** 1610 (2001).

[25] S. Chubukov and Ye, Phys. Rev. B **49,** 11919 (1994).

[26] Morr and Pines, Phys. Rev. lett. **81,** 1086 (1998).

[27] B. Vojta and Sachdev, Phys. Rev. B **61,** 15152 (2000).

[28] S. R. B. I. M. A. Fong, Bourges and Keimer, Phys. Rev. B **61,** 14773 (2000).

[29] H. Dai, Mook and Doğan, Phys. Rev. B **63,** 054525 (2000).

[30] J. M. Luttinger, Phys. Rev. **119,** 1153 (1960).

[31] B. et. al, Phys. Rev. B **74,** 224452 (2006).

[32] A. M. A. Luscher and O. Shushkov, Phys. Rev. lett. **98,** 37001 (2007).

[33] B. I. Shraiman and E. Siggia, Phys. Rev. Lett. **61,** 467 (1988).

[34] X. J. Zhou *et al.*, Phys. Rev. Lett. **92,** 187001 (2004).

[35] S. Danzenbächer *et al.*, Phys. Rev. lett. **96,** 106402 (2006).

[36] M. Civelli, M. Capone, S. S. Kancharla, O. Parcollet, and G. Kotliar, Phys. Rev. Lett. **95,** 106402 (2005).

[37] P. L. et. al., Phys. Rev. Lett. **91,** 016401 (2003).

[38] G. D. Mahan, *Many-Particle Physics* (Plenum Press, 1990).

[39] J. Kondo, Progr. Theoret. Phys. (Kyoto) **36,** 429 (1966).

[40] S. Doniach, Physica B. **91,** 231 (1977).

[41] P. Nozieres, Eur. Phys. B **6,** 447 (1998).

[42] P. W. Anderson, Phys. Rev. **124,** 41 (1961).

[43] J. H. V. Vleck, Rev. Mod. Phys. **34,** 681 (1962).

[44] P. Coleman, C. Pepin, Q. Si, and R. Ramazashvili, J. Phys.: Condens. Matt. **13,** 723 (2001).

[45] L. L. et. al., Phys. Rev. Lett. **72,** 3262 (1994).

[46] T. Senthil, M. Vojta, and S. Sachdev, Phys. Rev. B **69,** 035111 (2004).

[47] A. de Visser et. al., Phys. Rev. Lett. **85,** 3005 (2000).

[48] T. S. Pouyan Ghaemi and P. Coleman, Phys. Rev. B **77,** 245108 (2008).

[49] P. Ghaemi and T. Senthil, Phys. Rev. B **75,** 144412 (2007).

[50] P. Ghaemi and T. Senthil, Phys. Rev. B **73,** 054415 (2006).

[51] N. Read and S. Sachdev, Phys. Rev. Lett. **66,** 1773 (1991).

[52] X.-G. Wen, Phys. Rev. B **44,** 2664 (1991).

[53] T. Senthil and M. P. A. Fisher, Phys. Rev. B **62,** 7850 (2000).

[54] J. Moreno and P. Coleman, Physical Review letters **84,** 342 (2000).

[55] H. Ikeda and K. Miyake, Journal of Physical Society of Japan **65,** 1769 (1996).

[56] K. S. Burch, S. V. Dordevic, F. P. Mena, A. B. Kuzmenko, D. van der Marel, J. L. Sarrao, J. R. Jeffries, E. D. Bauer, M. B. Maple, and D. N. Basov, Phys. Rev. B **75,** 054523 (2007).

[57] R. Kubo, J. Phys. Soc. Jpn. **12,** 570 (1957).

[58] G. E. Volovik, Pis'ma ZhETF **66,** 492 (1997).

[59] T. Senthil, J. B. Marston, and M. P. A. Fisher, Phys. Rev. B **60,** 4245 (1999).

[60] M. A. Tanatar, J. Paglione, C. Petrovic, and L. Taillefer, Science **316,** 1320 (2007).

[61] N. Doiron-Leyraud, C. Proust, D. Leboeuf, J. Levallois, J. Bonnemaison, R. Liang, D. A. Bonn, W. N. Hardy, and L. Taillefer, Nature **447,** 565 (2007).

[62] E. A. Yelland, J. Singleton, C. H. Mielke, N. Harrison, B. D. F. F. Balakirev, and J. R. Cooper, Phys. Rev. Lett. **100,** 047003 (2008).

[63] A. F. Bangura *et al.*, Phys. Rev. Lett. **100,** 047004 (2008).

[64] G. Zwicknagl, Advances in Physics **41,** 201 (1992).

[65] D. L. Cox, *Exotic Kondo effects in metals : magnetic ions in a cystalline electric field and tunnelling centres* (Taylor and Francis Inc., 1999).

[66] J. R. Schreiffer and P. Wolff, Phys. Rev. **149,** 491 (1966).

[67] B. Coqblin and J. R. Schreiffer, Phys. Rev. **185,** 847 (1969).

[68] D. C. Langreth, Phys. Rev. **150,** 516 (1966).

[69] C. M. Varma, Phys. Rev. Lett. **55,** 2723 (1985).

[70] R. K. Kaul, Y. B. Kim, S. Sachdev, and T. Senthil, Nature Physics **4,** 28 (2008).

[71] L. Taillefer (unpublished).

[72] A. J. Millis and M. Norman, Phys. Rev. B **76,** 220503 (2007).

[73] N. Andrei and P. Coleman, Physical Review Letters **62,** 595 (1989).

[74] T. Senthil, S. Sachdev, and M. Vojta, Physical Review Letters **90,** 216403 (2003).

[75] M. Dzero and P. Coleman (unpublished).

[76] Q. Si, S. Rabello, K. Ingersent, and J. L. Smith, Nature **413,** 804 (2001).

[77] T. Senthil, Annals of Physics **321,** 1669 (2006).

[78] S. Kivelson, D. Rokhsar, and J. Sethna, Phys. Rev. B **35,** 8865 (1987).

[79] N. Read and S. Sachdev, Phys. Rev. Lett. **62,** 1694 (1989).

[80] S. Sachdev, Phys. Rev. B **40,** 5204 (1989).

[81] S. Sachdev, Rev. Mod. Phys **75,** 913 (2003).

[82] Z. Liu and Levin, Phys. Rev. lett. **75,** 4130 (1995).

[83] Millis and Monien, Phys. Rev. B **54,** 16172 (1996).

[84] Abanov and Chubukov, Phys. Rev. Lett. **83,** 1652 (1999).

[85] M. N. Norman, Phys. Rev. B **61,** 14751 (2000).

[86] J. Brinckmann and P. A. Lee, Phys. Rev. B **65,** 014502 (2002).

[87] S. A. K. E. W. Carlson, V. J. Emery and D. Orgad, in *Physics of conventional and unconventional superconductors*

[88] M. Hermele, T. Senthil, M. P. A. Fisher, P. A. Lee, N. Nagaosa, and X.-G. Wen, Phys. Rev. B **70,** 214437 (2004).

[89] I. Affleck and J. B. Marston, Phys. Rev. B **37,** 3774 (1988).

[90] J. B. Marston and I. Affleck, Phys. Rev. B **39,** 11538 (1989).

[91] X.-G. Wen and P. A. Lee, 'Phys. Rev. Lett. .

[92] D. H. Kim and P. A. Lee, Annals of Physics **272,** 130 (1999).

[93] W. Rantner and X.-G. Wen, Phys. Rev. B **66,** 144501 (2002).

[94] T. Senthil and P. A. Lee, Phys. Rev. B **71,** 174515 (2005).

[95] M. Hermele, T. Senthil, and M. Fisher, Phys. Rev. B **72,** 104404 ('2005).

[96] W. Rantner and X.-G. Wen, Phys. Rev. Lett. **86,** 3871 (2001).

[97] D. A. Ivanon, MIT PhD Thesis (2000).

[98] M. R. A. Paramekanti and N. Trivedi, Phys. Rev. B **71,** 094421 (2005).

[99] M. P. A. F. L. Balents and C. Nayak, Phys. Rev. B **60,** 1654 (1999).

[100] C. Gros, Ann. Phys. (N.Y.) **189,** 53 (1988).

[101] T. K. Lee and C. T. Shih, Phys. Rev. B **55,** 5983 (1997).

[102] M. P. A. F. L. Balents and C. Nayak, Int. J. of Mod. Phys. B **12,** 1033 (1998).

[103] J. Zinn-Justin, *Quantum Field Theory and Critical Phenomena*

[104] V. T. O. Vafek and M. Franz, Phys. Rev. Lett. **89,** 157003 (2002).

[105] V. T. M. Franz and O. Vafek, Phys. Rev. Lett. **66,** 054535 (2002).

[106] M. E. Peskin and D. V. Schroeder, *An Introduction to Quantum Field Theory* (Perseus Books Publishing L.L.C., 1995).

[107] F. Oberhettinger, in *Handbook of Mathematical Functions with Formulas, Graphs, and Mathematical Tables* (Dover, 1972), p. 555, edited by: Milton Abramowitz and Irene A. Stegun.

[108] N. W. Ashcroft and N. D. Mermin, *Solid State Physics* (Saunders College Publishing, 1976).

[109] L. E. Ballentine, *Quantum Mechanics: A Modern Development* (World Scientific Publishing Co. Pte. Ltd., 2003).